Climate drivers of Douglas-fir growth in the western United States

Christina Marie Restaino

A dissertation

submitted in partial fulfillment of the

requirements for the degree of

Doctor of Philosophy

University of Washington

2014

Reading Committee:

Gregory J. Ettl, Chair

David L. Peterson

Donald McKenzie

Program Authorized to Offer Degree:

School of Environmental and Forest Sciences

Acknowledgements

My committee has provided a tremendous amount of academic and emotional support along the way. I could not have asked for better guidance from such an amazingly intelligent and creative group of individuals. My advisor, Dave Peterson, has had more of an impact on my professional and scientific development than any other sole individual. His patience, support, and expertise are appreciated beyond measure. Dave changed my life and I will be forever grateful. Don McKenzie worked as a co-advisor in many respects and his critical eye and analytical expertise have contributed immensely to my development as a quantitative scientist. His support for our lab is enormous and I greatly appreciate his eagerness to see us improve. Greg Ettl provided me with guidance beyond my dissertation, aiding in my development as a teacher and leader in my community. He has provided an incredible sounding board for me at times when I was nearly broken. I thank him for his kindness and genuine advice. Soo-Hyung Kim has provided insight and education regarding the finest scales of plant response to environmental change. Any good forest ecologist must learn the mechanisms that drive plant productivity and behavior, and his attention to detail is exemplary. Janneke Hille ris Lambers has provided exceptional guidance in how to participate in new, cutting edge fields of ecological sciences. She has given me the inspiration to pursue academia and the world of tenure as a young woman.

The Fire and Mountain Ecology lab is comprised of role models and peers and I have been lucky enough to be a part of this lab for seven years. Starting at the beginning, the cast of characters contributed enormously to my humbling and intellectual development. A big thank you to Karen Kopper, Morris Johnson, Clint Wright, Crystal Raymond, Rich Gwozdz, and Jessica Halofsky. The later cohort of students helped me transition to a leadership role and I greatly appreciate their willingness to learn from me and help me with my development along the way. Thank you to Whitney Albright, Kailey Marcinkowski, Natasha Stavros, Jim Cronan, and Keala Hagmann. A huge thank you to Maureen Kennedy, post-doc of the universe! I honestly could not have done any of this without her help. Rob Norheim has provided incredible support and critical advice on cartography needs and I thank him for always providing flawless maps. Without Nick Povak, I would have never learned to actually love coding in R, and I will be forever grateful for his help (and am likely not done asking for it). Thank you, Nick.

I reserve a special thank you to Alina Cansler – we have been at it together all along! I would not be the scientist or teacher that I am without her incredible friendship, constructive criticism, and camaraderie. She is one of the most brilliant scientists I have met and I look forward to our many career and wilderness endeavors in the future.

The field effort required to complete this study was enormous and overwhelming and it would have been impossible without a few key players. Sarah Lyons-Tinsley accompanied me on my first field season, exploring the western mountains for the best study sites (and breweries

and climbing crags). Mike Tjoelker and Seth Cowdery worked with me on my second and third field seasons, coring hundreds of trees. Their patience and hard work is greatly appreciated. Mike Tjoelker also helped with processing and measuring all of the cores. Mike, this project would not have been possible without you!

This project would have never happened if it were not for the brilliance of Jeremy Littell. I followed in his footsteps and expanded on a project that he completed for his dissertation. Jeremy is incredibly intelligent and provides the most thoughtful and smart comments and ideas. I am very grateful that our worlds were able to collide. Thank you, Jeremy, for sharing your thoughts and knowledge of the mighty Douglas-fir with me.

I have an incredibly supportive group of family and friends. Mary Ann, Josh and Sarah Lyons-Tinsley have been my rock for 30 years. Thanks for always rallying to support me in all my crazy adventures. Maddy, Mic and Mike Restaino – I could not ask for a better family to marry. Your unwavering support does not go unnoticed. I love you all very much.

My husband, Joe, is the most supportive, caring and patient man. I have been in school for almost our entire relationship of 13 years. I would not exist as the person that I am without him. When I was a freshman at UC Berkeley he told my mom, “If we can just make it through all of the years that she wants to go to school, we can make it through anything.” Well, here we are! We’ve got stayin’ power, you and I, through thick and thin. Thank you, Joe, and I love you.

University of Washington

Abstract

Climate drivers of Douglas-fir growth in the western United States

Christina Marie Restaino

Chair of the Supervisory Committee:
Gregory J. Ettl
School of Environmental and Forest Sciences

Douglas-fir (*Psuedotsuga menziesii*) spans the entire mountain system of the western United States, successfully occupying many different climatic and ecological niches. Its occupation of many different growth environments, and its temporal persistence on the landscape, make this species an ideal representative of forest-climate interactions in western mountain ecosystems. To quantify climate-growth relationships in Douglas-fir, I developed a comprehensive network of chronologies collected across the "climate space" of the species. By sampling throughout climate space at the continental scale, I account for a large percentage of variability in growing environments for Douglas-fir. Data are summarized across six regions – Pacific Northwest, Northern Rockies, Central Rockies, Southern Rockies, California, and Southwest. Tree growth data were combined with data from the Variable Infiltration Capacity Hydrologic Model, which includes typical climate variables as well as "plant relevant" variables. Climate data include precipitation, temperature, potential evapotranspiration, actual evapotranspiration, and vapor pressure deficit. Climatic water deficit was calculated as actual evapotranspiration minus potential evapotranspiration. The relationship between tree growth and climate was analyzed at four spatial scales (plot, watershed, region, and continent) and three temporal scales (monthly, interannual, interdecadal).

Results suggest that variability in growth is tightly coupled to both interannual and decadal climatic variability, with evident linkages to the El Niño Southern Oscillation (ENSO) and Pacific Decadal Oscillation (PDO). Temperature exerts a top-down control on tree growth, regardless of the magnitude of precipitation. As air temperature increases, evaporative demand also increases, causing increased vapor pressure deficit and climatic water deficit (potential evapotranspiration minus actual evapotranspiration), altering the dynamics of water availability in forest ecosystems. Additional analyses focus on how large-scale climate teleconnections modify regional climate patterns that ultimately limit tree growth. Proximity to the dipole dictates the relative effect of ENSO events from region to region, and the strength and location of the dipole change when ENSO and PDO are in phase. ENSO- and PDO-related changes in regional climate result in increased variability and extremes in tree growth. Changes in tree growth occur in phase with ENSO across all regions, but the strongest response is at the extreme ends of the dipole. The complex relationship between tree growth and climate documented in this study can provide parameters for growth models, inform climate-change adaptation plans, and project future growth in Douglas-fir forests.

Table of Contents

List of Figures

significant: Southwest (SW, $\beta = -2.985$, $p < 0.001$), California (CA, $\beta = -1.084$, $p < 0.001$), Southern Rockies (SR, $\beta = -2.295$, $p < 0.001$), Central Rockies ($\beta = -0.8704$, $p = 0.023$), Northern Rockies ($\beta = -2.068$, $p < 0.001$), Pacific Northwest ($\beta = -0.994$, $p = 0.002$).

Figure S1. Distribution of sampling sites in climate space. The climatic limits of Douglas-fir (as defined by Thompson et al. 2000) are represented as 10^{th} and 90^{th} (dotted line) and 50^{th} percentiles (dashed line). The hatched box symbolizes the fundamental climate niche of Douglas-fir. Sampling sites are plotted in this climate space based on average values (1916-2006) of the variables indicated. The distribution of sample sites represents the realized climate niche of Douglas-fir

Figure S2. Climatic water deficit **(A)** and vapor pressure deficit **(B)** anomalies. Fitted lines are loess smoothed curves with a 13-year segment length. Interannual variability is lowest in the Pacific Northwest and increases towards the Southwest. Recent increases are most evident in the more southerly regions.

Figure S3. Temperature alone decreases tree growth only in the southern latitude regions. Solid lines represent linear regression models with 95% confidence intervals (shaded colors). Only southern latitude slopes are significant: Southwest (SW, $\beta = -0.147$, $p < 0.001$), California (CA, $\beta = -0.043$, $p = 0.032$), Southern Rockies (SR, $\beta = -0.087$, $p < 0.001$), Central Rockies ($\beta = 0.015$, $p = 0.403$), Northern Rockies ($\beta = -0.024$, $p = 0.302$), Pacific Northwest ($\beta = -0.024$, $p = 0.116$).

Figure 3.1. Distribution of study locations in the western United States. Grey depicts the distribution of Douglas-fir, and triangles indicate the location of plots in each location.

Figure 3.2. Precipitation anomalies depicting the El Niño dipole as illustrated in Wise (2010). Positive and negative values indicate low and high precipitation, respectively. When the El Niño Southern Oscillation and Pacific Decadal Oscillation are in phase the position of the dipole shifts and becomes stronger.

Figure 3.3. El Niño (red triangles) and La Niña (blue triangles) events overlaid on precipitation anomalies. Regions are denoted in the upper left. PNW = Pacific Northwest, NR = Northern Rockies, CR = Central Rockies, SR = Southern Rockies, CA = California, SW = Southwest. Phases of the Pacific Decadal Oscillation are represented in light red (warm) and blue (cool). El Niño event years bring opposite effects with below and above average precipitation in the PNW and SW, respectively. The effect of event years is also seen in CA and NR but is much weaker in the CR and SR, which can be explained by the location of these sites in the transitional zone of the ENSO dipole.

Figure 3.4. El Niño (red triangles) and La Niña (blue triangles) events overlaid on maximum temperature anomalies. Regions are denoted in the upper left. PNW = Pacific Northwest, NR = Northern Rockies, CR = Central Rockies, SR = Southern Rockies, CA = California, SW = Southwest Phases of the Pacific Decadal Oscillation are represented in light red (warm) and blue (cool). In the more northerly latitudes, El Niño years have consistently higher temperatures. The signal is more mixed in centrally located sites. In the SW, El Niño events have historically

brought lower temperatures but in the most recent decades warmer temperatures are coinciding with these events. Temperature anomalies are higher during the warm phases of the PDO. Both high and low peaks in temperature do occur during ENSO event years across all regions.

Figure 3.5. El Niño (red) and La Niña (blue) events overlaid on the first principal component of regional tree-ring time series. Percent variability explained by the principal component is indicated on the bottom right. Extremes in growth are not always linked to ENSO events, but some synchrony can be seen in the PNW, SW, NR and CA. The highest variability is observed in the SW and SR, whereas the lowest variability is in CA and the PNW. Length of times series vary based on common time periods of chronologies used in the PCA. PNW = Pacific Northwest, NR = Northern Rockies, CR = Central Rockies, SR = Southern Rockies, CA = California, SW = Southwest.

Figure 3.6. Pearson's product-moment correlations between the Oct-Mar "Best" Index and tree-ring indices for all study sites. Correlations are weak (≤ 0.30) for all sites, although values >0.16 or <-0.16 are significant at $\alpha = 0.05$. The strongest correlations are found in the Southwest, eastern Oregon and the California coast. Weak correlations with the ENSO index are consistent with findings in St. George (2014). See Appendix 3.1 for coefficients and significance level.

Figure 3.7. First principal component (PC1) of each regional time series overlaid on different phases of the Pacific Decadal Oscillation (PDO). Warm phases are denoted in red and cool phases in blue. All times series are smoothed with a 10-year smoothing spline**.** Regions vary in the growth response to PDO and there is little commonality among regions in the interdecadal signal. PC1 for each region appears to respond to PDO either positively (Pacific Northwest, Central Rockies, and California) or negatively (Northern Rockies, Southern Rockies, and Southwest).

Figure 3.8. Results of cross-wavelet analysis of tree growth and El Niño Southern Oscillation displayed in Plots of the bias-corrected power normalized by the variance for all regions. Wavelet-coherence is evident in all regions, ranging between low frequency and high frequency throughout the time series. Wavelet-coherence has increased in recent decades (coinciding with the latest warm-phase PDO), and is occurring at smaller periods for all regions except the Southern Rockies. Portions of the time series within the cone of influence should not be interpreted, because edge effects result in inaccurate wavelet transformations.

List of Tables

Chapter 1

A multi-scale approach to understanding climate sensitivity in *Psuedotsuga menziesii* (Douglas-fir): rationale and methods

1. BACKGROUND

Mechanistic understanding of the effects of climatic variability on forest ecosystems has increased as studies have corroborated the explicit relationships among forest productivity, tree mortality, and climate-induced stress (Breshears et al. 2009, Allen et al. 2010, Littell et al. 2010, Niinemets 2010, Chmura et al. 2011, Williams et al. 2013). Current climate models project that mean global surface temperatures will likely exceed 1.5° C by 2100, whereas precipitation projections are still uncertain (IPCC 2013). The short- and long-term consequences of these climate projections on forest productivity are still being explored, and models are commonly used to simplify some of the more complex relationships inherent in forest systems (Neilson 1995, Iverson and Prasad 2001, Constable and Friend 2000, Bachelet et al. 2001, Crookston et al. 2010, Coops and Waring 2011). The results from these models are only as reliable as the data used for inputs and parameterization (Loehle and Leblanc 1996). Consequently, fine-scale empirical data are needed to both populate models and increase our understanding of the relationship between trees and their growth environments.

Forest responses to climate can be identified by characterizing individual tree response to different growth environments, and this response is termed the *climate-growth relationship*. Growth environments can be considered water-limited, in which the strongest limiting factors are related to water availability (e.g., precipitation, snow water equivalent), or energy-limited, in which the strongest limiting factors are related to energy (e.g., temperature, growing degree days, or light), but these limitations are always interacting (Stephenson 1998, Peterson 1998, Albright

and Peterson 2013). Trees express changes in growth that relate to these different growth environments via radial growth increment. Therefore, changes in radial growth serve as a primary metric for quantifying relative changes in overall tree growth in relation to climatic variability (Fritts 1974).

Water availability circumstantially accounts for a large amount of radial growth variation in trees. Water is directly linked to cell division and enlargement, but is also critical for photosynthensis and ecosystem productivity (Fritts 1976, Jassal et al. 2009, Ahuja et al. 2010, Krishnan et al. 2008). Water stress reduces stomatal conductance in Douglas-fir (*Psuedotsuga menziesii* (Mirb.) Franco) trees (Warren et al. 2004), allowing less carbon dioxide into the intercellular space and the chloroplast (i.e. the site of photosynthesis; Law et al. 2001, Irvine et al. 2002). Without sufficient carbon dioxide, plants are unable to fix enough carbon to maintain respiration costs, resulting in carbon starvation or hydraulic failure (McDowell et al. 2008, McDowell et al. 2010). In addition, when Douglas-fir is stressed by low water availability, Rubisco (catalyst for photosynthesis) loses its sensitivity for carbon dioxide reception, and consequently more electrons are used for photorespiration (Warren et al. 2004). This process decreases overall carbon assimilation, which decreases wood production (Bower et al. 2005). Low annual growth increment has been correlated with high soil moisture deficits and drought (Fritts 1974, Bower et al. 2005, Littell et al. 2008, Kardol et al. 2010). Water is a primary limiting factor to tree growth, but the interaction of water and temperature can sometimes be even more important.

Temperature can affect tree growth by exacerbating water stress, directly imposing limitations to growth, or affecting the length of the growing season. In the summer months, high temperatures often coincide with low precipitation, resulting in low soil moisture (McCabe and

Wolock 2002). Trees also respond to higher temperatures in spring, which control length of the growing season and phenology (Walther et al. 2002, Badeck et al. 2004, Parmesan 2006) and can increase photosynthesis by causing earlier leaf emergence in trees (Rollinson and Kaye 2012). By increasing surface leaf area, trees will be more productive in the most critical time of the growing season; a majority of annual carbon uptake occurs in the spring, varying by species and location (Krishnan et al. 2008). This phenomenon is evidenced by significant correlations between radial growth and spring temperature (Graumlich and Brubaker 1986, Peterson and Peterson 2001, Peterson et al. 2002, Fagre et al. 2003).

Spatial patterns of tree growth differ as a result of large-scale topographic climate forcing, but finer-scale topographic complexity also influences tree growth. To a large degree, elevation mediates the expression of climate on the landscape through adiabatic lapse rate and cold air drainage (Clements et al. 2003, Sheridan et al. 2010). At high elevation, growing environments are affected by snowpack and cold temperatures (Wang and Schimel 2003, Fritts 1976); snow reflects more solar radiation and reduces energy absorption on the site (Wiscombe and Warren 1980). Air density decreases with altitude, resulting in less scattering and absorption of direct solar radiation by the atmosphere, so plants are subjected to higher radiation loads and higher daytime temperatures during cloudless days (Fritts 1976, Lambers et al. 2008). Because spatial dissimilarities in climate affect tree growth, elevation is a potential proxy for climate (McKenzie et al. 2003, Lo et al. 2010). Aspect controls the amount of incident radiation on a site and soil moisture retention (Chen and Kumar 2001, Yard et al. 2005). It is critical to consider this topographic complexity because different temperature regimes are part of different growth environments across complex terrain.

Douglas-fir is one of the most widespread species in North America, occupying growing environments in complex terrain throughout the dominant mountain ranges of the western United States (Figure 1.1). Empirically based studies that have quantified climate-growth interactions in Douglas-fir (Watson and Luckman 2002, Case and Peterson 2005, Littell et al. 2008, Chen et al. 2010, Griesbauer and Green 2010a, Griesbauer and Green 2010b) agree that low precipitation and high temperature are correlated with low tree growth, but that the spatial and temporal context of climate variables can influence growth patterns in different ways across the species range. Tree growth in a given year is affected by climate in the growing season and in the previous-year growing season (Nakawatase and Peterson 2006, Case and Peterson 2005, Littell et al. 2008). In the North Cascade Range (Washington, USA), Douglas-fir growth is correlated with growing season temperature and precipitation, but is also correlated with previous year precipitation (Case and Peterson 2005, Littell et al. 2008). In the Olympic Mountains (Washington, USA), Douglas-fir on the west slopes is sensitive to summer precipitation and temperature in the growing year, and to April and November temperatures from the previous year (Nakawatase and Peterson 2006, Littell et al. 2008). Climate-growth interactions are also expressed differently in different spatial contexts (e.g., elevation and aspect).

Physiography affects how thermal stress is manifest across a given landscape. On the east side, but not the west side, of the Olympic Mountains, growth is limited by winter temperatures (Brubaker 1980, Littell et al. 2008). Growth-climate interactions also vary with elevation because the limiting factor changes from water at lower elevations to energy (i.e., temperature) at higher elevations (Stephenson 1990). For example, in the North Cascade Range, growing season and previous year temperatures are correlated with growth in high elevation stands, whereas precipitation is correlated with growth in low and mid elevation stands (Littell et

al. 2008). These results suggest that the growth of Douglas-fir is limited by different climate at relatively fine scales.

The spatial and temporal variability of Douglas-fir to climate is critical to a comprehensive assessment of the species. Most studies focused on Douglas-fir climate-growth interactions have been conducted in the Pacific Northwest (PNW) and northern portions of its range, whereas few studies have examined these relationships in the southernmost reaches of its range. In the southern Rocky Mountains and Colorado Plateau, climate is distinct enough from the PNW that climate limitations to growth may differ from the relationships derived from studies conducted in the PNW. Insights on climate-growth interactions can be gained from the Sierra Madre (Mexico), the southernmost location of Douglas-fir (Gonzalez-Elizondo et al. 2005, Reich et al. 2008), where Gonzalez-Elizondo et al. found that maximum temperature in winter months is negatively correlated with growth, because of high soil water evaporation in the growing season. Winter precipitation has a stronger and positive correlation with growth in this region (which is opposite of findings from the PNW), with November of the previous year to March of the growing year being most strongly correlated with precipitation. Although a majority of precipitation falls in the summer, the temperatures likely are too hot to offset evaporative demand. This growing environment will be particularly vulnerable to climate change, because the sites will experience higher evaporation as winter temperatures increase (i.e., this region will become more water-limited). Warmer growing seasons are beneficial in the northern distribution of Douglas-fir, but higher temperature may limit growth in the southern portion of its distribution.

Douglas-fir growth is sensitive to changes in climate, but the relationships are complex, involving feedbacks when more than one variable changes in magnitude and direction.

Temperature sensitivity is an example: increases in spring temperatures are beneficial for Douglas-fir growth, but the subsequent increase in summer temperatures could be detrimental. The magnitude and timing of the temperature increase is therefore critical. Douglas-fir clearly responds to these conditions, evidenced by changes in wood density and width, or dendroplasticity (i.e., phenotypic plasticity in radial growth; Martinez-Maier et al. 2009). Higher latewood-to-earlywood ratio is also a response to favorable early season growing conditions and stress during dry summers (Martinez-Meier et al. 2008). However, the point at which conditions are so unfavorable that short-term adaptation is no longer a possibility is unknown.

To better understand the effects of future climate on Douglas-fir, it is necessary to quantify climate-growth relationships across the entire species distribution and the climate space it occupies. The range of Douglas-fir extends from British Columbia to Mexico, and experiences mediterranean (Sierra Nevada), maritime (Olympic Mountains, Coast Range), transitional (North Cascades), continental (Rocky Mountains), and monsoonal (Colorado Plateau) climate; nested within each climate domain, Douglas-fir occurs at different elevations and aspects in distinctly separate mountain ranges. Two hypotheses can potentially explain Douglas-fir growth across its range: (1) the species has distinct growth responses to climate constrained by elevation, aspect, and geographic location or (2) the species growth response is synchronized regardless of geography (i.e., top-down driver is climate). It has been difficult to address these hypotheses in the absence of a dataset that covers the entire species range. Investigating these two hypotheses requires a multi-scale approach, with an assessment of climate-growth relationships from stand to continent.

Identifying the specific climate variables that limit tree growth and the spatial and temporal scales at which these processes operate can inform predictions of how forests will

respond to climate change. Models that predict forest growth lack annual resolution growth data, and specifically data regarding climate-growth relationships. There is a clear need to provide comprehensive datasets that address climate sensitivity in forests at large spatial and long temporal scales.

I studied Douglas-fir across its geographic distribution in the United States to determine how climate limits Douglas-fir growth. My study uses a geographically and climatically stratified sampling approach that spans the western mountain complex of the United States. I ask if climate limits growth differentially throughout the various regions of the western United States, and if inferences about these limitations differ depending on the scale of analysis. In the methods presented below, I outline the specifics of my sampling strategy, study domain, analysis of climate space, and chronology development. More complex analyses are reported in subsequent chapters.

2. SAMPLING STRATEGY AND DATA PREPARATION

2.1 Study Domain

I used a sampling approach that focused on both the climate space and geographic extent of Douglas-fir. To facilitate a multi-scale analysis, I sampled at four spatial scales: tree, plot, watershed, and region (Figure 1.2).

Species range was divided into regions that served as "climate domains," based on an analysis of historical climate data calculated by the Variable Infiltration Capacity hydrologic model (VIC; Liang et al. 1994, Njissen et al. 1997) and summarized to the USGS HUC 4 level. The HUC 4 level is a second-level, subregion watershed. The climate data were aggregated at this level to match the scale of climate domain delineations. After summarizing the data in terms

of magnitude and timing of precipitation, I divided the Douglas-fir distribution into six regions: Pacific Northwest, California, Northern Rockies, Central Rockies, Southern Rockies, and Southwest. The climate domain delineation was verified by Bailey's ecoprovince divisions used nationwide (Bailey 2004; Figure 1.3), therefore these regions are likely representative of climatically distinct zones of the Douglas-fir range. In each region, I selected watersheds and placed plots (within each watershed) on opposing aspects at different elevations to account for topographic complexity. Plots were chosen based on field reconnaissance conducted in 2010.

2.2 Tree-core collections

In each plot, I sampled 15 trees (with few exceptions) in either dominant or codominant canopy positions, with no signs of pathogens, insects, or injuries. All trees were a minimum of 125 years-old at breast height; this age cut-off was employed to allow the exclusion of juvenile growth in the time series. I extracted one core from the side-slope of each tree, measured diameter at breast height, and geo-referenced each plot with a handheld Global Positioning System device.

The tree-core data are combined with data from Littell et al. (2008) to create a robust dataset that covers the entire geographic range of Douglas-fir in the United States. To match the sampling density of my plots in geographic space, I subsampled watersheds in each of their study sites, retaining two watersheds from each sample site and all plots in the chosen watersheds. Instead of a random sample of watersheds, I chose an informed sampling approach because my sampling strategy was designed to control for non-climatic factors (i.e., elevation, aspect) that may mediate the tree response to climate. I calculated growing season (April-September) water deficit (PET-AET) for each watershed (climate data below), and then graphically compared these

curves to other watersheds in the site. This approach allowed me to choose watersheds based on a range of deficit to surplus in growing season months, resulting in paired watersheds of wet vs. dry and/or warm vs. cool. Watersheds where deficit values differed only slightly were evaluated based on age of trees and temporal resolution.

2.3 Climate Data

I used historical climate data generated by the VIC model (Liang et al. 1994, Njissen et al. 1997), which is developed by the University of Washington Climate Impacts Group. The historical data are derived from a combination of Historical Climate Network observations and weather stations. These are daily resolution data, differing from PRISM data (Daly et al. 2008) which are monthly. The finer temporal resolution of the VIC data allows for the calculation of evapotranspiration and vapor pressure deficit, which are considered "plant-relevant" variables (Stephenson 1998, Albright and Peterson 2013). VIC data is calculated at 1/16 degree (6 km^2) resolution, and is interpolated to individual coordinates using adjustments based on elevation. Data available encompass a 91-year period (1916-2006).

Climate variables used in this study are monthly precipitation (mm), monthly maximum temperature (C), monthly minimum temperature (C), monthly average temperature (C), vapor pressure deficit (kPa), potential evapotranspiration (PET; mm), and actual evapotranspiration (AET; mm), and deficit (PET – AET). Climate anomalies were calculated for each climate variable by subtracting yearly values from the total time series mean. Anomalies were used to visualize departures in average climate during the period of analysis.

2.4 Climate space graphs

The distribution of sampled sites in climate space was visualized by plotting the geographic locations of plots based on their respective climate. I used climate parameters described in Thompson et al (2000), as these specific values define the climatic limits of Douglas-fir distribution. Climate variables are January temperature (C), July temperature (C) and annual precipitation (mm), all of which are derived from VIC model output. Climate space was also visualized using the plant-relevant variables growing season evapotranspiration (AET; mm) and growing season deficit (DEF; mm).

2.5 Chronology Development

I employed standard dendrochronological techniques to measure, detrend, standardize and "prewhiten" each tree-ring time series (Stokes and Smiley 1968, Fritts 1976, Cook and Kairiukstis 1989). All of the cores were measured using a Velmex sliding stage (precision = 0.001 mm), and crosschecked for errors using COFECHA (Holmes 1999). To account for the geometric bias of ring width imposed by age/size (e.g. larger trees put on narrow rings), I detrended the time series with a cubic smoothing spline for which the frequency response was 0.50 (retained 50% of the variance) at a wavelength equal to 2/3 the length of the series. The cubic smoothing spline is appropriate for a dataset with such a large geographic extent because the curve fit to each series is unique, taking into consideration different ages, competition, and stand disturbance histories. Detrended time series were then subtracted from the fitted spline to create a ring width index (RWI), a unit-less metric used as a proxy for annual ring-width. Finally, prewhitened or residual chronologies were calculated to remove the temporal

autocorrelation in each time series by performing autoregressive modeling, with the autoregressive order based on the persistence identified in each time series. The residual chronologies are preferred over raw chronologies for analysis because after detrending, standardization, and prewhitening the remaining inter-annual variance can be attributed to climate. For both the standardized and residual chronologies, years were retained only if sampling depth was at least 5 cores.

I developed chronologies at three spatial scales: plot, watershed and region (delinated from climate domain analysis). All cores from each plot were retained in chronology development. Plot-scale chronologies were calculated by aggregating tree-scale chronologies with a Tukey's bi-weight robust mean. For the watershed scale, the chronologies were recalculated starting from the individual tree, and followed the same methods used for the plot scale chronologies for detrending, standardization, and prewhitening. Regional-scale chronologies were calculated as a mean of the watershed-scale chronologies in a given region. To aid in visual interpretations, regional-scale chronologies were also calculated as z-scores which scale all data to a mean of 0 and standard deviation of 1.

Descriptive statistics were calculated for all chronologies (at both plot and watershed scales) using the dplR package (Bunn 2008) in the R Statistical Computing Environment. Statistics include series length, r bar, mean sensitivity, first-order autocorrelation, and expressed population signal. We tested the chronologies for suitability in parametric analyses using quantile-quantile plots (Appendix A).

3. VISUALIZATIONS AND DESCRIPTIVE STATISTICS

3.1 Capturing the climate space

Sample sites were distributed throughout 24 watersheds and 123 plots (Figure 1.4, Table 1). To assess if the breadth of climatic variability experienced by Douglas-fir were captured, I visualized the distribution of our plots in climate niche (Figure 1.5), following Littell et al. 2008. The hatched box in all panels of Figure 1.4 represents the fundamental climate "niche" of Douglas-fir, as defined by the space bound by the 10^{th} and 90^{th} percentiles (dotted lines) of suitable climate for Douglas-fir growth.

When comparing extremes in temperature (Figure 1.4 A), I am missing only the portions of the climate niche where July temperatures are very high and January temperatures are very low. Those growing environments may not actually exist for Douglas-fir. The few sites that fall outside of the climate niche are located in California where anomalously high temperatures in January and July exist.

The plots covered the climate niche sufficiently when plotted as a function of annual precipitation and July temperature (Figure 1.4 B). The anomalously high annual precipitation in the Pacific Northwest placed those sites in the 10^{th} percentile for climate generally experienced by the species. There are also sites in California that are found outside of the climate niche with regard to extreme July temperature.

The magnitude of precipitation in both January and July varies widely among regions, as evidenced by Figure 1.4 C. Again, sites in California and the Pacific Northwest experience anomalous climate, with low July precipitation in the former and high January precipitation in

the latter. Most of the other sites are grouped around moderate July precipitation and very low January precipitation.

To encompass plant-relevant variables in my climate-space visualization, I plotted growing season AET versus DEF as a way to understand productivity in terms of water stress (Figure 1.4 D). The distribution of points across this space demonstrates that trees growing in a broad range of water stress conditions were sampled.

3.2 Chronology summaries

Watershed-scale chronology characteristics and descriptive statistics are summarized in Table 2, and statistics for individual trees and plots are summarized in Appendix B. I sampled a total of 1,608 trees, with a minimum of 29, maximum of 92, and mean of 62 in a given watershed. The average length of series was 208 years, and the average ring width was 1.36 ± 0.43. First-order autocorrelation values range from 0.49 to 0.88, justifying the need for autoregressive modeling to remove the persistence in the time series. Expressed population signal ranges from 0. 88 to 0.99, confirming that I sampled enough trees per plot to obtain the climate signal from trees. Mean sensitivity was not reported, because the recent findings of Bunn et al. (2013) suggest that the statistic is misleading and does not provide useful information about the properties of a tree-ring time series.

4. SUMMARY

In this chapter, I summarize the rationale, sampling design, chronology development and descriptive statistics of the tree-ring data. The multi-scale sampling strategy facilitated the development of stand, watershed, and regional chronologies, which will be used in analyses presented in subsequent chapters. Descriptive statistics confirm that these data are temporally robust (> 125 years) and are sensitive enough to ascertain a climate signal (EPS > 0.9). Exploratory tests for normality verify that these data are appropriate for the parametric statistics used in the following chapters, including Pearson's product-moment correlations, ordinary least squares regression, and principal components analysis.

5. REFERENCES

Ahuja, I., R. C. H. de Vos, A. M. Bones, and R. D. Hall. 2010. Plant molecular stress responses in the face of climate change. Trends in Plant Science **15**: 664-674.

Albright, W. L., and D. L. Peterson. 2013. Tree growth and climate in the Pacific Northwest, North America: a broad-scale analysis of changing growth environments. Journal of Biogeography **40**: 2119-2133.

Allen, C. D., A. K. Macalady, H. Chenchouni, D. Bachelet, N. McDowell, M. Vennetier, T. Kitzberger, A. Rigling, D. D. Breshears, E. H. Hogg, P. Gonzalez, R. Fensham, Z. Zhang, J. Castro, N. Demidova, J. H. Lim, G. Allard, S. W. Running, A. Semerci, and N. Cobb. 2010. A global overview of drought and heat-induced tree mortality reveals emerging climate change risks for forests. Forest Ecology and Management **259**: 660-684.

Bachelet, D., R. P. Neilson, J. M. Lenihan, and R. J. Drapek. 2001. Climate change effects on vegetation distribution and carbon budget in the United States. Ecosystems **4**: 164-185.

Badeck, F. W., A. Bondeau, K. Bottcher, D. Doktor, W. Lucht, J. Schaber, and S. Sitch. 2004. Responses of spring phenology to climate change. New Phytologist **162**: 295-309.

Bailey, R. G. Identifying ecoregion boundaries. 2004. Environmental Management **34**: S14-S26.

Bower, A.D., W.T. Adams, D. Birkes, and D. Nalle. 2005. Response of annual growth ring components to soil moisture deficit in young, plantation-grown Douglas-fir in coastal British Columbia. Canadian Journal of Forest Ecology **35**: 2491-2499.

Breshears, D. D., O. B. Myers, C. W. Meyer, F. J. Barnes, C. B. Zou, C. D. Allen, N. G. McDowell, and W. T. Pockman. 2009. Tree die-off in response to global change-type drought: mortality insights from a decade of plant water potential measurements. Frontiers in Ecology and the Environment **7**: 185-189.

Brubaker, L. B. 1980. Spatial patterns of tree growth anomalies in the Pacific Northwest. Ecology **61**: 798-807.

Bunn, A. G. 2008. A dendrochronology program library in R (dplR). Dendrochronologia **28**: 115-124.

Bunn, A. G., E. Jansma, M. Korpela, R. D. Westfall, and J. Baldwin. 2013. Using simulations and data to evaluate mean sensitivity (< i> ζ</i>) as a useful statistic in dendrochronology. Dendrochronologia **31**: 250-254.

Case, M. J., and D. L. Peterson. 2005. Fine-scale variability in growth-climate relationships of Douglas-fir, North Cascade Range, Washington. Canadian Journal of Forest Research **35**: 2743-2755.

Chen, J., and P. Kumar. 2001. Topographic influence on the seasonal and interannual variation of water and energy balance of basins in North America. Journal of Climate **14**: 1989-2014.

Chen, P. Y., C. Welsh, and A. Hamann. 2010. Geographic variation in growth response of Douglas-fir to interannual climate variability and projected climate change. Global Change Biology **16**: 3374-3385.

Chmura, D. J., P. D. Anderson, G. T. Howe, C. A. Harrington, J. E. Halofsky, D. L. Peterson, D. C. Shaw, and J. B. St Clair. 2011. Forest responses to climate change in the northwestern United States: Ecophysiological foundations for adaptive management. Forest Ecology and Management **261**: 1121-1142.

Constable, J. V. H., and A. L. Friend. 2000. Suitability of process-based tree growth models for addressing tree response to climate change. Environmental Pollution **110**: 47-59.

Cook, E. R., and L. A. Kairiukstis (Ed.) 1990. Methods of dendrochronology: Applications in the Environmental Sciences. Kluver Academic Publishers, The Netherlands.

Coops, N. C., and R. H. Waring. 2011. A process-based approach to estimate lodgepole pine (*Pinus contorta* Dougl.) distribution in the Pacific Northwest under climate change. Climatic Change **105**: 313-328.

Clements C. B., C. D. Whiteman, and J. D. Horel. 2003. Cold-air-pool structure and evolution in a mountain basin: Peter sinks. Utah Journal of Applied Meteorology **42**: 752-768.

Crookston, N. L., G. E. Rehfeldt, G. E. Dixon, and A. R. Weiskittel. 2010. Addressing climate change in the forest vegetation simulator to assess impacts on landscape forest dynamics. Forest Ecology and Management **260**: 1198-1211.

Daly, C., M. Halbleib, J. I. Smith, W. P. Gibson, M. K. Doggett, G. H. Taylor, J. Curtis, and P. P. Pasteris. 2008. Physiographically sensitive mapping of climatological temperature and

precipitation across the conterminous United States. International Journal of Climatology **28**: 2031-2064.

Fagre, D. B., D. L. Peterson, and A. E. Hessl. 2003. Taking the pulse of mountains: Ecosystem responses to climatic variability. Climatic Change **59**: 263-282.

Fritts, H. C. 1974. Relationships of ring widths in arid-site conifers to variations in monthly temperature and precipitation. Ecological Monographs **44**: 411-440.

Fritts, H. C. 1976. Tree rings and climate. Academic Press, New York.

Gonzalez-Elizondo, M., E. Jurado, J. Navar, M. S. Gonzalez-Elizondo, J. Villanueva, O. Aguirre, and J. Jimenez. 2005. Tree-rings and climate relationships for Douglas-fir chronologies from the Sierra Madre Occidental, Mexico: A 1681-2001 rain reconstruction. Forest Ecology and Management **213**: 39-53.

Graumlich, L. J., and L. B. Brubaker. 1986. Reconstruction of annual temperature (1590-1979) for Longmire, Washington, derived from tree rings. Quaternary Research **25**: 223-234.

Griesbauer, H. P., and D. S. Green. 2010a. Assessing the climatic sensitivity of Douglas-fir at its northern range margins in British Columbia, Canada. Trees, Structure and Function **24**: 375-389.

Griesbauer, H. P., and D. S. Green. 2010b. Regional and ecological patterns in interior Douglas-fir climate-growth relationships in British Columbia, Canada. Canadian Journal of Forest Research **40**: 308-321.

Holmes, R. L. 1999. User's manual for program COFECHA. University of Arizona Press, Tucson, AZ.

Irvine, J., B. E. Law, P. M. Anthoni, and F. C. Meinzer. 2002. Water limitations to carbon exchange in old-growth and young ponderosa pine stands. Tree Physiology **22**: 189-196.

Iverson, L. R., and A. M. Prasad. 2001. Potential changes in tree species richness and forest community types following climate change. Ecosystems **4**: 186-199.

Intergovernmental Panel on Climate Change (IPCC). 2013. Summary for Policymakers. In: Climate Change 2013: The Physical Science Basis. Contribution of Working Group I to the Fifth Assessment Report of the Intergovernmental Panel on Climate Change [Stocker, T.F., D. Qin, G.-K. Plattner, M. Tignor, S.K. Allen, J. Boschung, A. Nauels, Y. Xia, V.

Bex and P.M. Midgley (eds.)]. Cambridge University Press, Cambridge, United Kingdom and New York, NY, USA.

Jassal, R. S., T. A. Black, D. L. Spittlehouse, C. Brummer, and Z. Nesic. 2009. Evapotranspiration and water use efficiency in different-aged Pacific Northwest Douglas-fir stands. Agricultural and Forest Meteorology **149**: 1168-1178.

Kardol, P., D. E. Todd, P. J. Hanson, and P. J. Mulholland. 2010. Long-term successional forest dynamics: species and community responses to climatic variability. Journal of Vegetation Science **21**: 627-642.

Krishnan, P., T.A. Black, R.S. Jassal, B. Chen, and Z. Nesic. 2008. Interannual variability of the carbon balance of three different-aged Douglas-fir stands in the Pacific Northwest. Journal of Geophysical Research **114**: 1-18.

Lambers, H., F. S. Chapin, and T. L. Pons. 2008. Plant physiological ecology. Springer Science and Business Media, New York.

Law, B. E., A. H. Goldstein, P. M. Anthoni, M. H. Unsworth, J. A. Panek, M. R. Bauer, J. M. Fracheboud, and N. Hultman. 2001. Carbon dioxide and water vapor exchange by young and old ponderosa pine ecosystems during a dry summer. Tree Physiology **21**: 299-308.

Liang, X., D. P. Lettenmaier, E. F. Wood, and S. J. Burges. 1994. A simple hydrologically based model of land surface water and energy fluxes for general circulation models. Journal of Geophysical Research **99**: 14415-14428.

Littell, J. S., D. L. Peterson, and M. Tjoelker. 2008. Douglas-fir growth in mountain ecosystems: water limits tree growth from stand to region. Ecological Monographs **78**: 349-368.

Littell, J. S., E. E. Oneil, D. McKenzie, J. A. Hicke, J. A. Lutz, R. A. Norheim, and M. M. Elsner. 2010. Forest ecosystems, disturbance, and climatic change in Washington State, USA. Climatic Change **102**: 129-158.

Little, E. L., Jr. 1971. Atlas of United States trees, volume 1, conifers and important hardwoods: U.S. Department of Agriculture Miscellaneous Publication 1146, 9 p., 200 maps.

Lo, Y. H., J. A. Blanco, B. Seely, C. Welham, and J. P. Kimmins. 2010. Relationships between climate and tree radial growth in interior British Columbia, Canada. Forest Ecology and Management **259**: 932-942.

Loehle, C., and D. LeBlanc. 1996. Model-based assessments of climate change effects on forests: A critical review. Ecological Modelling **90**: 1-31.

Martinez-Meier, A., L. Sanchez, M. Pastorino, L. Gallo, and P. Rozenberg. 2008. What is hot in tree rings? The wood density of surviving Douglas-firs to the 2003 drought and heat wave. Forest Ecology and Management **256**: 837-843.

Martinez-Meier, A., L. Sanchez, G. Dalla-Salda, L. Gallo, M. Pastorino, and P. Rozenberg. 2009. Ring density record of phenotypic plasticity and adaptation to drought in Douglas-fir. Forest ecology and management **258**: 860-867.

McCabe, G.J., and D.M. Wolock. 2002. Trends and temperature sensitivity of moisture conditions in the coterminous United States. Climate Research 20: 19-29.

McDowell, N., W. T. Pockman, C. D. Allen, D. D. Breshears, N. Cobb, T. Kolb, J. Plaut, J. Sperry, A. West, D. G. Williams, and E. A. Yepez. 2008. Mechanisms of plant survival and mortality during drought: why do some plants survive while others succumb to drought? New Phytologist **178**: 719-739.

McDowell, N. G., and S. Sevanto. 2010. The mechanisms of carbon starvation: how, when, or does it even occur at all? New Phytologist **186**: 264-266.

McKenzie, D., D. W. Peterson, and D. L Peterson. 2003. Modeling conifer species distributions in mountain forests of the Pacific Northwest. Forestry Chronicle **79**: 253-258.

Nakawatase, J. M., and D. L. Peterson. 2006. Spatial variability in forest growth – climate relationships in the Olympic Mountains, Washington. Canadian Journal of Forest Research **36**: 77-91.

Neilson, R. P. 1995. A model for predicting continental-scale vegetation distribution and water-balance. Ecological Applications **5**: 362-385.

Niinemets, U. 2010. Responses of forest trees to single and multiple environmental stresses from seedlings to mature plants: Past stress history, stress interactions, tolerance and acclimation. Forest Ecology and Management **260**: 1623-1639.

Njissen B. N., D. P. Lettenmaier, X. Liang, S. W. Wetzel, and E. F. Wood. 1997. Streamflow simulation for continental-scale river basins. Water Resources Research **33**: 711-724.

Parmesan, C. 2006. Ecological and evolutionary responses to recent climate change. Annual Review of Ecology Evolution and Systematics **37**: 637-669.

Peterson, D. W., and D. L. Peterson. 1994. Effects of climate on radial growth of sub-alpine conifers in the north Cascade Mountains. Canadian Journal of Forest Research **24**: 1921-1932.

Peterson, D. L. 1998. Climate, limiting factors and environmental change in high-latitude forests of western North America. In Climatic Variability and Extremes: The Impact on Forests (ed. by Beniston, M and J. L. Innes) Springer-Verlag, Heidelberg, Germany.

Peterson, D. W., and D. L. Peterson. 2001. Mountain hemlock growth responds to climatic variability at annual and decadal time scales. Ecology **82**: 3330-3345.

Peterson, D. W., D. L. Peterson, and G. J. Ettl. 2002. Growth responses of subalpine fir to climatic variability in the Pacific Northwest. Canadian Journal of Forest Research **32**: 1503-1517.

Reich, R. M., C. Aguirre-Bravo, and V. A. Bravo. 2008. New approach for modeling climatic data with applications in modeling tree species distributions in the states of Jalisco and Colima, Mexico. Journal of Arid Environments **72**: 1343-1357.

Rollinson, C. R., and M. W. Kaye. 2012. Experimental warming alters spring phenology of certain plant functional groups in an early successional forest community. Global Change Biology **18**: 1108-1116.

Sheridan, P., S. Smith, A. Brown, and S. Vosper. 2010. A simple height-based correction for temperature downscaling in complex terrain. Meteorological Applications **17**: 329-339.

Speer, J. H. 2010. Fundamentals of tree-ring research. University of Arizona Press, Tucson, AZ.

Stephenson, N. L. 1990. Climatic control of vegetation distribution- the role of water balance. American Naturalist **135**: 649-670.

Stephenson, N. L. 1998. Actual evapotranspiration and deficit: biologically meaningful correlates of vegetation distribution across spatial scales. Journal of Biogeography **25**: 855-870.

Stokes, M. A., and T. L. Smiley. 1968. An introduction to tree-ring dating. University of Chicago Press, Chicago, Illinois, USA.

Thompson, R. S., K. H. Anderson, P. J. Bartlein. 2000. Atlas of relations between climatic parameters and distributions of important trees and shrubs in North America: introduction and conifers. USGS Prof. Paper 1650-A, Reston, VA.

Walther, G. R., E. Post, P. Convey, A. Menzel, C. Parmesan, T. J. C. Beebee, J. M. Fromentin, O. Hoegh-Guldberg, and F. Bairlein. 2002. Ecological responses to recent climate change. Nature **416**: 389-395.

Wang, G. L., and D. Schimel. 2003. Climate change, climate modes, and climate impacts. Annual Review of Environment and Resources **28**: 1-28.

Warren, C. R., N. J. Livingston, and D. H. Turpin. 2004. Water stress decreases the transfer conductance of Douglas-fir (Pseudotsuga menziesii) seedlings. Tree Physiology **24**: 971-979.

Watson, E., and B. H. Luckman. 2002. The dendroclimatic signal in Douglas-fir and ponderosa pine tree-ring chronologies from the southern Canadian Cordillera. Canadian Journal of Forest Research **32**: 1858-1874.

Williams, A. P., C. D. Allen, C. I. Millar, T. W. Swetnam, J. Michaelsen, C. J. Still, and S. W. Leavitt. 2010. Forest responses to increasing aridity and warmth in the southwestern United States. Proceedings of the National Academy of Sciences of the United States of America **107**: 21289-21294.

Williams, A. P., C. D. Allen, A.K. Macalady, D. Griffin, C.A. Woodhouse, D. M. Meko, T. W. Swetnam, S. A. Rauscher, R. Seager, H. D. Grissino-Mayer, J. S. Dean, E. R. Cook, C. Gangodagamage, M. Cai, and N. G. McDowell. 2013. Temperature as a potent driver of regional forest drought stress and tree mortality. Nature Climate Change **3**: 292-297.

Wiscombe, W. J., and S. G. Warren. 1980. A model for the spectral albedo of snow. I: Pure snow. Journal of Atmospheric Sciences **37**: 2712-2733.

Yard, M. D., G. E. Bennett, S. N. Mietz, L. G. Coggins, L. E. Stevens, S. Hueftle, and D. W. Blinn. 2005. Influence of topographic complexity on solar insolation estimates for the Colorado River, Grand Canyon, AZ. Ecological Modelling **183**: 157-172.

6. TABLES

Table 1.1. Locations and mean annual climate parameters for all study plots. PPT = precipitation, TMAX = maximum temperature, TMIN = minimum temperature.

State	Region	Site	Plot Name	Latitude	Longitude	Elevation (m)	Annual PPT (mm)	Annual TMAX (°C)	Annual TMIN (°C)
Oregon	PNW	HJ Andrews Experimental Forest	ORHJ-S1	44.24181	-122.12393	1450.1	2410.25	12.10	1.78
Oregon	PNW	HJ Andrews Experimental Forest	ORHJ-S2	44.23140	-122.12652	1096.0	2410.44	13.82	2.98
Oregon	PNW	HJ Andrews Experimental Forest	ORHJ-S3	44.23581	-122.12275	1196.4	2410.44	13.82	2.98
Oregon	PNW	HJ Andrews Experimental Forest	ORHJ-N1	44.22372	-122.14030	1267.4	2353.74	13.81	3.14
Oregon	PNW	HJ Andrews Experimental Forest	ORHJ-N2	44.22675	-122.14173	1115.9	2353.74	13.81	3.14
Oregon	PNW	HJ Andrews Experimental Forest	ORHJ-N3	44.23008	-122.14608	951.1	2190.88	14.75	3.77
Washington	PNW	North Cascades National Park	WACR-N3	48.92506	-121.39314	1241.4	1963.06	9.78	1.09
Washington	PNW	North Cascades National Park	WACR-N1	48.93036	-121.39132	865.2	1949.70	10.92	1.25
Washington	PNW	North Cascades National Park	WACR-N2	48.92697	-121.39209	1061.7	1963.06	9.78	1.09
Washington	PNW	North Cascades National Park	WACR-S3	48.95416	-121.41528	1298.7	2048.69	8.50	0.37
Washington	PNW	North Cascades National Park	WACR-S1	48.95202	-121.40216	797.4	1951.83	11.02	1.41
Washington	PNW	North Cascades National Park	WACR-S2	48.95372	-121.40663	1025.1	1955.75	10.05	1.35
Washington	PNW	Olympic National Park	WADR-N3	47.72999	-123.20496	1327.4	1761.34	10.14	2.13
Washington	PNW	Olympic National Park	WADR-N1	47.74224	-123.20587	579.1	1756.78	12.84	3.89
Washington	PNW	Olympic National Park	WADR-N2	47.73636	-123.20830	1025.1	1761.34	10.14	2.13
Washington	PNW	Olympic National Park	WADR-S3	47.76480	-123.20225	1458.0	2240.60	7.50	-0.38
Washington	PNW	Olympic National Park	WADR-S1	47.74785	-123.20651	680.8	1752.51	11.98	3.55
Washington	PNW	Olympic National Park	WADR-S2	47.75611	-123.20842	1080.3	2007.42	10.21	2.34
Washington	PNW	Olympic National Park	WAHR-N3	47.81682	-123.96458	835.9	3532.27	13.20	4.90
Washington	PNW	Olympic National Park	WAHR-N1	47.82462	-123.97487	237.5	3247.47	14.17	5.06
Washington	PNW	Olympic National Park	WAHR-N2	47.82127	-123.96544	550.3	3344.42	14.78	4.92
Washington	PNW	Olympic National Park	WAHR-S3	47.83745	-124.02712	786.3	3405.90	13.67	4.56
Washington	PNW	Olympic National Park	WAHR-S1	47.82154	-124.02217	190.6	3260.70	14.31	5.10
Washington	PNW	Olympic National Park	WAHR-S2	47.83448	-124.02305	583.2	3405.90	13.67	4.56
Washington	PNW	North Cascades National Park	WAST-N1	48.31158	-120.67930	411.2	930.70	13.82	2.08
Washington	PNW	North Cascades National Park	WAST-N3	48.30789	-120.68574	738.1	930.70	13.82	2.08

Washington	PNW	North Cascades National Park	WAST-N2	48.29505	-120.68946	1379.6	1016.92	8.87	0.04
Washington	PNW	North Cascades National Park	WAST-S3	48.31123	-120.60912	1691.0	1320.13	8.05	-1.29
Washington	PNW	North Cascades National Park	WAST-S1	48.31056	-120.65139	501.3	932.27	14.25	2.81
Washington	PNW	North Cascades National Park	WAST-S2	48.30848	-120.62460	1213.0	1211.93	10.35	1.35
Idaho	NR	Idaho Panhandle National Forest	IDBO-N3	48.97356	-116.60042	1417.4	799.77	9.65	0.38
Idaho	NR	Idaho Panhandle National Forest	IDBO-N1	48.98780	-116.60350	726.6	695.86	13.07	1.48
Idaho	NR	Idaho Panhandle National Forest	IDBO-N2	48.98166	-116.60179	1088.3	732.03	11.80	0.80
Idaho	NR	Idaho Panhandle National Forest	IDBO-S3	48.99818	-116.65075	1600.5	999.34	8.17	0.36
Idaho	NR	Idaho Panhandle National Forest	IDBO-S1	48.98875	-116.65484	972.7	913.02	11.11	0.77
Idaho	NR	Idaho Panhandle National Forest	IDBO-S2	48.99345	-116.65257	1256.6	896.92	10.38	0.44
Montana	NR	Glacier National Park	MTLM-N3	48.55858	-113.90741	1413.5	838.28	9.86	-2.24
Montana	NR	Glacier National Park	MTLM-N1	48.57992	-113.90205	993.6	741.15	12.22	-0.53
Montana	NR	Glacier National Park	MTLM-N2	48.54595	-113.93873	1242.0	779.97	11.77	-0.90
Montana	NR	Glacier National Park	MTLM-S3	48.61694	-113.84409	1709.9	1133.30	8.05	-2.58
Montana	NR	Glacier National Park	MTLM-S1	48.61226	-113.86427	1112.6	795.95	11.45	-0.88
Montana	NR	Glacier National Park	MTLM-S2	48.61295	-113.84806	1466.2	941.32	9.03	-2.24
Montana	NR	Glacier National Park	MTTM-N3	48.46644	-113.37814	1767.8	1090.48	8.38	-1.21
Montana	NR	Glacier National Park	MTTM-N1	48.47366	-113.37648	1600.1	976.57	9.34	-1.97
Montana	NR	Glacier National Park	MTTM-N2	48.47068	-113.37583	1647.2	1090.48	8.38	-1.21
Montana	NR	Glacier National Park	MTTM-S3	48.52064	-113.34128	1952.1	1023.23	8.19	-0.89
Montana	NR	Glacier National Park	MTTM-S1	48.51048	-113.34008	1591.8	879.81	9.49	-1.95
Montana	NR	Glacier National Park	MTTM-S2	48.51731	-113.34301	1801.3	1023.23	8.19	-0.89
Idaho	NR	Idaho Panhandle National Forest	IDTR-N3	48.82192	-116.45527	1335.6	860.03	11.72	1.52
Idaho	NR	Idaho Panhandle National Forest	IDTR-N1	48.82679	-116.45795	951.0	860.03	11.72	1.52
Idaho	NR	Idaho Panhandle National Forest	IDTR-N2	48.82422	-116.45784	1113.1	860.03	11.72	1.52
Idaho	NR	Idaho Panhandle National Forest	IDTR-S3	48.84185	-116.46086	1727.8	912.12	7.63	0.63
Idaho	NR	Idaho Panhandle National Forest	IDTR-S1	48.82956	-116.46442	1081.8	934.17	9.99	0.53
Idaho	NR	Idaho Panhandle National Forest	IDTR-S2	48.83354	-116.46579	1337.1	934.17	9.99	0.53
Idaho	CR	Payette National Forest	IDBL-S1	45.17256	-116.47835	1893.3	1199.41	10.72	-1.62
Idaho	CR	Payette National Forest	IDBL-S2	45.19576	-116.52554	1930.8	1209.41	10.73	-1.79
Idaho	CR	Payette National Forest	IDBL-S3	45.18402	-116.48935	1485.1	1060.50	12.23	-1.45
Idaho	CR	Payette National Forest	IDBL-S4	45.12772	-116.60034	2101.0	1166.68	9.49	-2.43

Idaho	CR	Payette National Forest	IDMC-W1	45.05391	-116.15057	1912.0	1240.11	9.71	-2.83
Idaho	CR	Payette National Forest	IDMC-W2	45.03281	-116.13945	1941.3	1227.35	9.84	-2.86
Montana	CR	Gallatin National Forest	MTGT-N1	45.85834	-110.87770	1732.2	790.23	11.55	-3.51
Montana	CR	Gallatin National Forest	MTGT-N2	45.84902	-110.86966	2103.0	826.67	10.21	-3.05
Montana	CR	Gallatin National Forest	MTGT-N3	45.85388	-110.87219	1956.6	815.47	10.54	-3.07
Montana	CR	Gallatin National Forest	MTGT-S1	45.91430	-110.95727	2365.6	129.92	6.69	-3.77
Montana	CR	Gallatin National Forest	MTGT-S2	45.86057	-110.87810	1833.8	790.23	11.55	-3.51
Montana	CR	Gallatin National Forest	MTGT-S3	45.91087	-110.92451	1923.5	937.10	9.62	-2.37
Oregon	CR	Umatilla National Forest	ORUT-N1	44.99828	-118.98540	981.5	429.98	16.67	1.31
Oregon	CR	Umatilla National Forest	ORUT-W1	44.99966	-118.98780	942.7	430.81	16.52	1.25
Oregon	CR	Wallowa-Whitman National Forest	ORWT-S1	46.09643	-117.78622	1664.6	1511.13	9.48	0.26
Oregon	CR	Wallowa-Whitman National Forest	ORWT-S2	46.09514	-117.78361	1681.8	1457.22	10.45	1.00
Oregon	CR	Wallowa-Whitman National Forest	ORWT-W1	46.09731	-117.78704	1706.9	1511.13	9.48	0.26
Oregon	CR	Wallowa-Whitman National Forest	ORWW-E1	45.14546	-116.83314	1691.3	1019.61	11.41	0.60
Oregon	CR	Wallowa-Whitman National Forest	ORWW-W1	45.14581	-116.83565	1700.9	1019.61	11.41	0.60
Colorado	SR	Gunnison National Forest	COMP-N1	38.44258	-106.35025	3158.8	664.69	9.13	-4.53
Colorado	SR	Gunnison National Forest	COMP-N2	38.44646	-106.34871	3045.0	663.24	9.89	-4.12
Colorado	SR	Gunnison National Forest	COMP-N3	38.44885	-106.34814	2958.4	663.24	9.89	-4.12
Colorado	SR	Gunnison National Forest	COMP-S1	38.45056	-106.37699	3018.0	657.66	9.44	-4.41
Colorado	SR	Gunnison National Forest	COMP-S2	38.44553	-106.37841	2966.5	632.73	10.67	-4.13
Colorado	SR	Gunnison National Forest	COMP-S3	38.43744	-106.37733	2779.4	598.79	11.16	-6.17
Colorado	SR	Roosevelt National Forest	CORO-N1	40.41250	-105.29578	2347.0	485.62	14.55	1.47
Colorado	SR	Roosevelt National Forest	CORO-N2	40.41506	-105.28864	2087.9	481.98	15.52	2.12
Colorado	SR	Roosevelt National Forest	CORO-N3	40.41684	-105.28029	1874.5	476.06	15.97	0.85
Colorado	SR	Roosevelt National Forest	CORO-S1	40.45681	-105.43896	2270.8	451.30	13.13	-0.89
Wyoming	SR	Bridger-Teton National Forest	WYJK-N1	43.46260	-110.75688	2383.7	569.82	10.83	-3.70
Wyoming	SR	Bridger-Teton National Forest	WYJK-N2	43.46455	-110.73258	1943.6	618.59	11.32	-4.36
Wyoming	SR	Bridger-Teton National Forest	WYJK-N3	43.46119	-110.73388	2122.9	685.13	10.15	-2.38
Wyoming	SR	Bridger-Teton National Forest	WYJK-S1	43.47999	-110.71121	2605.9	794.92	8.49	-3.69
Wyoming	SR	Bridger-Teton National Forest	WYJK-S2	43.47420	-110.72632	2355.7	652.25	9.63	-2.73
Wyoming	SR	Bridger-Teton National Forest	WYJK-V1	43.51136	-110.63581	2386.9	800.59	9.20	-2.85
Wyoming	SR	Bridger-Teton National Forest	WYJK-V2	43.51023	-110.64938	2299.2	714.16	10.09	-3.22

California	CA	UC Angelo Reserve	CAAG-N1	39.71793	-123.63020	719.0	2166.73	18.40	6.14
California	CA	UC Angelo Reserve	CAAG-N2	39.72436	-123.63300	568.4	2091.71	19.04	5.52
California	CA	UC Angelo Reserve	CAAG-N3	39.72954	-123.63415	452.8	2023.21	20.34	5.46
California	CA	UC Angelo Reserve	CAAG-S1	39.72557	-123.62563	471.6	2171.00	19.21	5.37
California	CA	UC Angelo Reserve	CAAG-S2	39.73496	-123.64447	421.2	1991.09	20.28	5.54
California	CA	BLM Headwaters Reserve	CAHW-N1	40.63498	-124.07886	484.8	1517.01	18.44	7.51
California	CA	BLM Headwaters Reserve	CAHW-N2	40.63889	-124.08482	474.0	1502.34	18.70	7.59
California	CA	BLM Headwaters Reserve	CAHW-S1	40.64104	-124.07084	483.2	1511.89	18.38	7.61
California	CA	BLM Headwaters Reserve	CAHW-S2	40.64659	-124.07425	498.9	1473.50	18.82	7.26
California	CA	Plumas National Forest	CAPL-N1	39.92889	-121.07053	1201.3	1025.59	19.47	2.74
California	CA	Plumas National Forest	CAPL-N2	39.93278	-121.08183	1142.3	1058.32	19.30	2.94
California	CA	Plumas National Forest	CAPL-N3	39.94880	-121.11241	1511.4	1248.33	17.13	4.29
California	CA	Plumas National Forest	CAPL-S1	39.95737	-121.11212	1644.4	1214.21	16.28	3.69
California	CA	Plumas National Forest	CAPL-S2	39.95479	-121.10964	1529.3	1214.21	16.28	3.69
California	CA	Plumas National Forest	CAPL-S3	39.95282	-121.10769	1399.4	1248.33	17.13	4.29
California	CA	Stanislaus National Forest	CAST-N1	37.97918	-120.06102	1085.7	1113.39	19.90	5.61
California	CA	Stanislaus National Forest	CAST-N2	37.96742	-120.03341	1300.2	1112.67	19.25	4.61
California	CA	Stanislaus National Forest	CAST-N3	37.97418	-120.12519	1461.4	1115.21	17.44	5.50
Idaho	CR	Payette National Forest	IDBL-N1	45.18934	-116.54463	2115.2	1279.61	9.71	-2.49
Arizona	SW	Grand Canyon National Park	AZGC-E1	36.21474	-112.05323	2340.7	605.07	14.78	0.29
Arizona	SW	Grand Canyon National Park	AZGC-N1	36.24319	-111.99254	2561.2	619.63	13.77	-0.66
Arizona	SW	Grand Canyon National Park	AZGC-W1	36.28624	-112.07986	2674.7	728.84	14.14	-0.32
New Mexico	SW	Chama River Wilderness Area	NMCH-E1	36.27455	-106.61571	2423.2	518.11	15.22	1.71
New Mexico	SW	Chama River Wilderness Area	NMCH-W1	36.27487	-106.61445	2425.1	518.11	15.22	1.71
New Mexico	SW	Valles Caldera National Preserve	NMVC-N1	35.87654	-106.57639	2908.0	758.57	10.80	-1.85
New Mexico	SW	Valles Caldera National Preserve	NMVC-N2	35.89028	-106.54670	3023.0	768.74	10.40	-1.78
New Mexico	SW	Valles Caldera National Preserve	NMVC-S1	35.93067	-106.60437	2823.1	694.96	11.16	-1.59
New Mexico	SW	Valles Caldera National Preserve	NMVC-S2	35.93371	-106.61557	3007.2	696.84	10.71	-1.75
New Mexico	SW	Valles Caldera National Preserve	NMVC-V1	36.27413	-106.61719	2489.5	518.11	15.22	1.71
Utah	SW	Henry Mountains	UTHM-N1	38.04960	-110.75899	2710.6	595.76	12.52	-0.52
Utah	SW	Henry Mountains	UTHM-S1	38.06890	-110.82055	2876.0	750.72	10.90	-1.98
Utah	SW	Henry Mountains	UTHM-W1	38.09111	-110.80494	3171.9	830.34	9.50	-3.54

Table 1.2. Descriptive statistics of detrended watershed-scale chronologies. First and last year are computed as an average of all cores in each chronology. First-order autocorrelation suggests that biological persistence is strong in all cores (which is corrected with autoregressive modelling). Expressed population signal values are very high and confirm that sample size is sufficient in each watershed to detect the influence of climate.

Site	# of trees	First year (mean)	Last year (mean)	Length of series	Average ring width (mm)	First-order autocorrelation	r bar*	Expressed population signal
AZGC	40	1809	2010	201	1.32	0.75	0.35	0.91
CAAG	72	1853	2010	158	2.32	0.77	0.27	0.92
CAHW	57	1854	2010	155	2.05	0.79	0.24	0.93
CAPL	91	1813	2010	197	1.71	0.80	0.27	0.95
CAST	41	1844	2010	166	2.00	0.78	0.26	0.88
COMP	89	1756	2011	255	0.76	0.74	0.34	0.96
CORO	59	1812	2008	195	0.77	0.60	0.57	0.98
IDBL	72	1814	2010	196	1.71	0.79	0.32	0.93
IDBO	70	1817	2004	187	1.14	0.78	0.32	0.95
IDTR	71	1853	2004	151	1.39	0.74	0.38	0.96
MTGT	92	1801	2009	209	1.01	0.83	0.35	0.95
MTLM	81	1821	2004	183	1.10	0.77	0.32	0.97
MTTM	68	1856	2004	148	1.35	0.70	0.30	0.92
NMCH	30	1794	2010	216	0.82	0.49	0.81	0.99
NMVC	74	1802	2010	208	1.25	0.72	0.39	0.96
ORHJ	85	1715	2010	295	1.22	0.81	0.24	0.94
ORUT	31	1824	2011	187	1.22	0.81	0.45	0.94
ORWT	45	1825	2011	186	1.45	0.72	0.37	0.94
ORWW	29	1870	2011	141	2.09	0.76	0.47	0.95
UTHM	43	1694	2010	316	0.94	0.69	0.48	0.95
WACR	76	1726	2004	278	0.98	0.87	0.25	0.92
WADR	70	1730	2004	274	0.99	0.88	0.18	0.93
WAHR	72	1685	2004	319	1.25	0.85	0.18	0.88
WAST	67	1794	2004	209	1.55	0.82	0.21	0.90
WYJK	83	1835	2010	175	1.65	0.77	0.39	0.97

*__rbar__ = the mean of all the correlations between different cores

7. FIGURES

Figure 1.1. Entire geographic distribution of Douglas-fir in North America. Douglas-fir is the most widespread commercial conifer species, and is found growing in all of the dominant mountain ranges of the western United States.

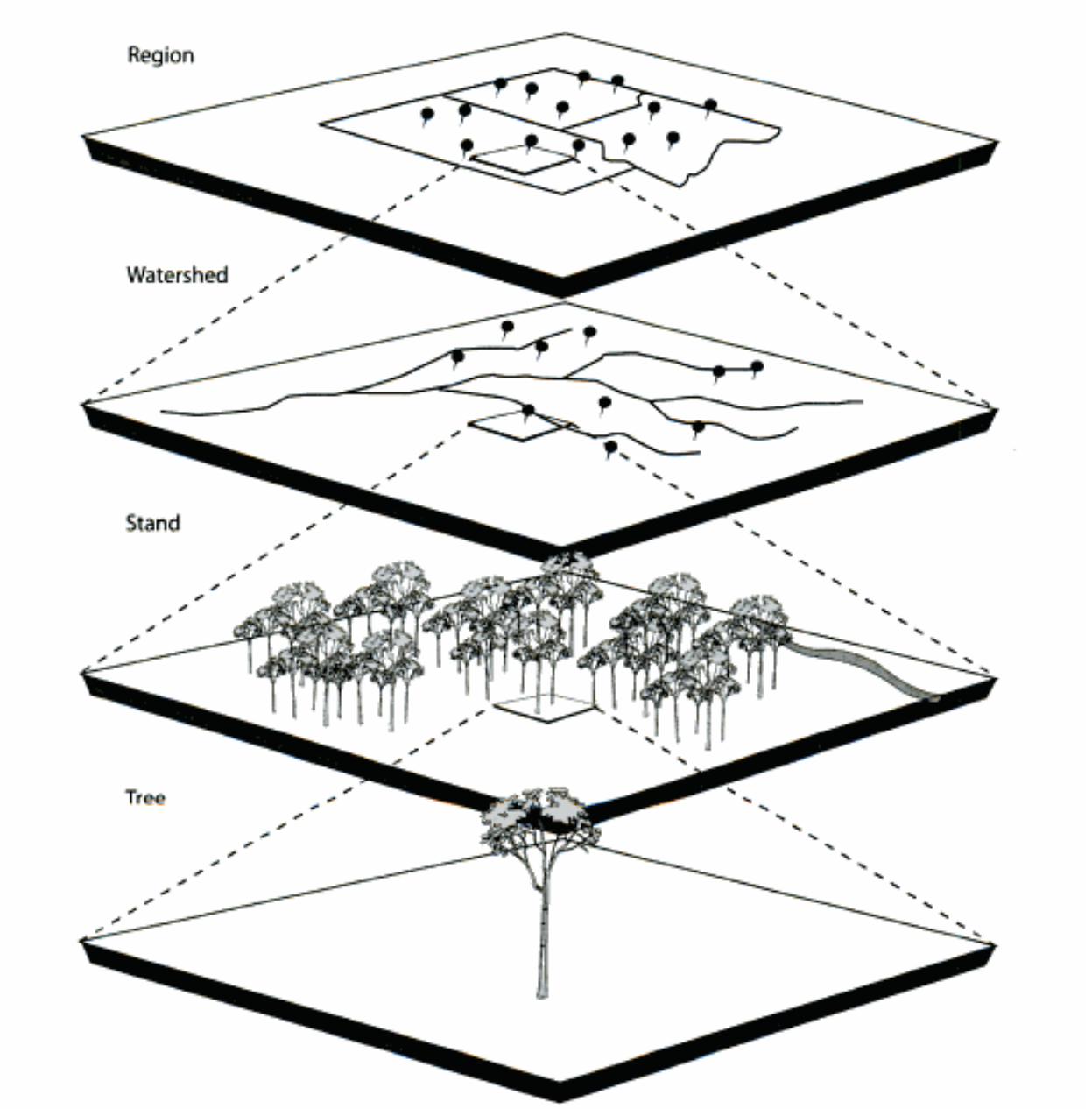

Figure 1.2. Schematic of multi-scale sampling approach. I sampled at multiple scales to provide replications for analysis at the stand (plot), watershed, and regional scales. Figure from Speer (2012).

Figure 1.3. Bailey's ecoprovinces in the western United States. I used these delineations as a proxy for climate domain.

Figure 1.4. Distribution of study sites across the western United States. Grey is the distribution of Douglas-fir from Little et al. (1971). Triangles represent the density of plots within land ownership perimeters.

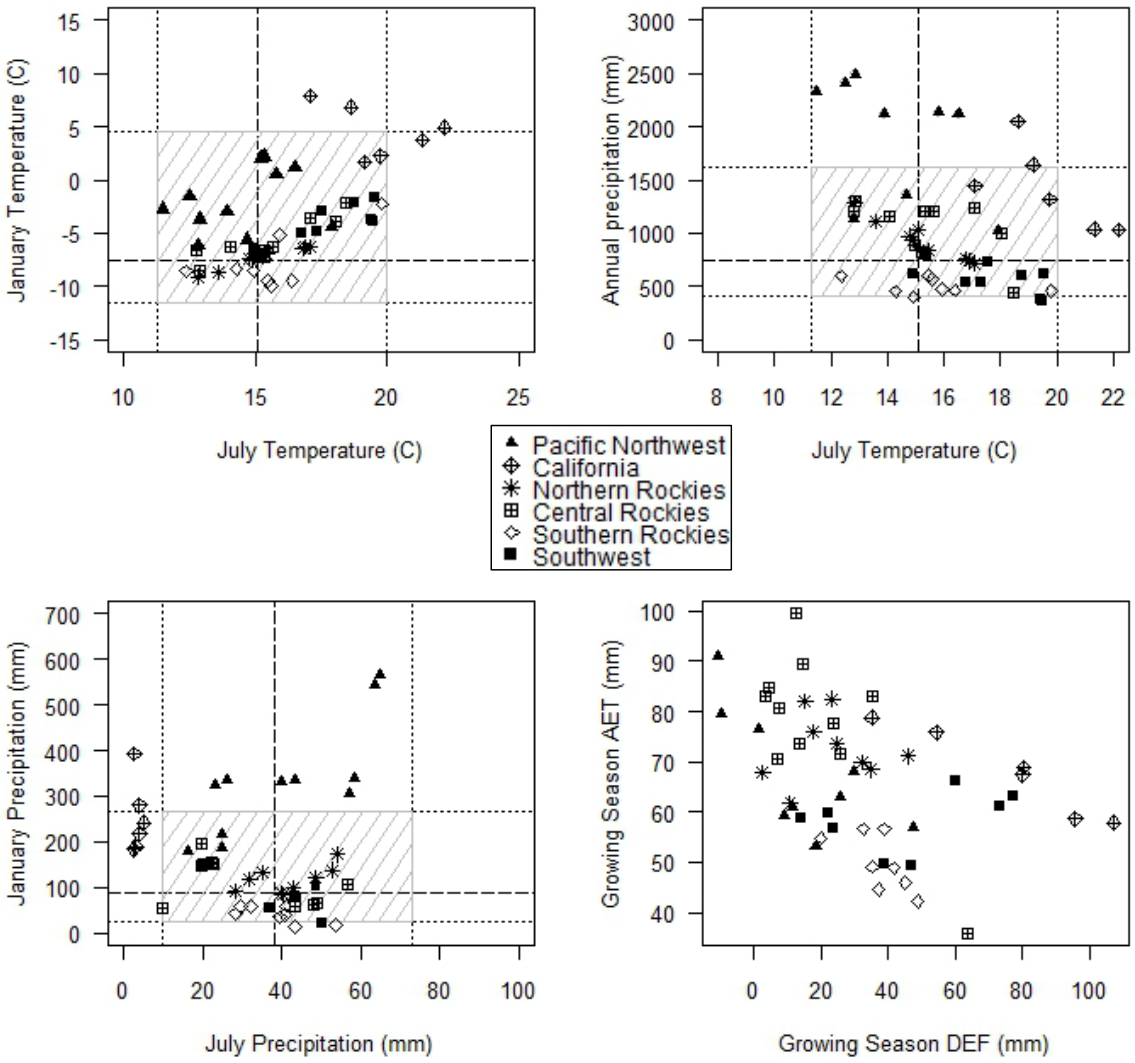

Figure 1.5. The distribution of sampling sites in climate space. The climatic limits of Douglas-fir (as defined by Thompson et al. [2000]) are represented as 10th and 90th (dotted line) and 50th percentiles (dashed line). The hatched box symbolizes the climate space of Douglas-fir. Sampling sites are plotted in this climate space based on average values (1916-2006) of the variables indicated.

8. APPENDICES

Appendix 1.1. Quantile-quantile plots of standardized watershed-scale chronologies. Pre-whitened chronologies were tested for normality using the same method, and the plots are nearly identical to the plots presented here.

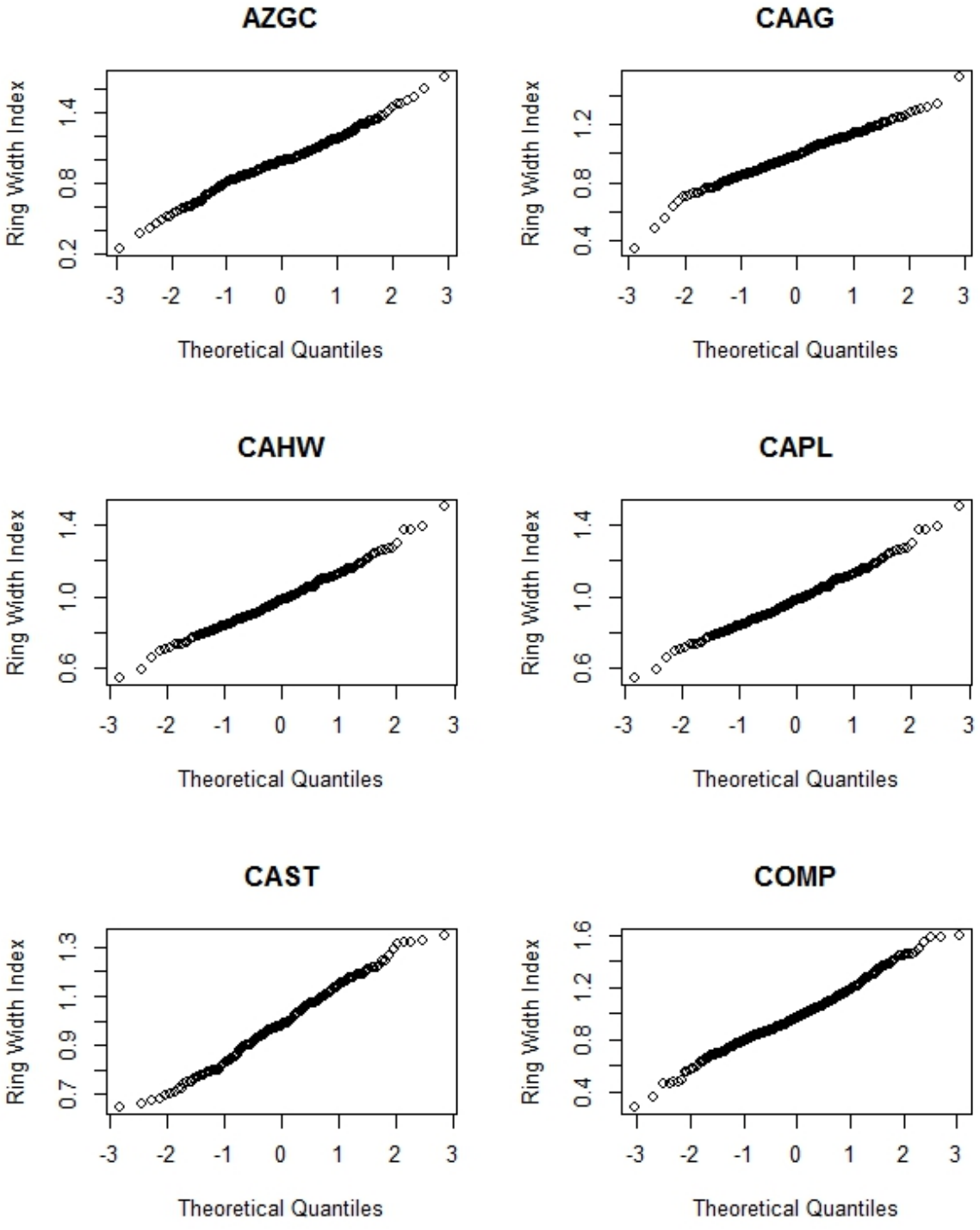

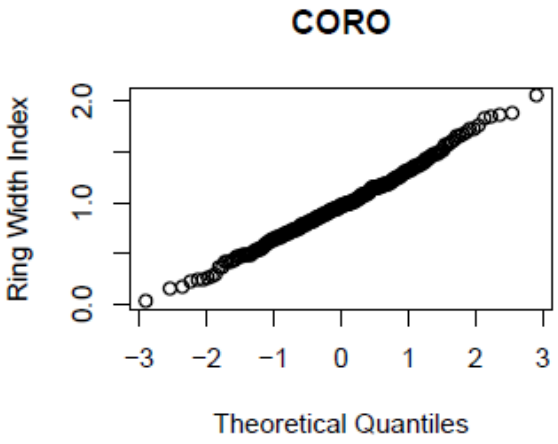
CORO
Ring Width Index
0.0
1.0
2.0
−3
−2
−1
0
1
2
3
Theoretical Quantiles

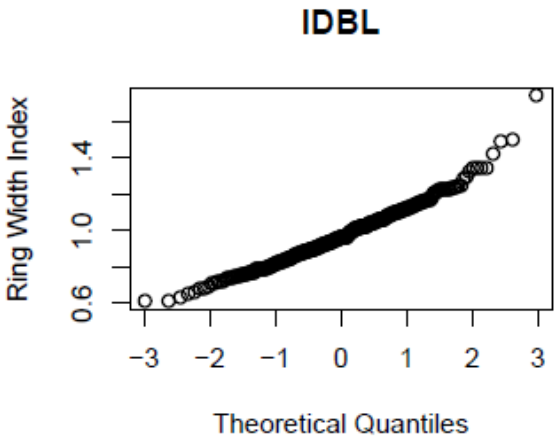
IDBL
Ring Width Index
0.6
1.0
1.4
−3
−2
−1
0
1
2
3
Theoretical Quantiles

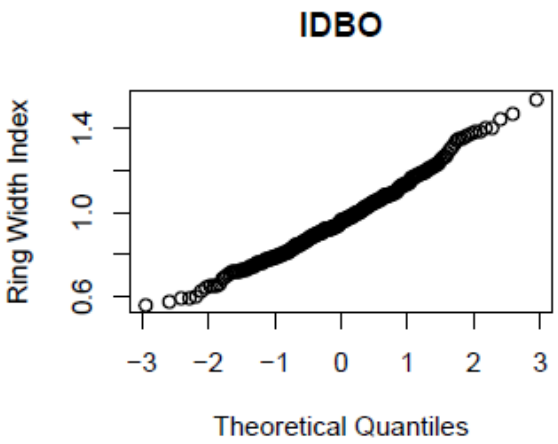
IDBO
Ring Width Index
0.6
1.0
1.4
−3
−2
−1
0
1
2
3
Theoretical Quantiles

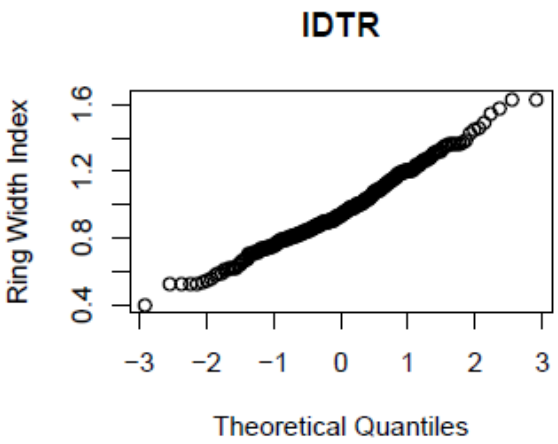
IDTR
Ring Width Index
0.4
0.8
1.2
1.6
−3
−2
−1
0
1
2
3
Theoretical Quantiles

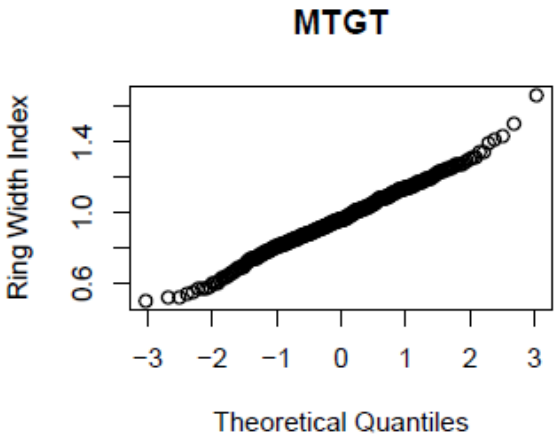
MTGT
Ring Width Index
0.6
1.0
1.4
−3
−2
−1
0
1
2
3
Theoretical Quantiles

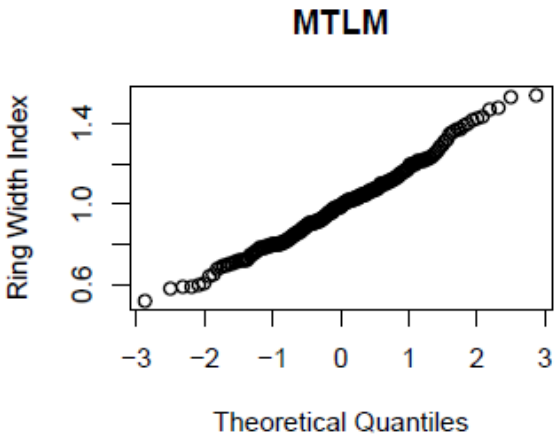
MTLM
Ring Width Index
0.6
1.0
1.4
−3
−2
−1
0
1
2
3
Theoretical Quantiles

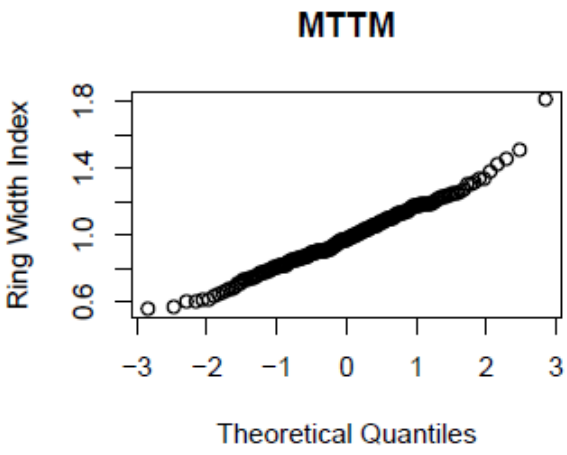
MTTM
Ring Width Index
0.6
1.0
1.4
1.8
−3
−2
−1
0
1
2
3
Theoretical Quantiles

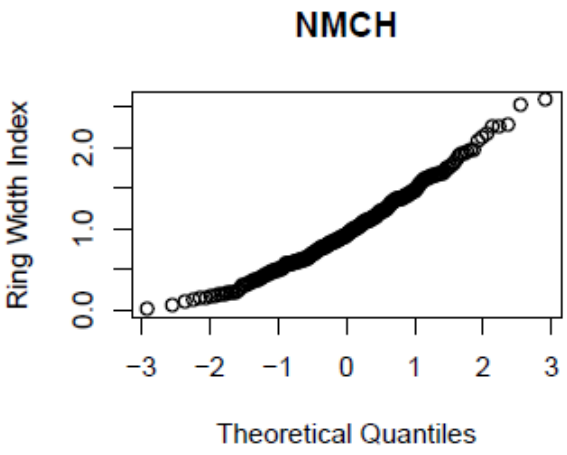
NMCH
Ring Width Index
0.0
1.0
2.0
−3
−2
−1
0
1
2
3
Theoretical Quantiles

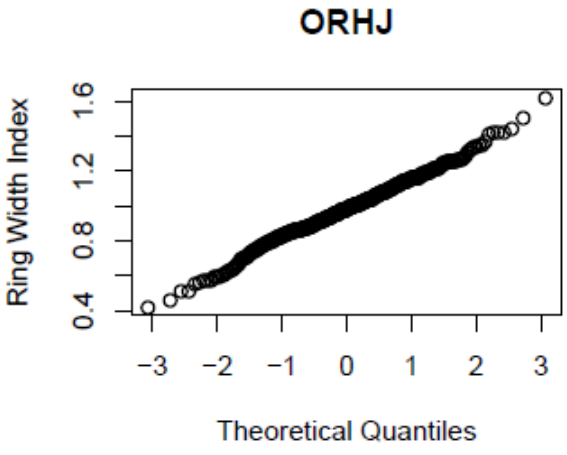
ORHJ
Ring Width Index
0.4
0.8
1.2
1.6
−3
−2
−1
0
1
2
3
Theoretical Quantiles

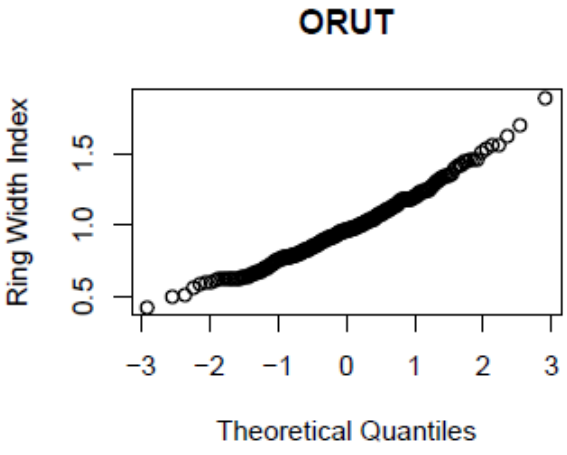
ORUT
Ring Width Index
0.5
1.0
1.5
−3
−2
−1
0
1
2
3
Theoretical Quantiles

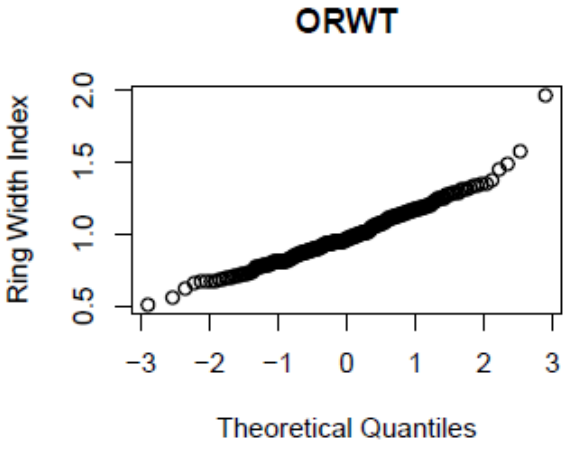
ORWT
Ring Width Index
0.5
1.0
1.5
2.0
−3
−2
−1
0
1
2
3
Theoretical Quantiles

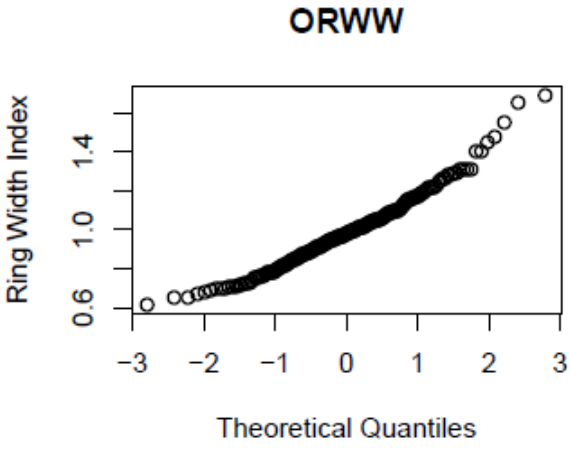
ORWW
Ring Width Index
0.6
1.0
1.4
−3
−2
−1
0
1
2
3
Theoretical Quantiles

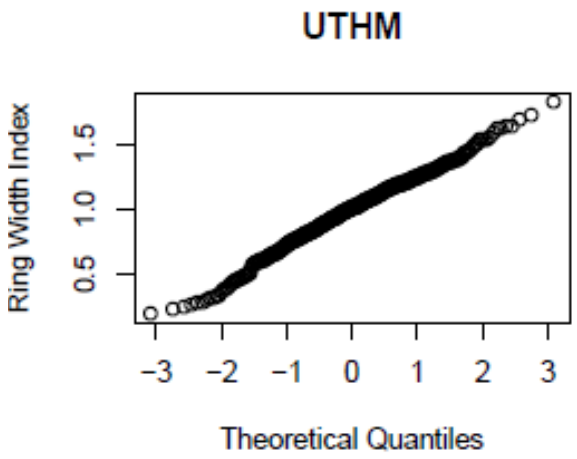
UTHM
Ring Width Index
0.5
1.0
1.5
−3
−2
−1
0
1
2
3
Theoretical Quantiles

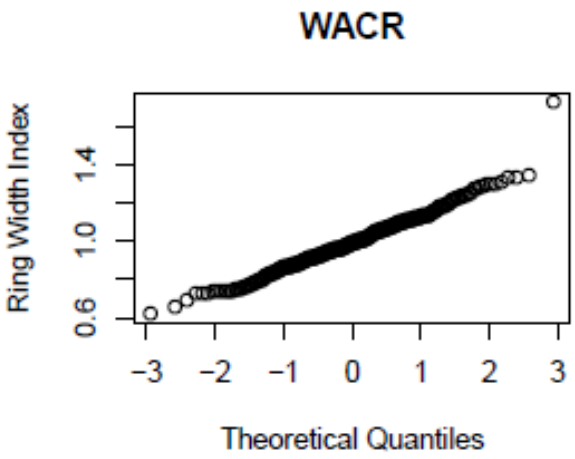
WACR
Ring Width Index
0.6
1.0
1.4
−3
−2
−1
0
1
2
3
Theoretical Quantiles

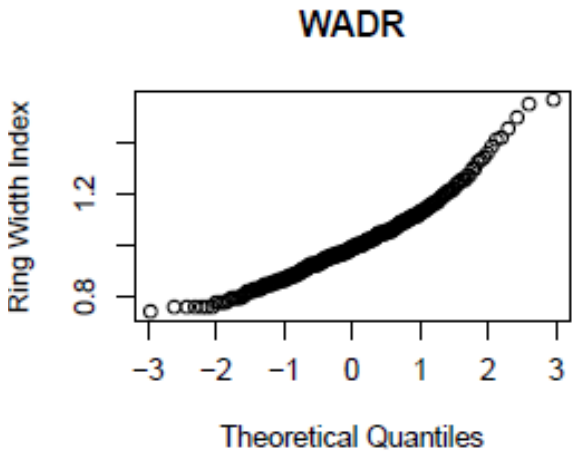
WADR
Ring Width Index
0.8
1.2
−3
−2
−1
0
1
2
3
Theoretical Quantiles

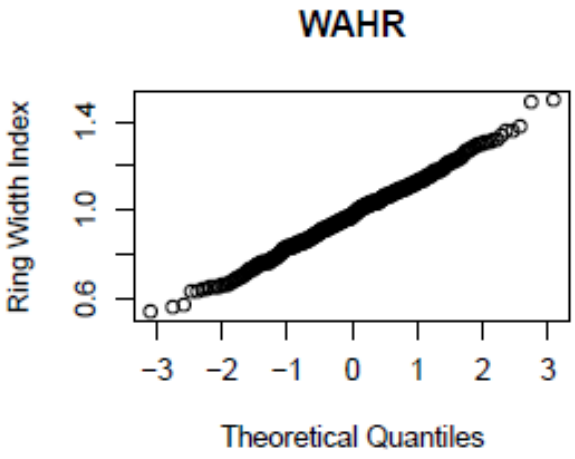
WAHR
Ring Width Index
0.6
1.0
1.4
−3
−2
−1
0
1
2
3
Theoretical Quantiles

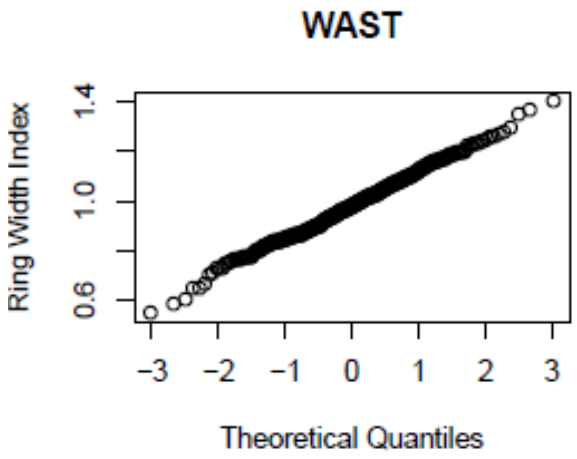
WAST
Ring Width Index
0.6
1.0
1.4
−3
−2
−1
0
1
2
3
Theoretical Quantiles

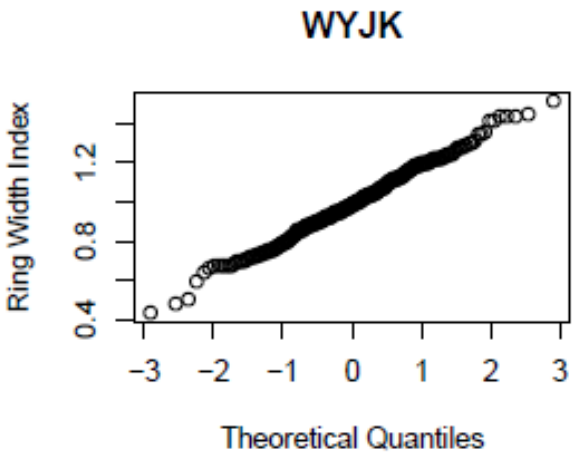
WYJK
Ring Width Index
0.4
0.8
1.2
−3
−2
−1
0
1
2
3
Theoretical Quantiles

Chapter 2

Higher temperatures drive deficit-related growth reductions in Douglas-fir forests of the western US

1. ABSTRACT

As air temperature increases, evaporative demand also increases, increasing vapor pressure deficit (VPD) and climatic water deficit (DEF; potential evapotranspiration minus actual evapotranspiration) and altering water availability in forest ecosystems. These integrated climate variables reflect the water and energy balance (strongly controlled by maximum temperature) of terrestrial ecosystems. As deficits increase, water is lost to the atmosphere through plant tissues and from the soil, which affects water use efficiency, individual tree growth and vigor, and forest productivity. Using a spatially comprehensive network of Douglas-fir (*Pseudotsuga menziesii*) chronologies from 122 locations that experience distinctly different climate in the western United States, I correlate growth with temperature, precipitation, VPD, and DEF. By sampling throughout "climate space" at the continental scale, these data account for a large percentage of variability in growing environments for Douglas-fir which allows for a full assessment of the species response to climatic variability. Results encompassing historical climate records (since 1916) indicate that temperature decreases growth via VPD. Increased VPD results in a steeper water potential gradient and stomatal closure, causing trees to lose water, and reduce carbon uptake and photosynthesis. Reductions in growth are observed at all latitudes, although the effects of VPD and DEF are most pronounced in the southernmost latitudes and at the lowest elevations. As temperature continues to increase in future decades, we

can expect deficits to increase and consequently Douglas-fir growth to decrease throughout its US range.

2. MAIN TEXT

Declines in forest growth decrease net primary productivity and alter the global carbon cycle (Allen et al. 2010, Schwalm et al. 2010, Zhao and Running 2010). Decreased tree vigor can also predispose forests to stress and disturbances, such as bark beetle-induced mortality (Bentz et al. 2010), subsequent accumulation of fine woody debris that contribute to short-term wildfire hazard (Hicke et al. 2012), and potential mortality associated with low soil moisture (McDowell et al 2008, Van Mantgem et al. 2009), all of which can have concomitant impacts on ecosystem processes and function (McKenzie et al. 2009). Changes in forest growth are often attributed to climatic variability (Fritts 1974, Littell et al. 2008), wherein periods of warm and dry conditions (i.e. water stress) result in the decrease of annual tree growth (Williams et al. 2010).

Water stress is a function of a combination of precipitation, water use by plants in photosynthesis, and the evaporative demand imposed by temperature. Increased air temperature exacerbates water stress by increasing deficits in both the soil and atmosphere. As these deficits increase, trees either lose water via the soil-plant-atmosphere continuum resulting in increased stress (Breda et al. 2006), or close stomata ceasing growth altogether (McDowell et al. 2008). Increased precipitation can ameliorate water stress to some degree, but changes in temperature can outweigh precipitation and ultimately increase deficit levels and water stress in forest ecosystems (Adams et al. 2009, Williams et al. 2013).

Measurements of precipitation and temperature are useful indicators of climate at any given time, but unlike "plant relevant" variables, do not directly reflect the energy and water balance of terrestrial systems (Stephenson 1998). Variables that express how plants "sense" climate are more useful in analyses that consider climatic limitations on plant growth and distributions (Stephenson 1990, Lutz et al. 2010, Williams et al. 2013). Climatic water deficit (DEF), calculated as potential evapotranspiration minus actual evapotranspiration, measures climate as the interaction of water (precipitation) and energy (temperature; Stephenson 1998). High DEF values indicate time periods when evaporative demand of plants is not met, and is often driven by soil moisture. Vapor pressure deficit (VPD), another plant relevant variable, is a function of relative humidity and maximum temperature. VPD increases with temperature and high VPD levels indicate periods when atmospheric deficits are so high that plants either lose water at faster rates as a reaction to steep water potential gradients or close stomata. DEF and VPD are variables that integrate water and energy and are sensitive to temperature increases (Williams et al. 2013).

I quantified the relationship between climate and Douglas-fir (*Psuedotsuga menziesii* (Mirb.) Franco) growth in forests throughout the western United States (US). Douglas-fir occupies diverse landscapes (from sea level to 3300 m) and a broad range of climate regimes (Figure S1) in the dominant mountain ranges of the western US, and is one of the most ecologically and economically important coniferous species in western US forests. My network of 122 newly developed tree-ring chronologies is a novel dataset representing tree growth in a breadth of growing environments and climate (Fig. 1), contrasting with previous attempts to assess climate-growth relationships at regional scales (Williams et al. 2013, Griesbauer and Green 2009, Littell et al. 2008) or with data mined from the International Tree-Ring Data Bank

(ITRDB), which largely represents extreme growing environments (Chen et al. 2010, Williams et al. 2013). Although the ITRDB is an excellent source of data, climate-growth relationships are difficult to quantify due to sampling bias inherent in reconstruction data (Nehrbass-Ahles et al. 2014). Here, I analyze the first comprehensive network of growth data sampled specifically to assess the relationship between climate and tree growth.

Historical climatic data (1916-2006) were summarized and modeled with the Variable Infiltration Capacity hydrologic model (VIC; Liang et al 1994, Njissen 1997, Elsner et al. 2010). The VIC model uses daily climatic data extracted from the Historical Climate Network (available online at http://cdiac.ornl.gov/epubs/ndp/ushcn/ushcn.html) to calculate evapotranspiration and relative humidity (needed for VPD and DEF). VIC outputs of plant-relevant climatic data are arguably the most temporally and spatially resolved in the western United States. Monthly precipitation and temperature time series are bias-corrected against the PRISM model and are therefore consistent with values used in other ecological studies (Daly 2007, Williams et al. 2013). Monthly climatic data include precipitation, maximum temperature, VPD, and DEF.

Growth was positively correlated (Pearson's $r \geq 0.2$, $p = 0.05$) with precipitation and negatively correlated (Pearson's $r \leq -0.2$, $p = 0.05$) with temperature, VPD, and DEF in the growing season (April – July; Figure 2.2), and correlations were much higher for the latter two variables. Correlations with precipitation and temperature mirror one another; higher temperatures decrease growth in the same months that precipitation enhances growth, so it is difficult to attribute the effect of one variable from the other. Conversely, VPD and DEF have a much stronger relationship with growth (Pearson's $r \leq -0.5$, $p \leq 0.001$) than precipitation,

suggesting that these integrated climatic variables are more representative of climate that limit growth.

The strength of growth-climate relationships differs in timing and by length of the growing season. A consistent negative relationship exists between growth and VPD in June and July across all regions, with strength of relationship increasing as latitude decreases (Figure 2.2). Growing season deficits decrease tree growth, but also evident is a lagged relationship in which previous-year, late-summer temperature and deficits decrease growth in all regions except California (Figure 2.2). Lagged responses provide evidence that climate can affect growth for more than one season because favorable or deleterious growing conditions alter carbon fixation and bud production. The influence of non-growing season and previous year climate increases with latitude and strength of correlation is higher in regions where water-stress appears less limiting. Warmer temperatures will likely increase water stress in the south, and change the timing of limiting factors in the north as water stress becomes more important as a limiting factor.

Growing season months (AMJJ) were aggregated into one climate variable and correlated with watershed-scale chronologies (Figure 2.3) to test if the relationships varied by scale. Correlation coefficients increased in strength for all variables, reinforcing the inference that high deficits during growing-season months drive reductions in tree growth at the plot- and watershed scales (Figure 2.3). Fine-scale variability in climate response can likely be attributed to genetic variability (Rehfeldt 1989), but coarse-scale patterns support the conclusion that Douglas-fir is sensitive to deficits throughout its range.

My results corroborate the effects of VPD on forest drought stress documented for forests in the southwestern United States (Williams et al. 2013). However, my data suggest that a strong

relationship exists between VPD and growth throughout Douglas-fir forests of the western United States, evidenced by decreased growth commensurate with VPD increases across all regions (Figure 2.4). Regressions conducted for temperature effects on growth did not yield significant downward slopes for all regions (Figure S3), suggesting that temperature does not directly decrease growth.

Although both high temperature and VPD decrease growth, the physiological mechanisms differ between climate variables. The effect of high temperature alone would cause growth to decrease as a function of biochemical limitations to growth, because photosynthesis decreases once leaf temperatures exceed a given threshold (Farquhar 1980, Medlyn et al. 2002). The mechanism is different, however, when VPD reduces growth: moisture stress results in stomatal closure, which ultimately decreases growth due to reduced CO_2 uptake (Stewart and Dwyer 1983). VPD is one of the most important climate variables linked to variation in stomatal closure (Bunce 1996), with stomatal conductance exponentially decreasing as VPD increases (Oren 1999). VPD limits growth across all latitudes, whereas temperature is limiting only in the southernmost sites, suggesting a latitudinal gradient of limiting factors. Higher temperatures drive stomatal closure (via water stress) in the northern latitudes, and a combination of stomatal closure and biochemical limitations inhibit photosynthesis in southern latitudes. Although the mechanisms vary, high temperatures result in decreased growth across all regions analyzed.

My results illustrate that forests are sensitive to changes in VPD and DEF, which reflect the relationship between temperature and precipitation in terrestrial ecosystems. Temperature, VPD, and DEF have already increased across all study regions (Fig.1, Figure S2) and are projected to increase throughout western North America (IPCC 2013). Model projections are

highly uncertain regarding precipitation, but suggest that precipitation will not increase substantially. Both deficit variables are highly sensitive to temperature, therefore if temperature increases, especially with no increase in precipitation, we can expect an increase in deficits. As temperatures increase in forested regions throughout the western US, I expect that growth will decrease commensurate to declines observed in historical warm periods. As warm periods become more common, reduced growth will prevail as the new normal.

Future temperature increases will strongly affect Douglas-fir forests of the western US, outweighing a potential fertilization effect (via increased water use efficiency) that higher ambient CO_2 concentration may have on tree growth (Gedalof and Berg 2010). The principle of limiting factors supports this conclusion: tree growth can proceed only as fast as allowed by the primary variables that limit growth (Fritts 1976). Once demands for CO_2 are met, the down-regulation of photosynthesis occurs in response to other limiting factors (i.e., water, nutrients, light; Ainsworth et al. 2005). In Douglas-fir forests, water is the principal limiting factor. Growth and productivity will therefore decrease in these and potentially other water-limited forests in response to a warmer climate.

3. REFERENCES

Adams, H. D., M. Guardiola-Claramonte, G. A. Barron-Gafford, J. C. Villegas, D. D. Breshears, C. B. Zou, P. A. Troch, and T. E. Huxman. 2009. Temperature sensitivity of drought-induced tree mortality portends increased regional die-off under global change-type drought. Proceedings of the National Academy of Sciences **106**: 7063-7064.

Ainsworth, E. A. and S. P. Long. 2005. What have we learned from 15 years of free-air CO2 enrichment (FACE)? A meta-analytic review of the responses of photosynthesis, canopy properties and plant production to rising CO2. New Phytologist **165**: 351-372.

Allen, C. D., A. K. Macalady, H. Chenchouni, D. Bachelet, N. McDowell, M. Vennetier, T. Kitzberger, A. Rigling, D. D. Breshears, E. H. Hogg, P. Gonzalez, R. Fensham, Z. Zhang, J. Castro, N. Demidova, J. H. Lim, G. Allard, S. W. Running, A. Semerci, and N. Cobb. 2010. A global overview of drought and heat-induced tree mortality reveals emerging climate change risks for forests. Forest Ecology and Management **259**: 660-684.

Bailey, R. G. 2004. Identifying ecoregion boundaries. Environmental Management **34**: S14-S26.

Bentz, B. J., J. Régnière, C. J. Fettig, E. M. Hansen, J. L. Hayes, J. A. Hicke, R. G. Kelsey, J. F. Negrón, and S. J. Seybold. 2010. Climate change and bark beetles of the western United States and Canada: direct and indirect effects. BioScience **60**: 602-613.

Bréda, N., R. Huc, A. Granier, and E. Dreyer. 2006. Temperate forest trees and stands under severe drought: a review of ecophysiological responses, adaptation processes and long-term consequences. Annals of Forest Science **63**: 625-644.

Bunn, A. G. 2008. A dendrochronology program library in R (dplR). Dendrochronolgia **26**: 115-124.

Chen, P. Y., C. Welsh, and A. Hamann. 2010. Geographic variation in growth response of Douglas-fir to interannual climate variability and projected climate change. Global Change Biology **16**: 3374-3385.

Daly, C., M. Halbleib, J. I. Smith, W. P. Gibson, M. K. Doggett, G. H. Taylor, J. Curtis, and P. Pasteris. 2008. Physiographically sensitive mapping of climatological temperature and precipitation across the conterminous United States. International Journal of Climatalogy **28**: 2031-2064.

Elsner, M. M., L. Cuo, N. Voisin, J. S. Deems, A. F. Hamlet, J. A. Vano, K. E. B. Mickelson, S. Lee, and D. P. Lettenmaier. 2010. Implications of 21st century climate change for the hydrology of Washington State. Climatic Change **102**: 225-260.

Farquhar, G. D., S. V. von Caemmerer, and J. A. Berry. 1980. A biochemical model of photosynthetic CO2 assimilation in leaves of C3 species. Planta **149**: 78-90.

Fritts, H. C. 1974. Relationships of ring widths in arid-site conifers to variations in monthly temperature and precipitation. Ecological Monographs **44**: 411-440.

Fritts, H. C. 1976. Tree rings and climate. Academic Press, New York.

Gedalof, Z. E. and A. A. Berg. 2010. Tree ring evidence for limited direct CO2 fertilization of forests over the 20th century. Global Biogeochemical Cycles **24**: 1-6.

Griesbauer, H. P., and D. S. Green. 2010. Regional and ecological patterns in interior Douglas-fir climate-growth relationships in British Columbia, Canada. Canadian Journal of Forest Research **40**: 308-321.

Hicke, J. A., M. C. Johnson, J. L, Hayes, and H. Preisler. 2012. Effects of bark beetle-caused tree mortality on wildfires: a review. Forest Ecology and Management **271**: 81-90.

Holmes, R. L. 1999. User's manual for program COFECHA. University of Arizona Press, Tucson, AZ.

IPCC. 2013. Annex I: Atlas of Global and Regional Climate Projections [van Oldenborgh, G.J., M. Collins, J. Arblaster, J.H. Christensen, J. Marotzke, S.B. Power, M. Rummukainen and T. Zhou (eds.)]. In: Climate Change 2013: The Physical Science Basis. Contribution of Working Group I to the Fifth Assessment Report of the Intergovernmental Panel on Climate Change [Stocker, T.F., D. Qin, G.-K. Plattner, M. Tignor, S.K. Allen, J. Boschung, A. Nauels, Y. Xia, V. Bex and P.M. Midgley (eds.)]. Cambridge University Press, Cambridge, United Kingdom and New York, NY, USA.

Liang, X., D. P. Lettenmaier, E. F. Wood, and S. J. Burges. 1994. A simple hydrologically based model of land surface water and energy fluxes for general circulation models. Journal of Geophysical Research **99**: 14415-14428.

Littell, J. S., D. L. Peterson, M. Tjoelker. 2008. Douglas-fir growth in mountain ecosystems: water limits tree growth from stand to region. Ecological Monographs **78**: 349-368.

Lutz, J. A., J. W. van Wagtendonk, and J. F. Franklin. 2010. Climatic water deficit, tree species ranges, and climate change in Yosemite National Park. Journal of Biogeography **37**: 936-950.

Medlyn, B. E., E. Dreyer, D. Ellsworth, M. Forstreuter, P. C. Harley, M. U. F. Kirschbaum, X. Le Roux, P. Montpied, J. Strassemeyer, A. Walcroft, K. Wang, D. and Loustau. 2002. Temperature response of parameters of a biochemically based model of photosynthesis. II. A review of experimental data. Plant, Cell & Environment **25**: 1167-1179.

McKenzie, D., D. L. Peterson, and J. Littell. 2009. Global warming and stress complexes in forests of western North America. Pages 317-337 in A. Bytnerowicz, M. J. Arbaugh, A. R. Riebau, and C. Andersen (eds.), Wildland Fires and Air Pollution. Elsevier Publishers, The Hague, Netherlands.

McDowell, N., W. T. Pockman, C. D. Allen, D. D. Breshears, N. Cobb, T. Kolb, J. Plaut, J. Sperry, A. West, D. G. Williams, and E. A. Yepez. 2008. Mechanisms of plant survival and mortality during drought: why do some plants survive while others succumb to drought? New Phytologist **178**: 719-739.

Nehrbass-Ahles, C., F. Babst, S. Klesse, M. Notzli, O. Bouriaud, R. Neukom, M. Dobbertin, and D. Frank. The influence of sampling design on tree-ring based quantification of forest growth. Global Change Biology in press (available at http://dx.doi.org/10.1111/gcb.12599).

Njissen, B. N., D. P. Lettenmaier, X. Liang, S.W. Wetzel, and E. F. Wood. 1997. Streamflow simulation for continental-scale river basins. Water Resources Research **33**: 711-724.

Oren, R., J. S. Sperry, G. G. Katul, D. E. Pataki, B. E. Ewers, N. Phillips, and K. V. R. Schäfer. 1999. Survey and synthesis of intra- and interspecific variation in stomatal sensitivity to vapour pressure deficit. Plant, Cell and Environment **22**: 1515-1526.

Schwalm, C. R., C. A. Williams, K. Schaefer, D. Baldocchi, T. A. Black, A. H. Goldstein, B. E. Law, W. C. Oechel, K. T. Paw U., and R. L. Scott. 2012. Reduction in carbon uptake during turn of the century drought in western North America. Nature Geoscience **5**: 551-556.

Stephenson, N. L. 1990. Climatic control of vegetation distribution- the role of water balance. American Naturalist **135**: 649-670.

Stephenson, N. L. 1998. Actual evapotranspiration and deficit: biologically meaningful correlates of vegetation distribution across spatial scales. Journal of Biogeography **25**: 855-870.

Stewart, D. W., and L. M. Dwyer. 1983. Stomatal response to plant water deficits. Journal of Theoretical Biology **104**: 655-666.

Stokes, M. A. and T. L. Smiley. 1968. An introduction to tree-ring dating. University of Chicago Press, Chicago, Illinois, USA.

Thompson, R. S., K. H. Anderson, P. J. Bartlein. 2000. Atlas of relations between climatic parameters and distributions of important trees and shrubs in North America: introduction and conifers. USGS Prof. Paper 1650-A, Reston, VA.

Van Mantgem, P. J., N. L. Stephenson, J. C. Byrne, L. D. Daniels, J. F. Franklin, P. Z. Fule, M. E. Harmon, A. J. Larson, J. M. Smith, A. H. Taylor, and T. T. Veblen. 2009. Widespread increase of tree mortality rates in the western United States. Science **323**: 521-524.

Williams, A. P., C. D. Allen, C. I. Millar, T. W. Swetnam, J. Michaelsen, C. J. Still, and S. W. Leavitt. 2010. Forest responses to increasing aridity and warmth in the southwestern United States. Proceedings of the National Academy of Sciences **107**: 21289-21294.

Williams, A. P., C. D. Allen, A. K. Macalady, D. Griffin, C. A. Woodhouse, D. M. Meko, T. W. Swetnam, S. A. Rauscher, R. Seager, H. D. Grissino-Mayer, J. S. Dean, E. R. Cook, C. Gangodagamage, M. Cai, and N. G. McDowell. 2013. Temperature as a potent driver of regional forest drought stress and tree mortality. Nature Climate Change **3**: 292-297.

Zhao, M. and S. W. Running. 2011. Drought-induced reduction in global terrestrial net primary production from 2000 through 2009. Science **329**: 940-943.

4. FIGURES

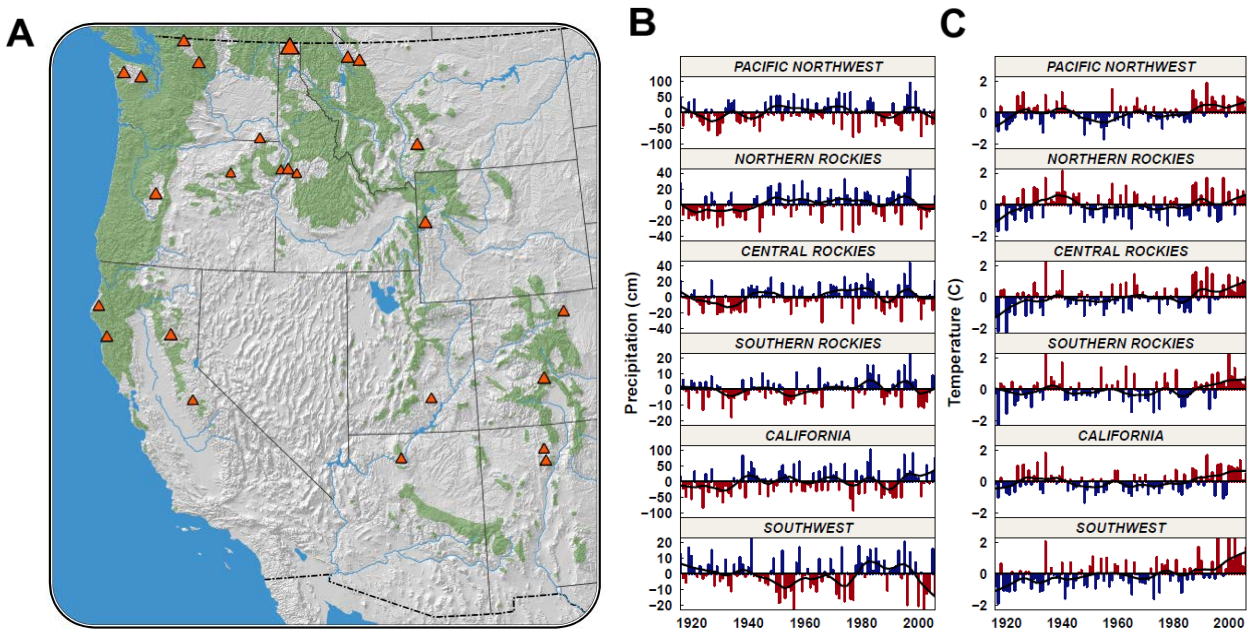

Figure 2.1. Distribution of study sites in the western United States; green is the range of Douglas-fir, and the size of triangles depicts density of sample plots **(A)**. Precipitation anomalies **(B)**, and temperature anomalies **(C)** for study regions. A clear upward trend in temperature is evident, whereas no trend in precipitation exists.

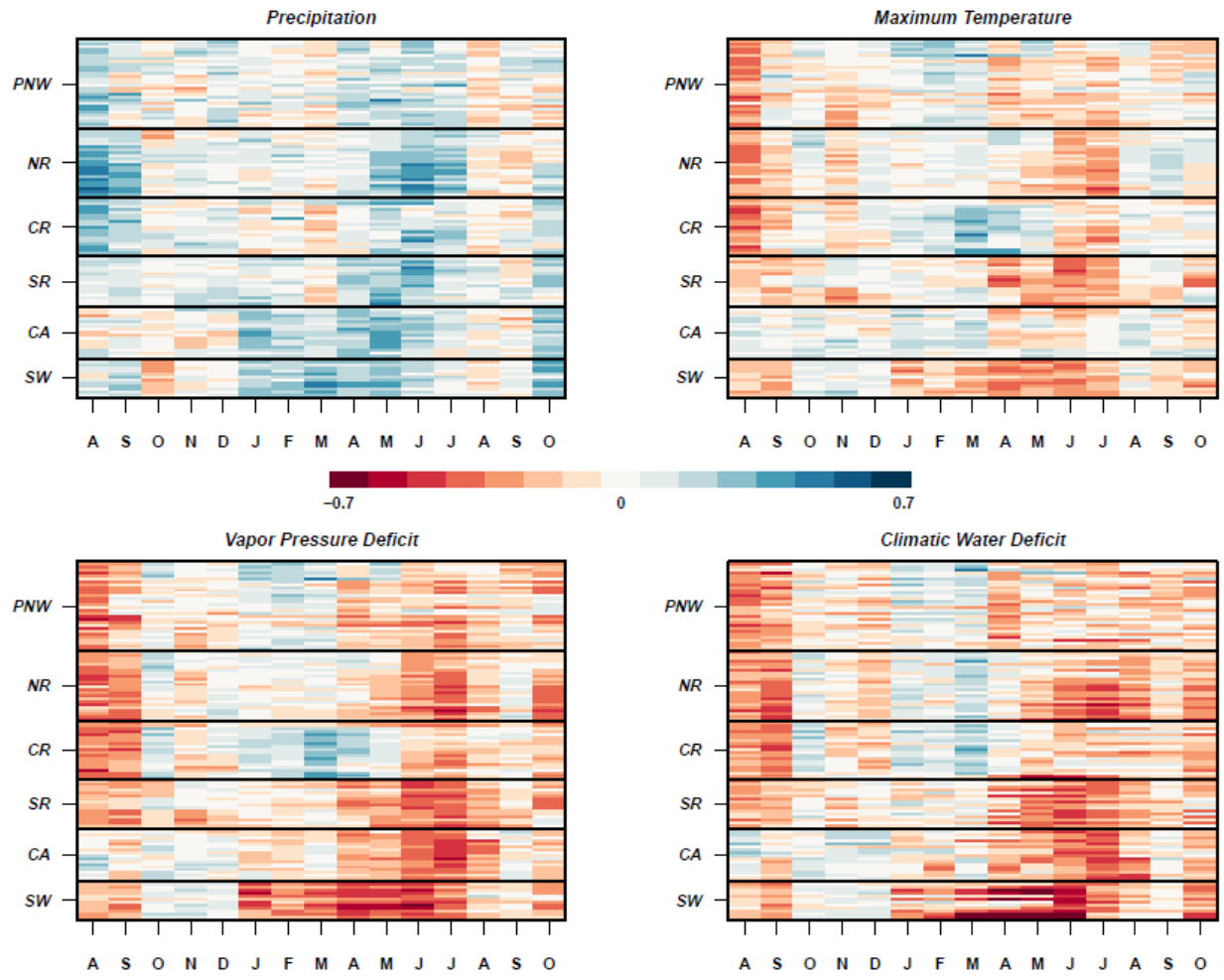

Figure 2.2. Correlations between monthly climate and annual growth at the plot scale. The x-axis denotes months spanning from August of the previous year to October of the current growing season. Plots are ordered within each region from high to low elevation. During the growing season (AMJJ), growth is tightly linked to climate with a strong negative relationship between growth VPD and DEF. PPT and TMP, while significant in the growing season, are less correlated with growth. **PNW** = Pacific Northwest, **NR** = Northern Rockies, **CR** = Central Rockies, **SR** = Southern Rockies, **CA** = California, **SW** = Southwest. Correlation coefficients > 0.2 and < -0.2 are significant at $\alpha = 0.05$.

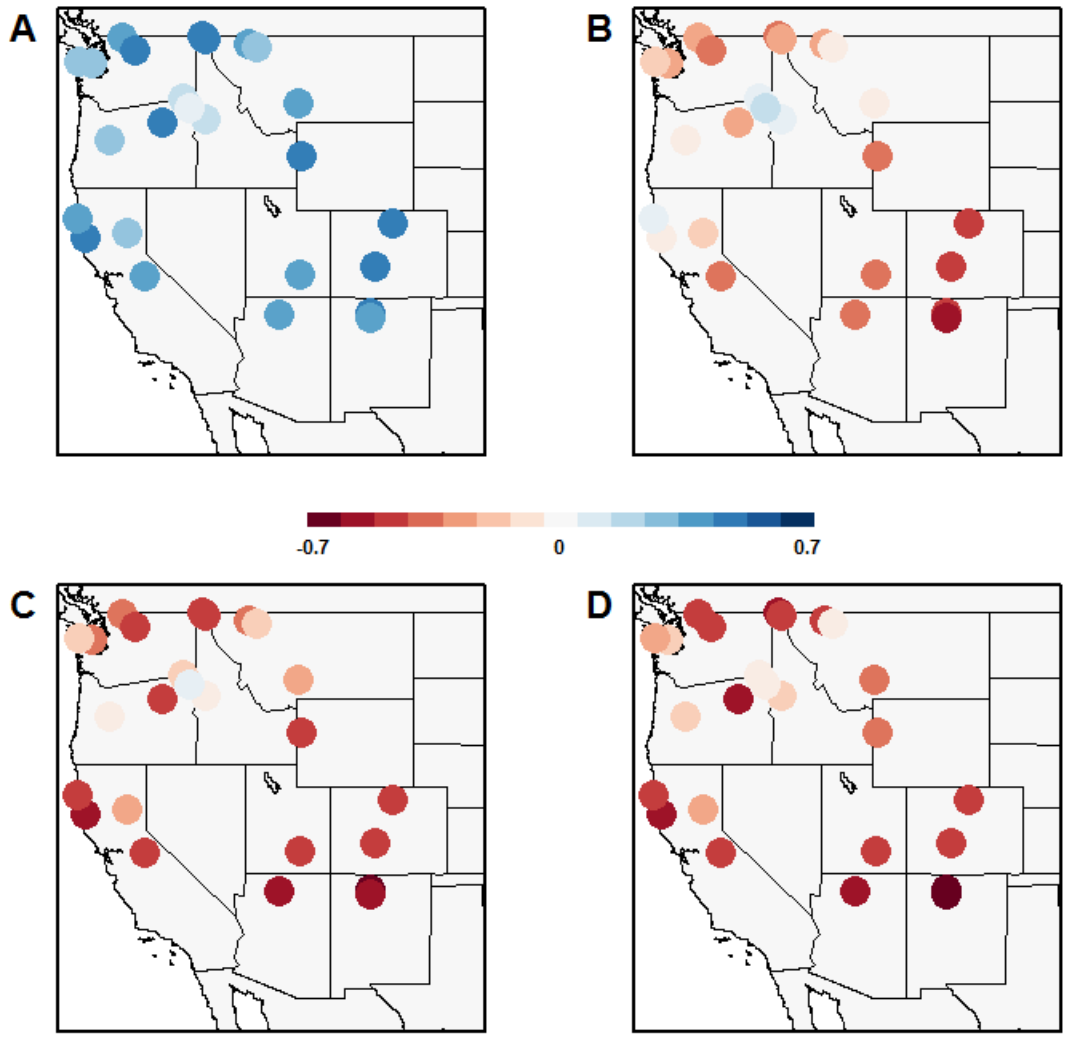

Figure 2.3. Correlations between watershed-scale chronologies and growing season (AMJJ) total precipitation **(A)**, mean maximum temperature **(B)**, total vapor pressure deficit **(C)**, and total climatic water deficit **(D)**. Correlation coefficients > 0.2 and < -0.2 are significant at $\alpha = 0.05$. Correlations between growth and AMJJ climate are stronger than monthly correlations. Panels **C** and **D** show the stronger relationships produced when using plant-relevant variables.

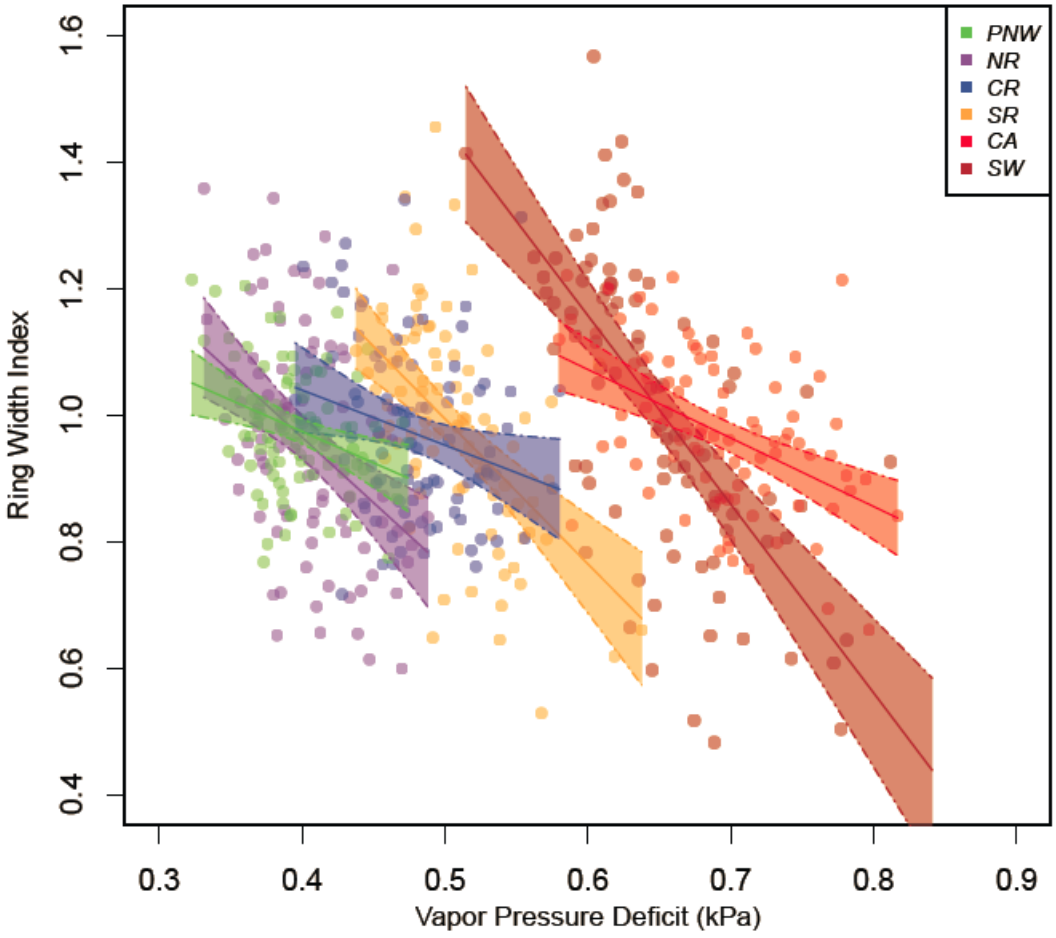

Figure 2.4. Ring width decreases with increasing vapor pressure deficit. Solid lines represent linear regression models with 95% confidence intervals (shaded colors). All slopes are significant: Southwest (SW, $\beta = -2.985$, $p < 0.001$), California (CA, $\beta = -1.084$, $p < 0.001$), Southern Rockies (SR, $\beta = -2.295$, $p < 0.001$), Central Rockies ($\beta = -0.8704$, $p = 0.023$), Northern Rockies ($\beta = -2.068$, $p < 0.001$), Pacific Northwest ($\beta = -0.994$, $p = 0.002$).

5. SUPPLEMENTARY MATERIALS

5.1 Materials and Methods

I used a sampling approach that focused on both the climate space and geographic extent of Douglas-fir. The species range was divided into regions that served as "climate domains," based on an analysis of historical climatic data calculated by the Variable Infiltration Capacity hydrologic model (VIC; Liang et al 1994, Njissen 1997). After summarizing the data in terms of magnitude and timing of precipitation, Douglas-fir distribution was divided into six regions: Pacific Northwest, California, Northern Rockies, Central Rockies, Southern Rockies, and Southwest. The climate domain delineation was verified by Bailey's ecoprovince divisions used nationwide (Bailey 2004), so I feel confident that these regions are representative of climatically distinct zones of the Douglas-fir range. In each region, I selected watersheds and placed plots (within each watershed) on opposing aspects at different elevations to account for topographic complexity.

In each plot, I sampled 15 trees in either dominant or codominant canopy positions, with no signs of pathogens, insects, or injuries. All trees were a minimum of 125 years at breast height; this age threshold was employed to avoid the inclusion of the juvenile portion growth in the time series. I extracted one core from the side-slope of each tree, measured diameter at breast height, and geo-referenced each plot with a handheld Global Positioning System device.

The tree-core data are combined with data from Littell et al. (2008) to create a robust dataset that covers the entire geographic range of Douglas-fir in the United States. To match the sampling density of the new plots in geographic space, I subsampled watersheds in each of their study sites, retaining two watersheds from each sample site and all plots in the chosen watersheds. Instead of a random sample of watersheds, I chose an informed sampling approach

because my sampling strategy was designed to control for non-climatic factors (i.e., elevation, aspect) that may mediate the tree response to climate. I calculated growing season (April-September) water deficit (PET-AET) for each watershed and then graphically compared these curves to other watersheds in the site. This approach allowed me to choose watersheds based on a range of deficit to surplus in growing season months, resulting in paired watersheds of wet vs. dry and/or warm vs. cool. Watersheds whose deficit values differed only slightly were evaluated based on age of trees and temporal resolution.

The distribution of sampled sites in climate space was visualized by plotting the geographic locations of plots based on their respective climatic conditions (fig. S1). I used climate parameters described in Thompson et al (2000), because these specific values define the climatic limits of Douglas-fir distribution. Climate variables are January temperature (C), July temperature (C) and annual precipitation (mm), all derived from VIC model output. Climate space was also visualized using the plant-relevant variables growing season evapotranspiration (mm) and growing season deficit (mm).

I employed standard dendrochronological techniques to measure, detrend, standardize, and "prewhiten" each tree-ring time series (Stokes and Smiley 1968, Fritts 1976, Cook and Kairiukstis 1989). All of the cores were measured using a Velmex sliding stage (precision = 0.001 mm), and crosschecked for errors using COFECHA (Holmes 1999). To account for the geometric bias of ring width imposed by age/size (e.g. larger trees put on narrow rings), I detrended the time series with a cubic smoothing spline for which the frequency response was 0.50 (retained 50% of the variance) at a wavelength equal to 2/3 the length of the series. The cubic smoothing spline is appropriate for a dataset with such a large geographic extent because the curve fit to each series is unique, taking into consideration different ages, competition, and

stand disturbance histories. Detrended time series were then subtracted from the fitted spline to create a ring-width index (RWI), a unit-less metric used as a proxy for annual ring width. Finally, prewhitened (or residual) chronologies were calculated to remove the temporal autocorrelation in each time series by performing autoregressive modeling, with the autoregressive order based on the persistence identified in each time series. The residual chronologies are preferred over raw chronologies for analysis because after detrending, standardization, and prewhitening, the remaining interannual variance can be attributed to climate. For both the standardized and residual chronologies, years were retained only if sampling depth was at least 5 cores.

I developed chronologies at the plot, watershed, and region scales using dplR (Bunn 2008). Plot-scale chronologies were calculated by aggregating tree-scale chronologies with a Tukey's bi-weight robust mean. For the watershed scale, the chronologies were recalculated starting from the individual tree, and followed the same methods used for the plot-scale chronologies for detrending, standardization, and prewhitening. Regional-scale chronologies were calculated as a mean of the watershed-scale chronologies in a given region. To aid in visual interpretations, regional-scale chronologies were also calculated as z-scores which scale all data to a mean of 0 and standard deviation of 1.

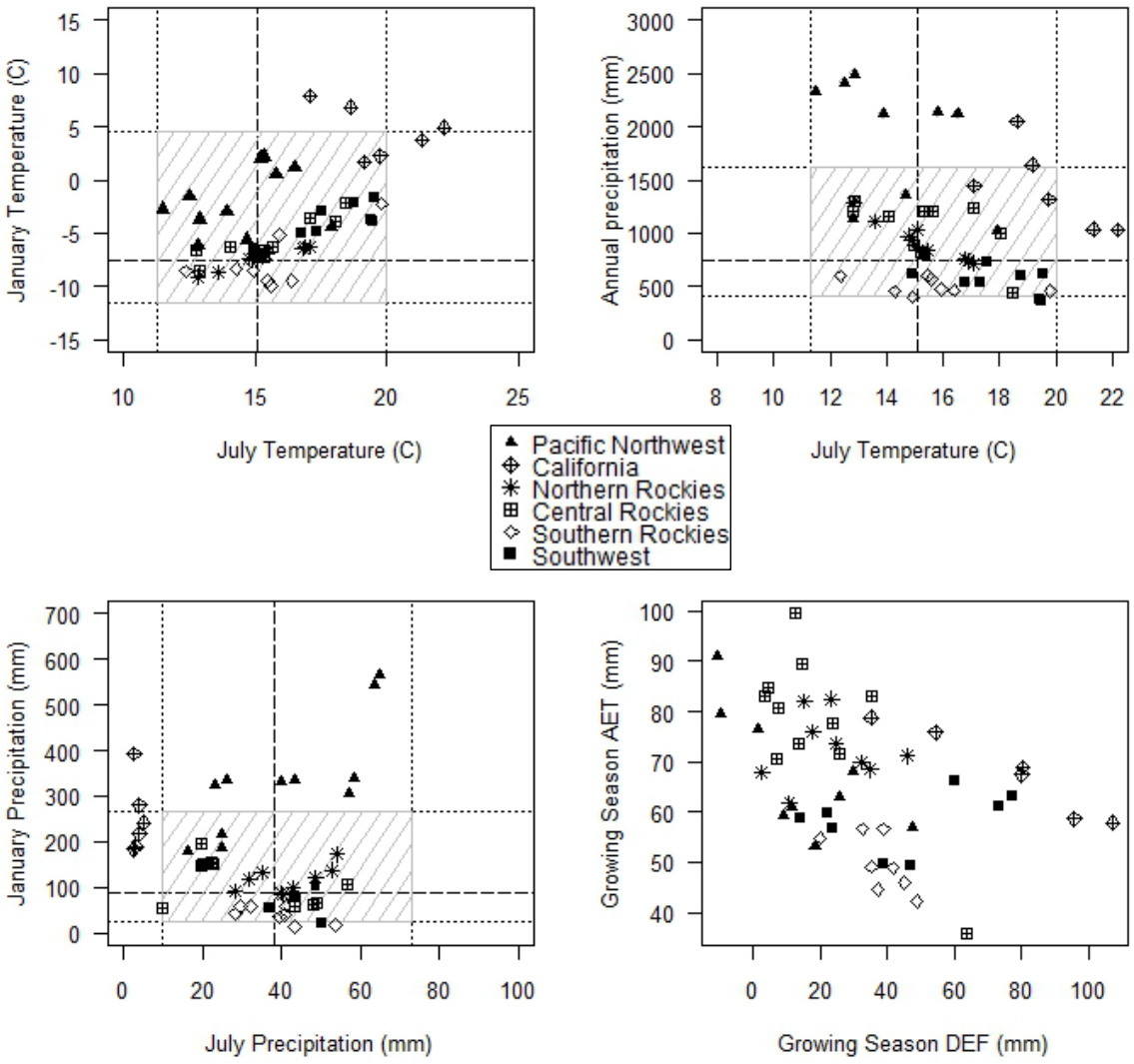

Figure S1. Distribution of sampling sites in climate space. The climatic limits of Douglas-fir (as defined by Thompson et al. 2000) are represented as 10th and 90th (dotted line) and 50th percentiles (dashed line). The hatched box symbolizes the fundamental climate niche of Douglas-fir. Sampling sites are plotted in this climate space based on average values (1916-2006) of the variables indicated. The distribution of sample sites represents the realized climate niche of Douglas-fir.

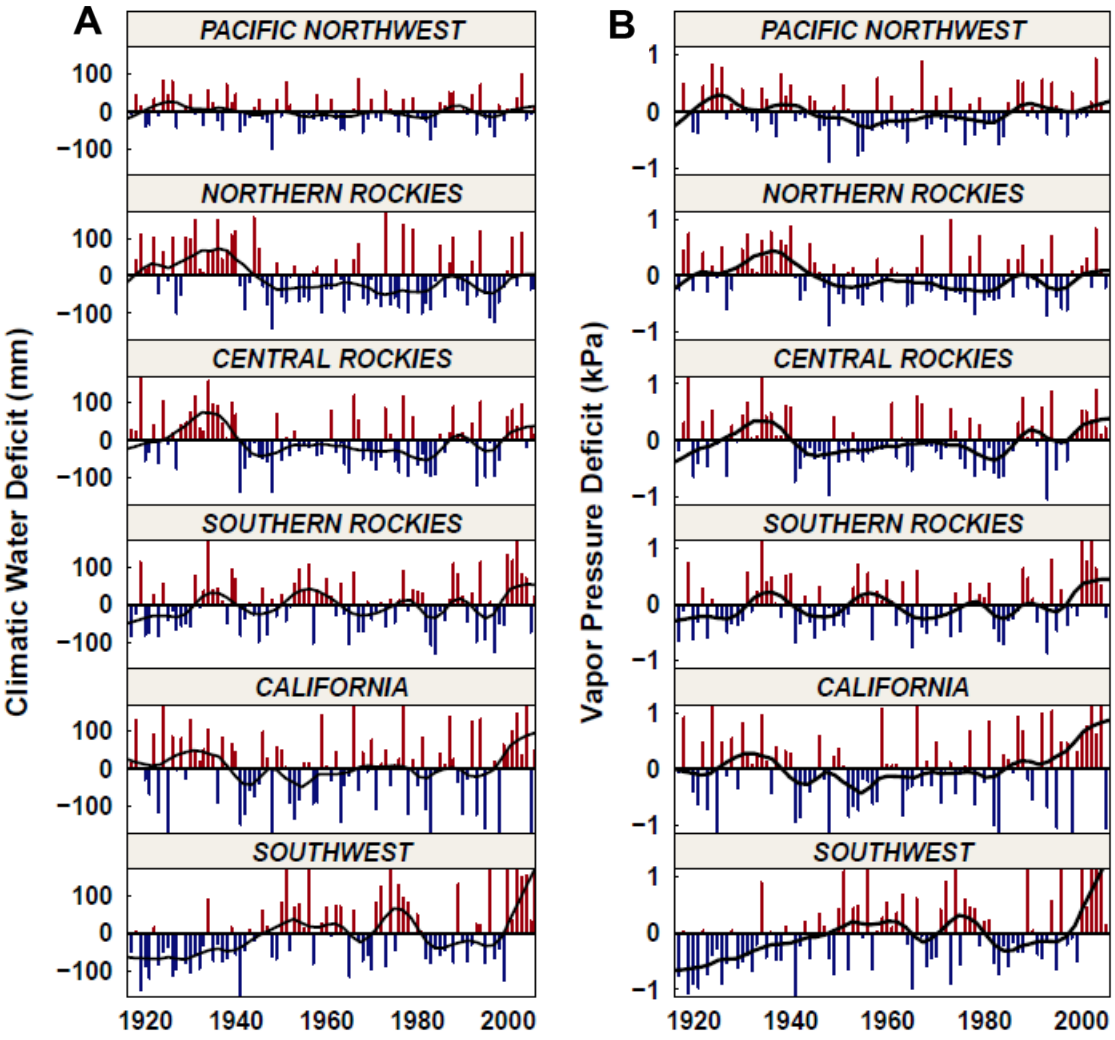

Figure S2. Climatic water deficit **(A)** and vapor pressure deficit **(B)** anomalies. Fitted lines are loess smoothed curves with a 13-year segment length. Interannual variability is lowest in the Pacific Northwest and increases towards the Southwest. Recent increases are most evident in the more southerly regions.

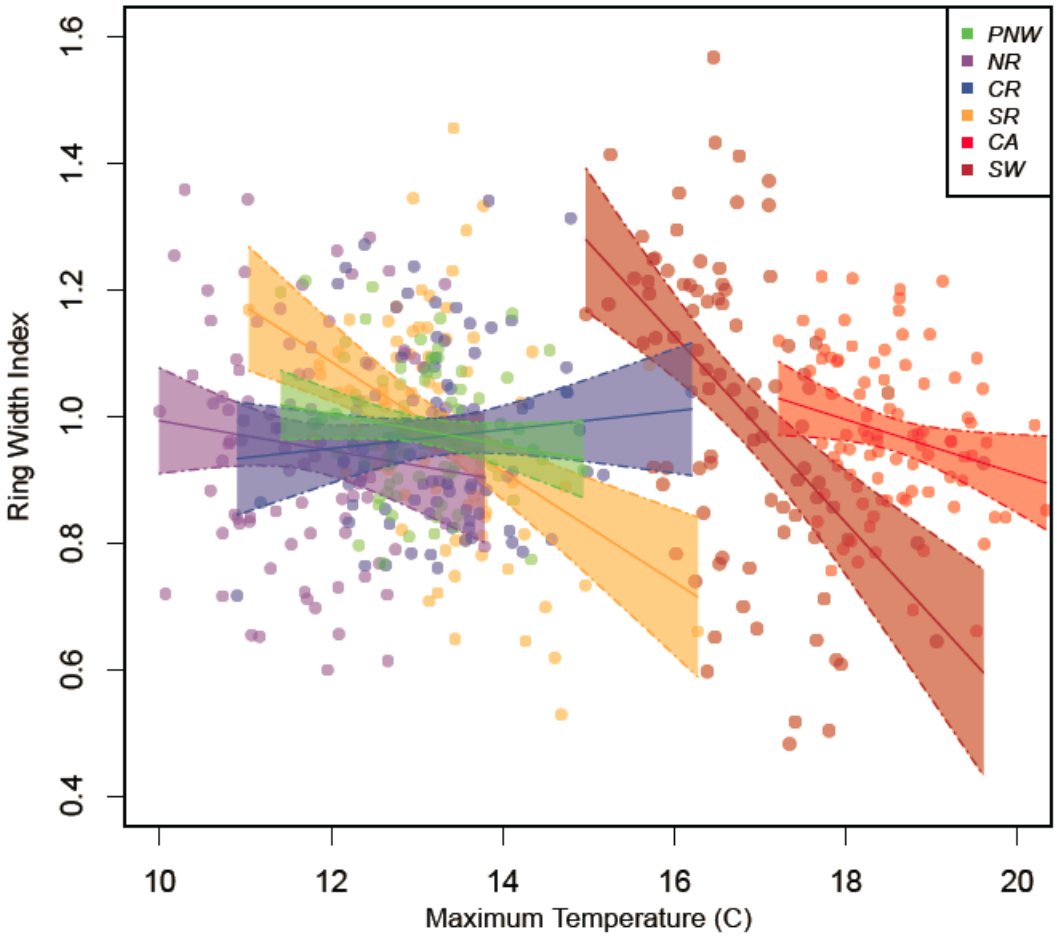

Figure S3. Temperature alone decreases tree growth only in the southern latitude regions. Solid lines represent linear regression models with 95% confidence intervals (shaded colors). Only southern latitude slopes are significant: Southwest (SW, $\beta = -0.147$, $p < 0.001$), California (CA, $\beta = -0.043$, $p = 0.032$), Southern Rockies (SR, $\beta = -0.087$, $p < 0.001$), Central Rockies ($\beta = 0.015$, $p = 0.403$), Northern Rockies ($\beta = -0.024$, $p = 0.302$), Pacific Northwest ($\beta = -0.024$, $p = 0.116$).

Table S1. Locations and mean annual climate parameters for all study watersheds. ELEV = elevation, PPT = precipitation, TMAX = maximum temperature, TMIN = minimum temperature.

Region	State	# of trees	Property Name	Latitude	Longitude	ELEV (m)	Annual PPT (cm)	Annual TMAX (C)	Annual TMIN (C)
Pacific Northwest	Washington	76	North Cascades National Park	48.94038	-121.40010	1048	197	10.0	1.1
Pacific Northwest	Washington	70	Olympic National Park	47.74623	-123.20605	1031	188	10.5	2.3
Pacific Northwest	Washington	72	Olympic National Park	47.82603	-123.99620	531	337	14.0	4.9
Pacific Northwest	Washington	67	North Cascades National Park	48.30747	-120.65660	989	106	11.5	1.2
Pacific Northwest	Oregon	85	HJ Andrews Experimental Forest	44.23159	-122.13355	1179	235	13.7	3.0
Northern Rockies	Montana	81	Glacier National Park	48.58777	-113.88410	1323	87	10.4	-1.6
Northern Rockies	Montana	68	Glacier National Park	48.49320	-113.35914	1727	101	8.7	-1.4
Northern Rockies	Idaho	70	Idaho Panhandle National Forest	48.98723	-116.62731	1177	84	10.7	0.7
Northern Rockies	Idaho	71	Idaho Panhandle National Forest	48.82964	-116.46036	1258	89	10.5	1.0
Central Rockies	Idaho	72	Payette National Forest	45.13659	-116.41832	1911	120	10.3	-2.2
Central Rockies	Montana	92	Gallatin National Forest	45.87449	-110.89657	1986	71	10.0	-3.2
Central Rockies	Oregon	31	Umatilla National Forest	44.99897	-118.98660	962	43	16.6	1.3
Central Rockies	Oregon	74	Wallowa-Whitman National Forest	45.71603	-117.40513	1689	130	10.4	0.5
Southern Rockies	Wyoming	83	Bridger-Teton National Forest	43.48059	-110.70658	2300	69	10.0	-3.3
Southern Rockies	Colorado	89	Gunnison National Forest	38.44524	-106.36330	2988	65	10.0	-4.6
Southern Rockies	Colorado	59	Roosevelt National Forest	40.42530	-105.32592	2145	47	14.8	0.9
California	California	72	UC Angelo Reserve	39.72647	-123.63349	527	209	19.5	5.6
California	California	57	BLM Headwaters Reserve	40.64037	-124.07719	485	150	18.6	7.5
California	California	91	Plumas National Forest	39.94591	-121.09904	1405	117	17.6	3.6
California	California	41	Stanislaus National Forest	37.97359	-120.07321	1282	111	18.9	5.2
Southwest	Arizona	40	Grand Canyon National Park	36.24806	-112.04188	2526	65	14.2	-0.2
Southwest	New Mexico	74	Valles Caldera National Preserve	35.98106	-106.59204	2850	69	11.7	-1.1
Southwest	New Mexico	30	Chama River Wilderness	36.27471	-106.61508	2424	52	15.2	1.7
Southwest	Utah	43	Henry Mountains	38.06987	-110.79483	2920	73	11.0	-2.0

6. APPENDICES

Appendix 2.1. Pearson's correlation coefficients between monthly precipitation and watershed-scale chronologies. Correlation coefficients > 0.2 and < -0.2 are significant at $\alpha = 0.05$.

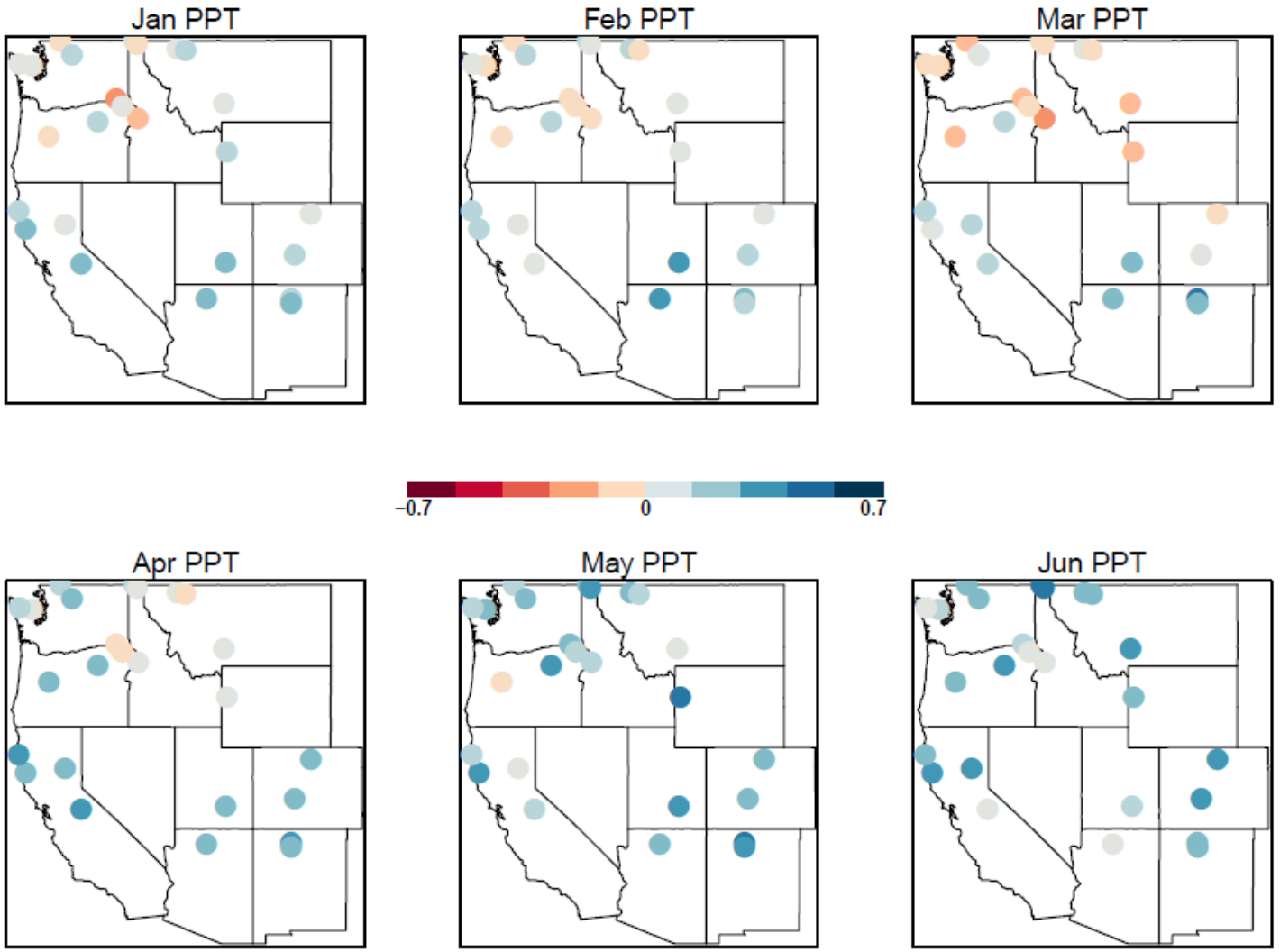

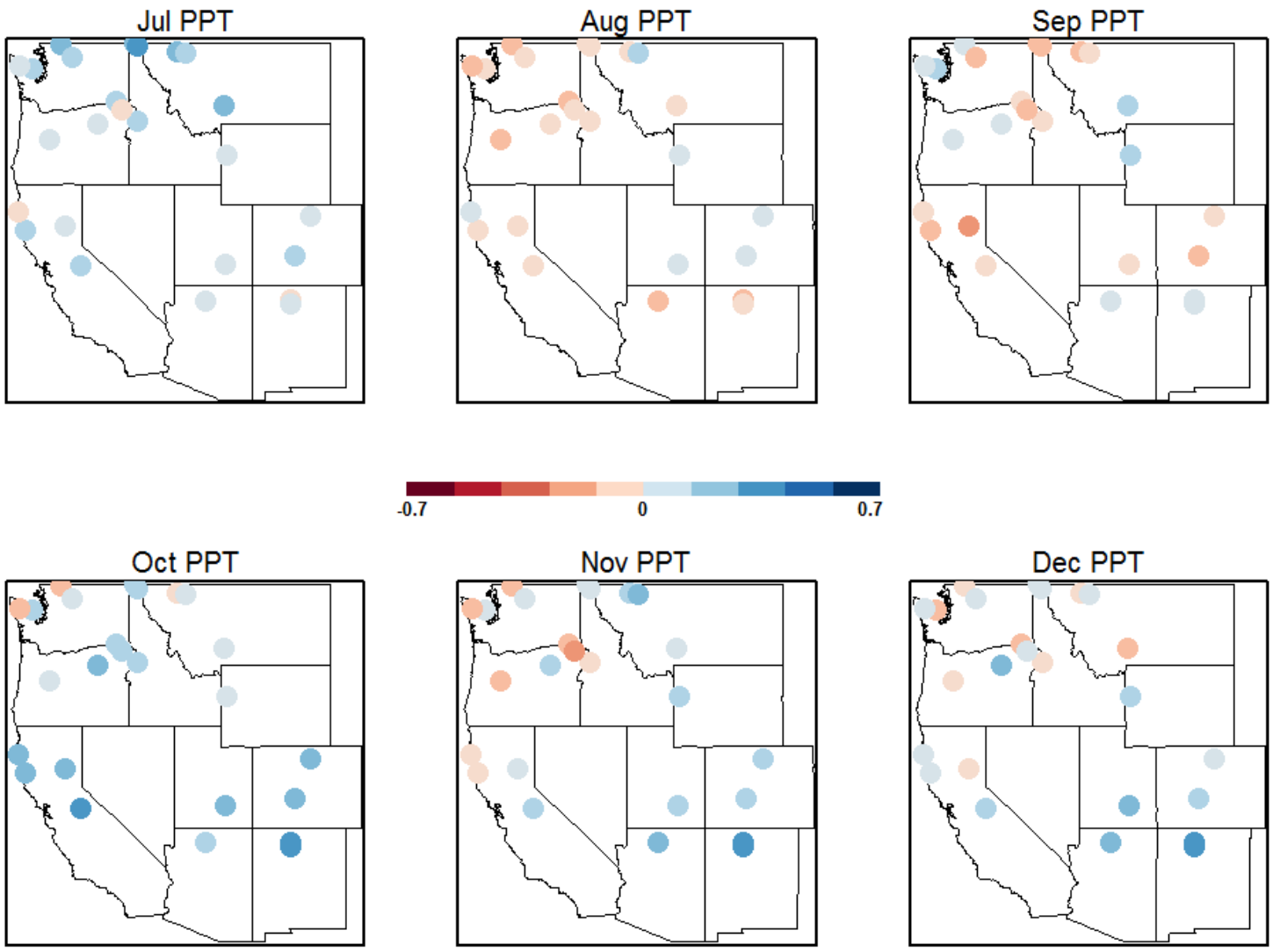
Jul PPT
Aug PPT
Sep PPT
-0.7
0
0.7
Oct PPT
Nov PPT
Dec PPT

Appendix 2.2. Pearson's correlation coefficients between monthly maximum temperature and watershed-scale chronologies. Correlation coefficients > 0.2 and < -0.2 are significant at $\alpha = 0.05$.

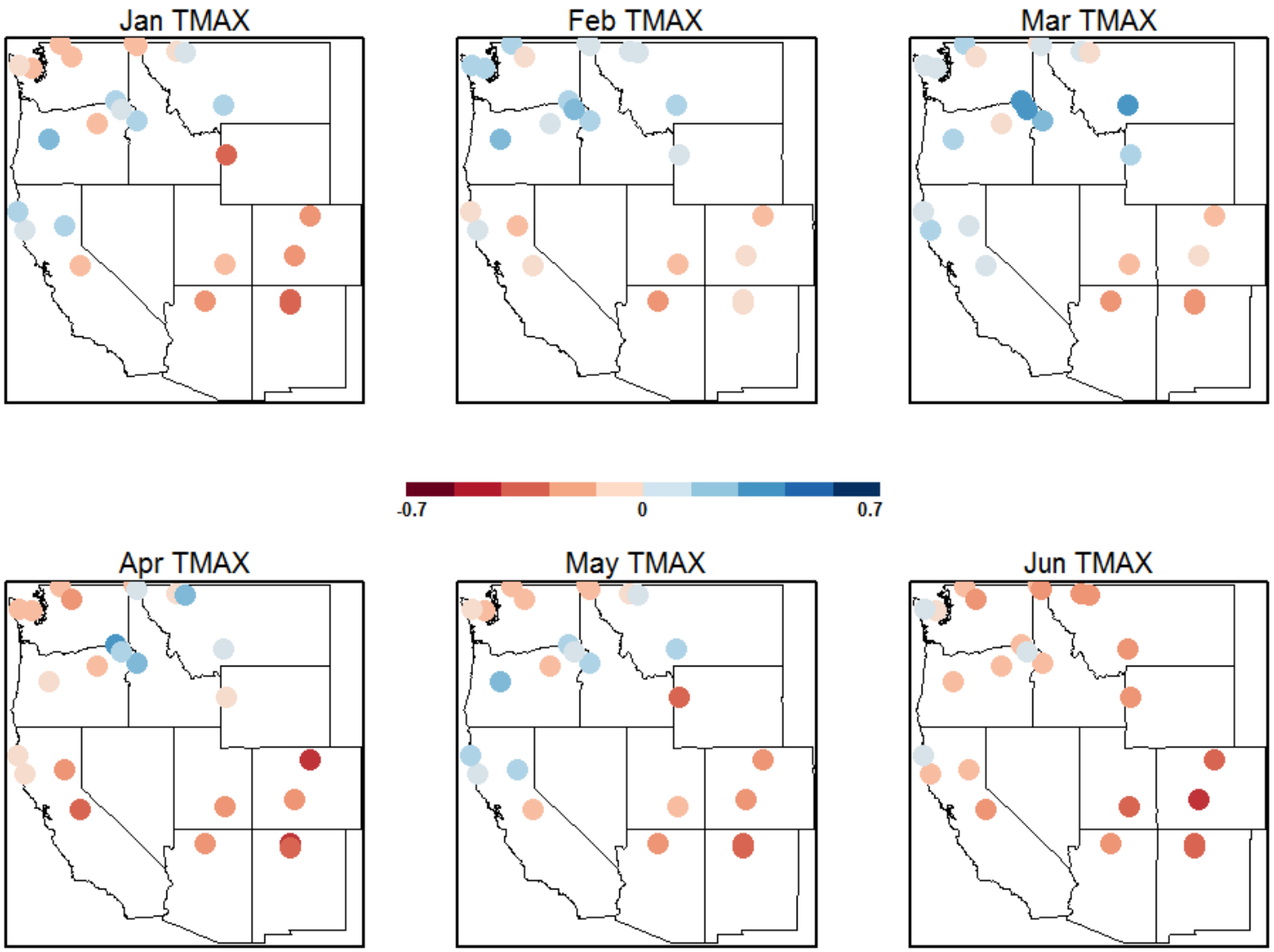

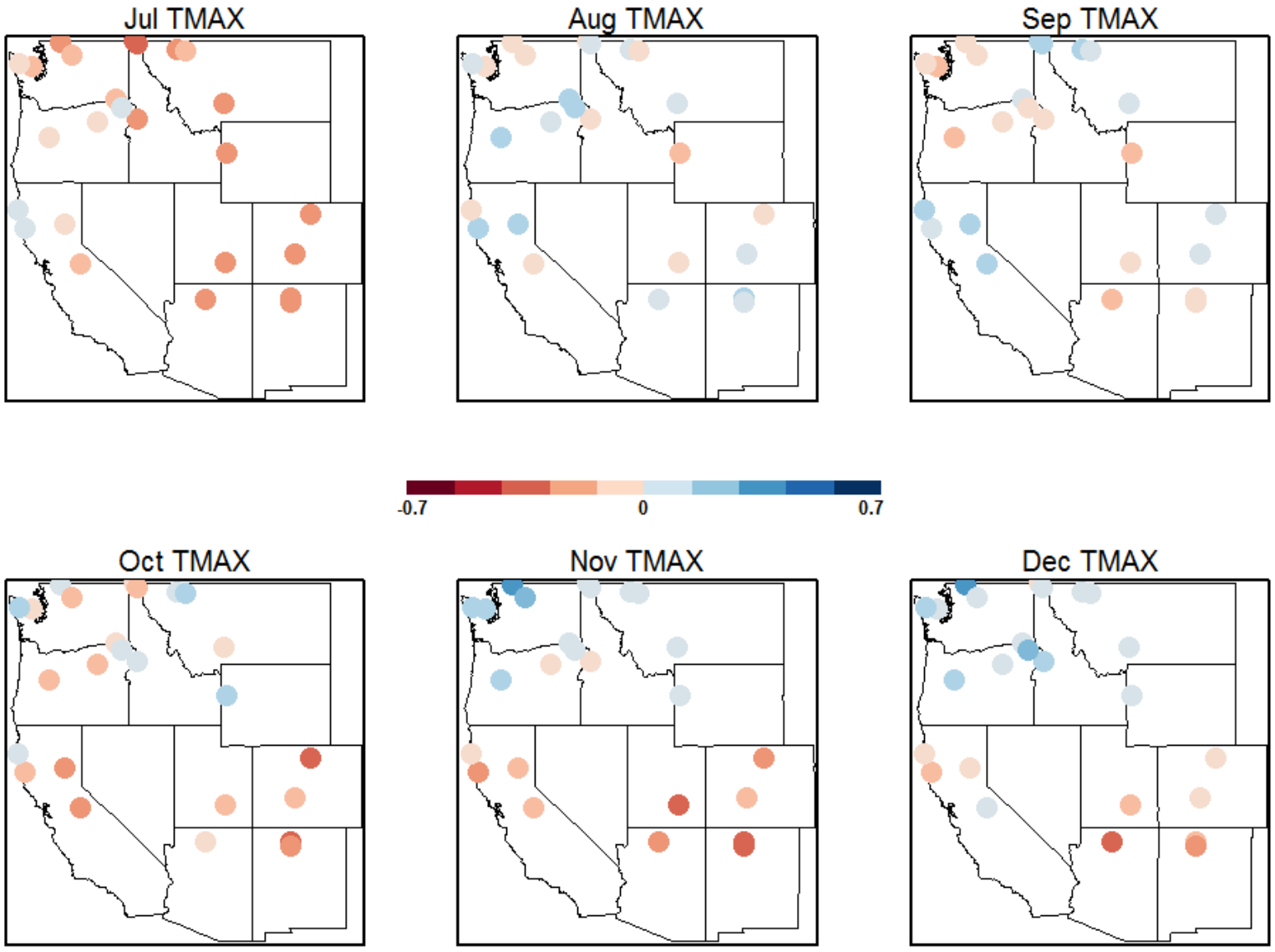
Jul TMAX
Aug TMAX
Sep TMAX
-0.7
0
0.7
Oct TMAX
Nov TMAX
Dec TMAX

Appendix 2.3. Pearson's correlation coefficients between monthly climatic water deficit and watershed-scale chronologies. Correlation coefficients > 0.2 and < -0.2 are significant at $\alpha = 0.05$.

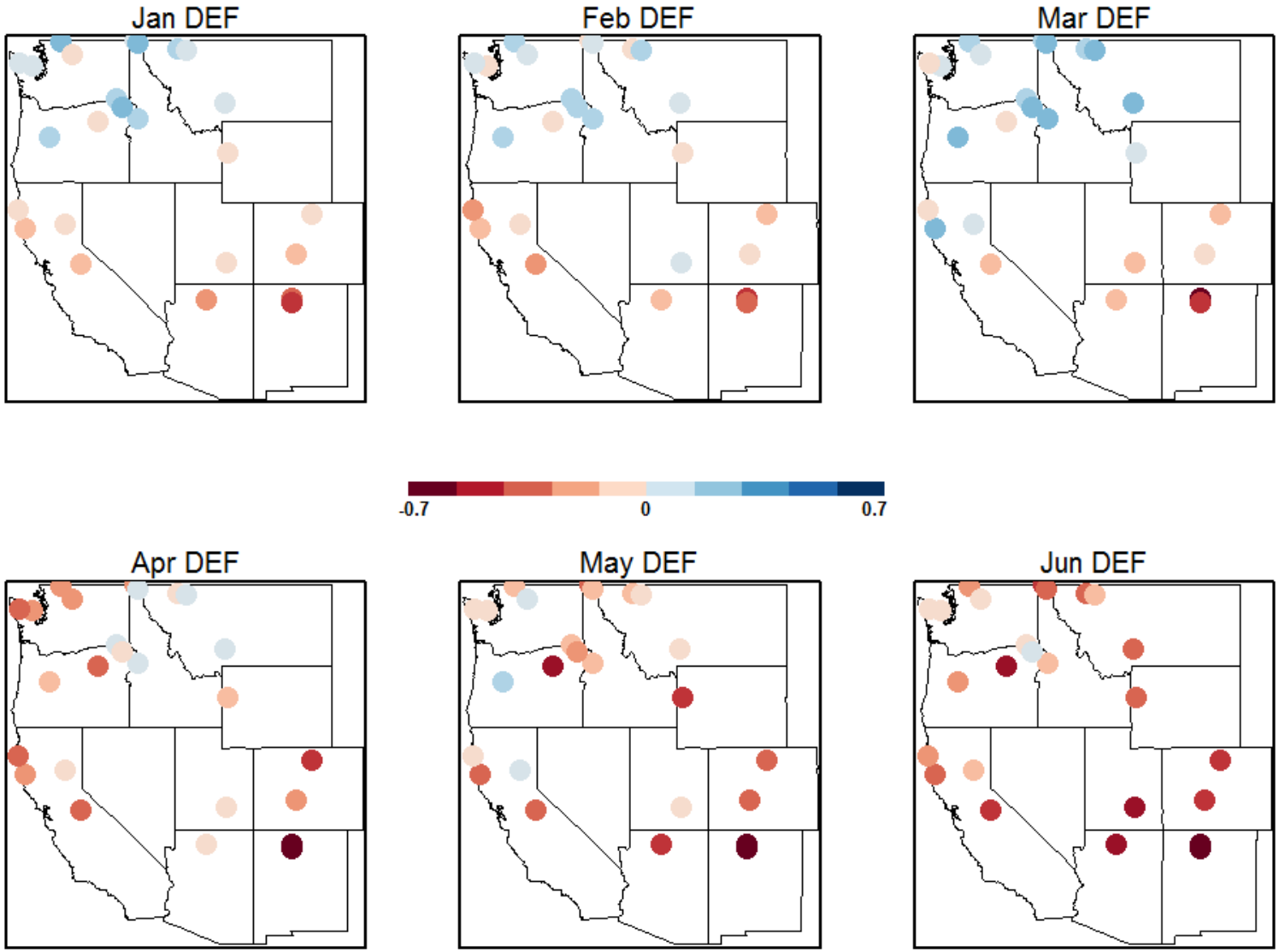

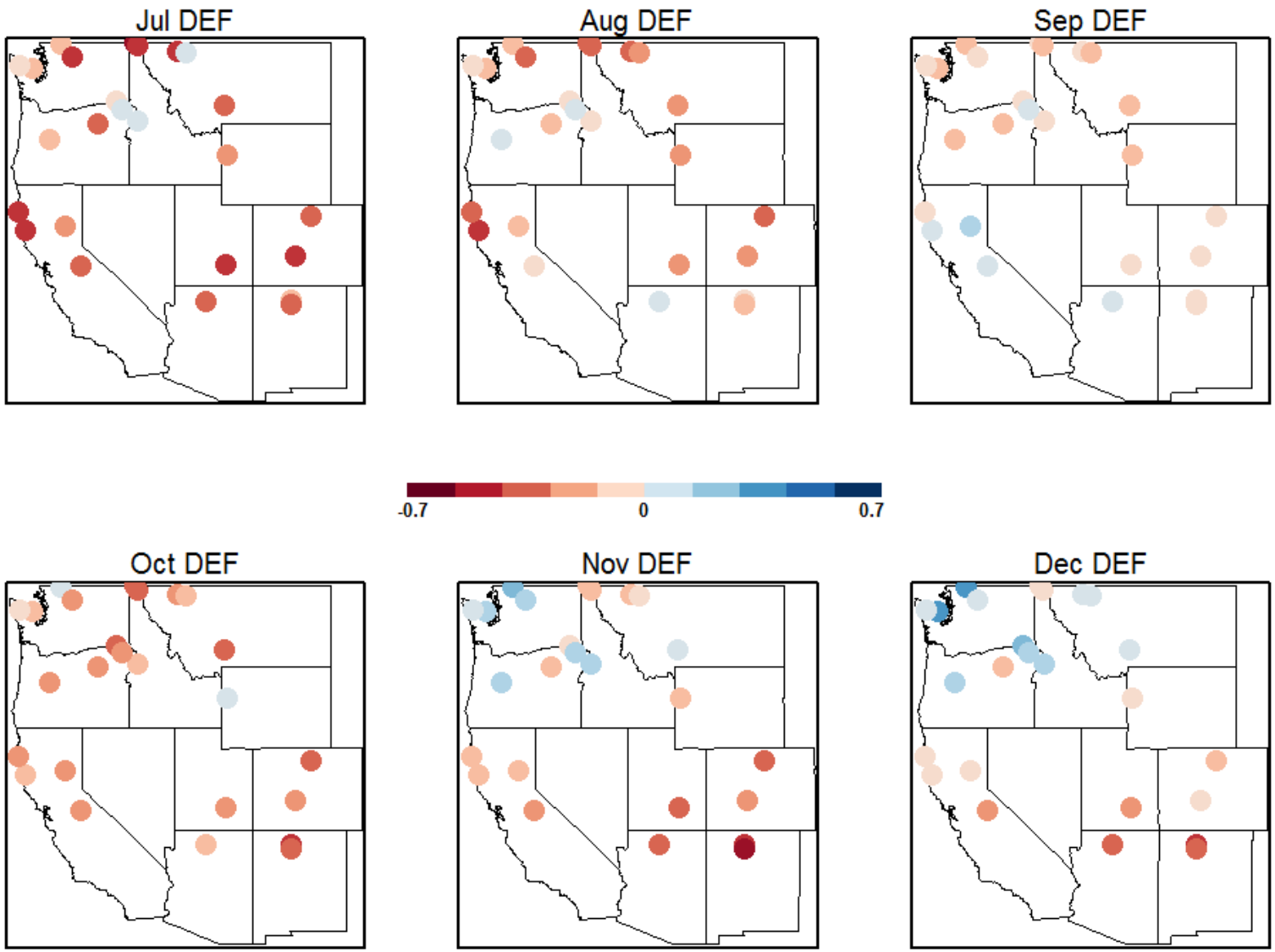
Jul DEF
Aug DEF
Sep DEF
-0.7
0
0.7
Oct DEF
Nov DEF
Dec DEF

Appendix 2.4. Pearson's correlation coefficients between monthly vapor pressure deficit and watershed-scale chronologies. Correlation coefficients > 0.2 and < -0.2 are significant at $\alpha = 0.05$.

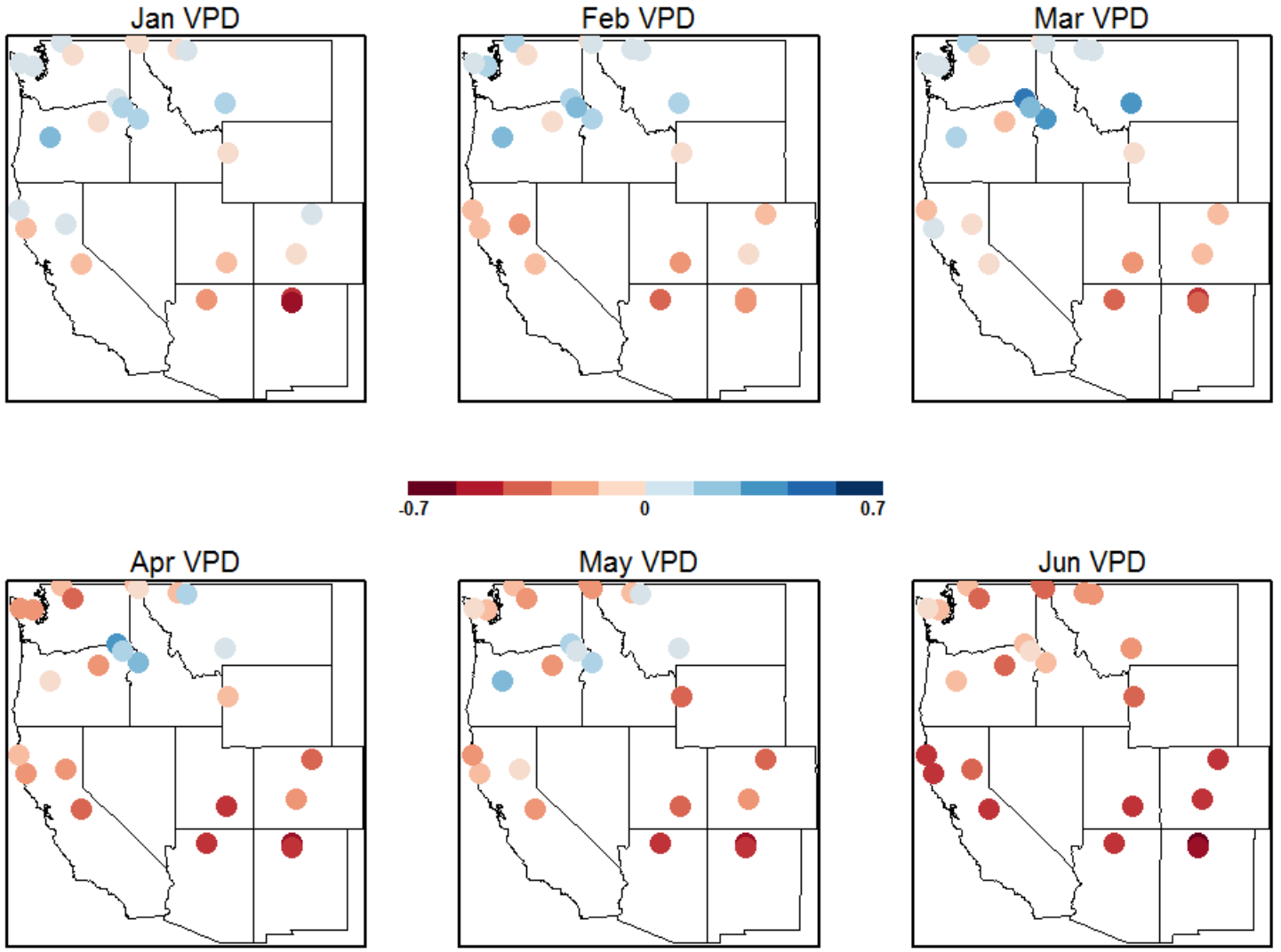

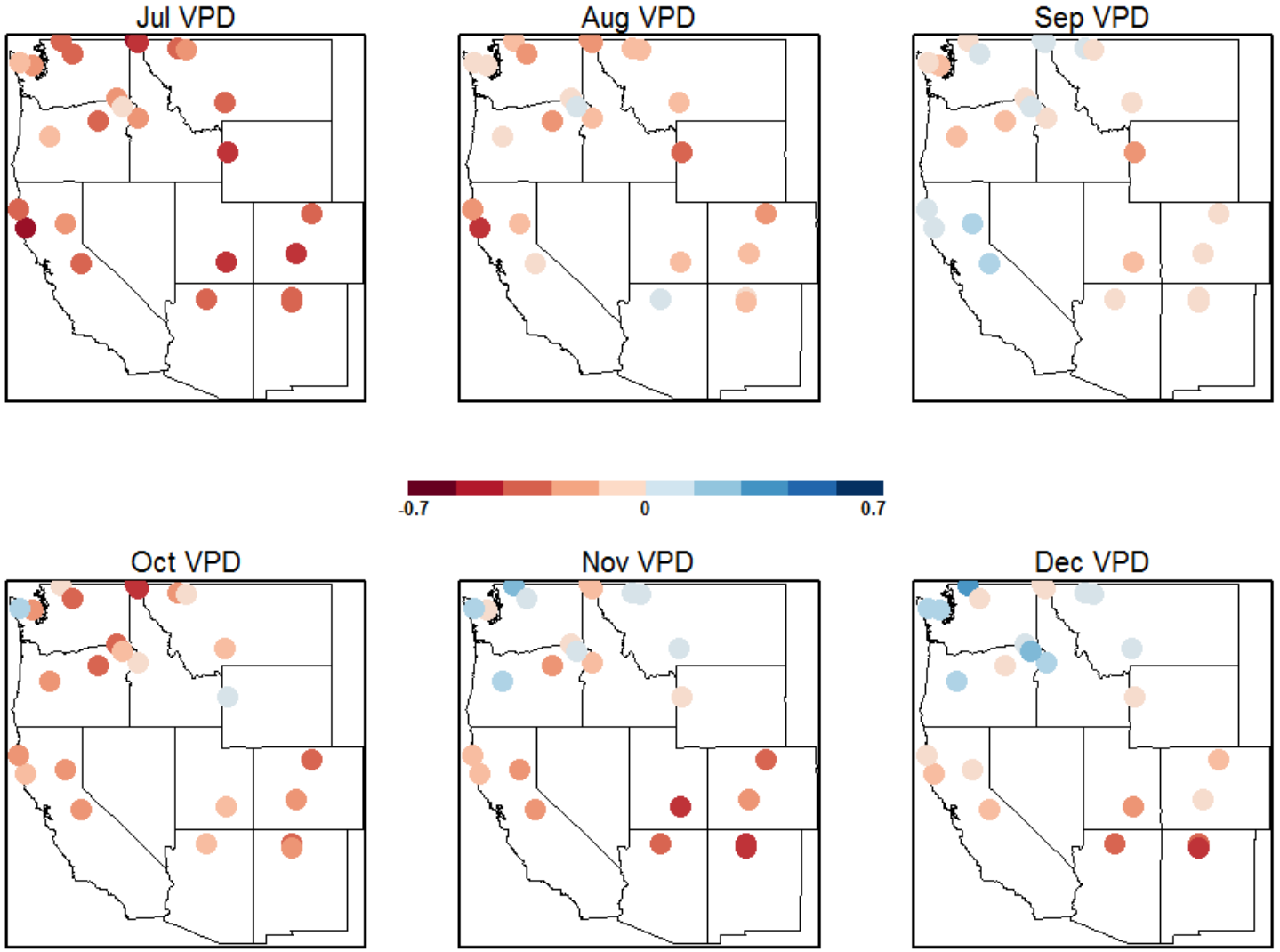
Jul VPD
Aug VPD
Sep VPD
-0.7
0
0.7
Oct VPD
Nov VPD
Dec VPD

Chapter 3

ENSO and PDO modify tree growth in Douglas-fir forests of the western United States

1. ABSTRACT

Large-scale patterns of moisture availability in the western United States are driven by variation in atmosphere-ocean circulation patterns, and these changes in moisture availability can be seen in inter-annual to decadal variability in tree rings. The direct link between climate teleconnections and variations in tree growth is difficult to decipher because the cause-and-effect relationship is obfuscated by the many temporal and spatial scales in which climate regulates plant communities. I quantified how climate teleconnections modify regional climate patterns that ultimately limit tree growth. Using principal components, superposed epoch, and cross-wavelet analyses, I first quantify how the El Niño Southern Oscillation (ENSO) and Pacific Decadal Oscillation (PDO) affect regional climate and tree growth. A spatially comprehensive network of Douglas-fir tree-ring data across the entire species range in the western United States is then used to represent tree growth response. Temperature and precipitation data from the Variable Infiltration Capacity Hydrologic Model were used to assess departures from the mean during ENSO events and warm and cool phases of the PDO. ENSO-related climatic variability manifests differently in northern and southern latitudes of North America based on the amplification or dampening of the Polar and Pacific jet streams, resulting in a "dipole" effect where opposite effects of warm and cool ENSO phases are observed to the north or south. Proximity to the dipole dictates the relative effect of ENSO events from region to region, and the strength and location of the dipole changes when ENSO and PDO are in phase. During El Niño

events, precipitation is significantly higher in the Southwest and lower in the Pacific Northwest; the converse is true for La Niña events. Temperature is significantly higher during El Niño events across all regions except in the Southwest. ENSO- and PDO-related changes in regional climate result in increased variability and extremes in tree growth. Changes in tree growth are synchronous with ENSO across all regions, but the strongest response is at the extreme ends of the dipole. Cross-wavelet analysis demonstrates a non-stationarity in the climate-growth response to ENSO, in which wavelet-coherence has increased in recent decades. This non-stationarity is attributed to warmer air temperatures in recent decades and the amplification of ENSO events during a warm phase PDO. Results suggest that Douglas-fir trees are sensitive to climate drivers that occur at the broadest scales (continental to global) where regional climatic variability is modified by atmospheric-ocean circulation patterns.

2. INTRODUCTION

The El Niño Southern Oscillation (ENSO) and Pacific Decadal Oscillation (PDO) are cyclical, inter- and multi-decadal modes of climatic variability that modify climate at local to regional scales. Extremes in ENSO, in particular, are known to cause variability in cool-season precipitation that can result in either widespread drought or flooding. In extreme dry years, drought (Piechota and Dracup 1996), decreased tree growth (Woodhouse 1993, Rigozo et al. 2002), and increased wildfire activity are attributed to ENSO events (Schoennagel et al. 2005), and the converse is true for extreme wet years. The PDO has fewer extreme events, but instead operates at 20-30 year cycles and provides background changes in temperature and precipitation that can amplify the shorter ENSO cycles. Warm phases of the PDO have been linked to altered

precipitation patterns (Dettinger et al. 1998), decreased streamflow (Mantua and Hare 2002), and wildfire occurrence (Heyerdahl et al. 2002, Hessl et al. 2004).

Variations in ENSO are caused by changes in the strength of trade winds and atmospheric pressure, and consequently the location of warm sea surface temperatures in the equatorial Pacific Ocean (Diaz et al. 2001, McPhaden et al. 2006). A dampening of the easterly trade winds causes a concentration of warm water in the western equatorial Pacific Ocean to move eastward and occupy a larger area of the ocean surface. This movement of warm water is characteristic of an "El Niño" event and shifts the location of thunderstorm development, which brings anomalously high precipitation to areas in the Southern Hemisphere and the southwestern United States (Vinnikov et al. 1996, Smith and Sardushmekh 2000). A "La Niña" event is characterized by the opposite effect, in which warmer sea surface waters are pushed westward in the equatorial Pacific Ocean, resulting in a westerly concentration in thunderstorm development.

In western North America, El Niño and La Niña events modify climate to varying degrees, with the strongest effects presented on the extreme ends of the ENSO "dipole." The dipole phenomenon arises due to variability in pressure systems off of western North America that modify the location and persistence of the Polar Jet Stream and the amplification or dampening of the Pacific Jet Stream from the warmer waters in the equatorial Pacific. During La Niña events, a high pressure blocking system in the northern Pacific Ocean forces the Polar Jet Stream north and the Pacific Jet Stream also moves northward resulting in moist cool air reaching northern latitudes of western North America with minimal moisture delivered to southern latitudes. During El Niño events, a low pressure system in the northern Pacific Ocean brings warm dry air via the Polar Jet Stream to northern latitudes and wet cool air to the southern latitudes via a persistent, extended Pacific Jet Stream. Different (almost opposite) climate arises

in northern and southern latitudes as a result of the changes in these atmospheric circulation patterns, creating a dipole. The location and strength of the dipole are transient (40°N - 42°N) and more pronounced when ENSO and other climate teleconnections are in sync (Cole and Cook 1998, Wise 2010; Figure 3.1). The strongest ENSO-related climate responses (especially precipitation) have been observed in the Southwest (where El Niño brings higher winter precipitation) and Pacific Northwest (where La Niña brings higher winter precipitation; Brown and Comrie 2004, Wise 2010). The effects of ENSO on climate in the transitional zones of the dipole (e.g. the central and southern Rocky Mountains and eastern Oregon) of the western United States are less clear.

The mechanisms that drive the PDO are still under investigation, but the multi-decadal variability it imposes on climate is evident in historical records of precipitation, temperature, tree growth, and fisheries (Mantua et al. 1997, Zhang et al. 1997). The PDO is mathematically represented by the first principal component of sea surface temperatures in the equatorial Pacific and is characterized by warm and cool phases similar to ENSO (Davis 1976, Mantua et al. 1997). It is hypothesized that PDO is not governed by clear processes (like ENSO) but instead is a response to a dynamically changing system that involves ocean circulation anomalies, changes in sea level pressure of the Aleutian low, and forcing by ENSO that is manifest in the readjustment of the Pacific Ocean via Rossby waves (Newman et al. 2003, Schneider and Cornuelle 2005). The PDO is known to modulate the ENSO (Gershunov and Barnett 1998), as evidenced by changes in the location of the dipole and strength of ENSO influence when both oscillations are in phase (Wise 2010; Figure 3.2).

Climate projections regarding the dynamism between increased atmospheric temperatures and ENSO events are uncertain (Zelle et al. 2005, Guilyardi et al. 2009). ENSO events manifest

via changes in sea surface temperatures, strength of the easterly trade winds, and thermocline gradients in the equatorial Pacific Ocean. One or all of these oceanic and atmospheric components are projected to change to some degree in response to a changing climate, although it is unclear if these processes will be dampened or accelerated (McPhaden et al. 2006, Collins et al. 2010). The direction of change in any mechanism responsible for ENSO will have implications for atmosphere-ocean feedbacks that ultimately modify climate and local weather patterns. Effects of climate change on the PDO are even less clear, because the mechanisms causing the phenomenon are uncertain.

It is well established that tree growth responds to climatic variability from interannual to decadal time scales (Littell et al. 2008, Chen et al. 2010). Dominant conifer species in western North America are sensitive to variation in winter and growing season temperatures (Case and Peterson 2005), seasonal variation in moisture availability (Watson and Luckman 2002, Griesbauer and Green 2010a, Griesbauer and Green 2010b), and prolonged periods of drought stress (Williams et al. 2013). Because ENSO events modify cold-season precipitation, it is suggested that ENSO indirectly affects tree growth at decadal time scales and that the frequency of these events can be seen in tree-ring time series. Consequently, tree-ring time series have been used to reconstruct ENSO beyond instrumental records (Stahle et al. 1998, D'Arrigo et al. 2005), although the implication of variability in ENSO intensity and frequency on tree growth has not been fully explored. The effects of ENSO and PDO on tree growth are difficult to explore because climate-growth relationships at inter-decadal scales are inherently non-stationary, causing significant correlations to be masked by frequent periods of non-significance.

In this study, I investigate the presence of climate-growth relationships at inter-decadal scales in Douglas-fir (*Pseudotsuga menziesii*) tree-ring chronologies distributed throughout the

western United States. I hypothesize that large-scale climate teleconnections modify regional climate patterns that ultimately limit tree growth. I test whether anomalous climatic conditions that arise during ENSO events, especially when these events occur in phase with PDO, result in extreme highs and lows in growth, using a spatially extensive database of Douglas-fir tree-ring chronologies. The data are stratified in six distinct regions that represent the dominant climate experienced by forests in the western United States: mediterranean (Sierra Nevada), maritime (Olympic Mountains, Coast Range), transitional (North Cascades), continental (Rocky Mountains), and monsoonal (Colorado Plateau). I further explore the effects of ENSO on tree growth by analyzing patterns in the frequency domain of both tree-ring and ENSO time series. Climate-growth relationships are interpreted in the context of how climatic variability and change may affect Douglas-fir growth in future decades.

3. METHODS

3.1 Climate Data

El Niño Southern Oscillation (ENSO) event years ("El Niño" and "La Niña") were calculated based on the "Best" index (Smith and Sardeshmukh 2000), which combines values from the Southern Oscillation Index (SOI) and Niño 3.4, creating a robust metric that integrates both departures in sea surface temperatures (Niño 3.4) and atmospheric processes (SOI). El Niño and La Niña years are determined by periods when both the SOI and Nino 3.4 are in agreement. Here I use only extreme conditions ($\pm$ 1.28 °C) as event years, as defined by 5-month running means (Table 3.2). Because events usually span a winter season, event years are denoted as latter year (e.g., if the event took place in the winter of 1982-1983, 1983 is marked as

the event year). A list of ENSO events is provided in Table 3.2. I calculated winter "Best" Index values as an average of Oct–Mar 1-month means.

Pacific Decadal Oscillation (PDO) index values were obtained from the University of Washington Climate Impacts Group (Mantua et al. 1997, Zhang et al. 1997) (http://jisao.washington.edu/pdo). Cool (1890 -1924 and 1947-1976) and warm phases (1925-1946 and 1977-mid 2000s) were defined by Mantua et al. (1997). It is presumed that we are currently in a cool phase of the PDO that began in the mid-2000s.

Temperature and precipitation data were extracted from the Variable Infiltration Capacity Hydrologic Model (VIC; Liang et al. 1994, Njissen et al. 1997) for our study sites only. Historical VIC data are derived from a combination of Historical Climate Network observations and weather stations. VIC data is calculated at 1/16 degree (6 km^2) resolution, and is interpolated to individual coordinates using adjustments based on elevation. Available data encompass a 91-year period (1916-2006). Annual temperature (°C) and precipitation (cm) anomalies were calculated as annual deviations from the mean time series length (1916-2006), and were summarized at the regional scale.

3.2 Tree growth data

I created a comprehensive network of 122 Douglas-fir tree-ring chronologies (23 sites, 1700 trees) that encompass distinct climate regimes in dominant mountain ranges of the western United States (Restaino et al. *in preparation*) (Figure 3.1, Table 3.1). The species range was divided into six regions. The regions are (1) Pacific Northwest (PNW), (2) California (CA), (3) Northern Rockies (NR), (4) Central Rockies (CR), (5) Southern Rockies (SR), and (6) Southwest (SW). In each region, sample watersheds were chosen and plots were placed within each

watershed on at least two different aspects at multiple elevations to account for topographic complexity. In each plot, I cored 15 dominant or codominant trees with no signs of pathogens, insects, or injuries. All trees were a minimum of 125 years at breast height. I extracted one core from the side-slope of each tree, measured diameter at breast height, and geo-referenced each plot with a handheld Global Positioning System device.

The tree-growth data were combined with data from Littell et al. (2008) to create a robust dataset that covers the entire geographic range of Douglas-fir in the United States. To match the sampling density of the new plots in geographic space, I subsampled watersheds in each study site sampled by Littell et al. (2008), retaining two watersheds from each sample site and all plots in the chosen watersheds. Instead of a random sample of watersheds, I chose an informed sampling approach because my sampling strategy was designed to control for non-climatic factors (i.e., elevation, aspect) that may mediate the tree response to climate. I calculated growing season (April-September) water deficit (PET – AET) for each watershed and then graphically compared these curves to other watersheds in the site. This approach allowed me to choose watersheds based on a range of deficit to surplus in growing-season months, resulting in paired watersheds of wet vs. dry and/or warm vs. cool. For watersheds whose deficit values differed only slightly, I retained those watersheds that had the oldest trees with the longest usable record of tree rings.

3.3 Chronology development

I used standard dendrochronological techniques to measure, detrend, and standardize each tree-ring time series (Stokes and Smiley 1968, Fritts 1976, Cook and Kairiukstis 1989). All cores were measured using a Velmex sliding stage (precision = 0.001 mm), and crosschecked for

errors using COFECHA (Holmes 1999). To account for the geometric bias of ring width imposed by age/size (e.g., recent rings of larger trees are narrow), I detrended the time series with a cubic smoothing spline for which the frequency response was 0.50 (retained 50% of the variance) at a wavelength equal to 2/3 the length of the series. The cubic smoothing spline is appropriate for a dataset with such a large geographic extent because the curve fit to each series is unique, taking into consideration different ages, competition, and stand disturbance histories. Detrended time series were then subtracted from the fitted spline to create a ring-width index (RWI), a unit-less metric used as a proxy for annual ring width. For the RWIs, years were retained only if sampling depth was at least 5 cores. I built chronologies at the watershed and regional scales (see Restaino et al. *in preparation*). Watershed-scale chronologies were calculated by aggregating tree-scale chronologies with a Tukey's bi-weight robust mean. Regional-scale chronologies were calculated as a mean of the watershed-scale chronologies in a given region. All cores from all plots in each watershed were retained in chronology development resulting in chronologies that represent the suite of variable conditions experienced by trees.

3.4 Analysis

I analyzed the relationship between ENSO events and climate using graphical representations and superposed epoch analysis (SEA). SEA is a useful approach in resolving signal-to-noise ratio, especially when the relationship being studied is easily obfuscated by other co-occurring drivers (Adams et al. 2003). An SEA uses a Monte Carlo simulation to test if "event years" are distinctly different than the baseline average, and has been used to study fire-climate relationships (Swetnam and Betancourt 1990, Hessl et al. 2003) and volcanic eruptions

(Adams et al. 2003). Using an SEA approach, I tested for significant differences ($\alpha = 0.05$) in growing season and winter precipitation and growing season maximum temperature during ENSO event years. PDO was not analyzed in the same fashion, because it is not characterized by event years. The relationship among ENSO, PDO and climate was explored graphically.

A principal components analysis (PCA) was performed on the covariance matrix of the standardized chronologies within each region. Length of the period of analysis varied by region based on common length of time series. The first principal component (PC1) was extracted for each region to represent the dominant mode of variability in the regional tree-ring data, and ENSO events were plotted over each PC to explore patterns of tree growth in relation to events. To test for significance between growth extremes and ENSO events, I sub-sampled the 10^{th} percentile extreme growth years from each regional PC1 and used an SEA to test if climate is significantly different in those years. Each regional PC1 was also used to visually compare growth with warm and cool phases of PDO in each region.

To further characterize the relationship between ENSO and tree growth, I conducted a wavelet analysis on the standardized chronologies to identify a possible signature of inter-decadal variability in the frequency domain. I used the RWIs instead of PC1 for this analysis, because I wanted to use the longest time series possible. However, the wavelet transformations are identical for either the RWIs or the PC1s, because the transformation captures the variation in amplitude which is retained in a PCA. I used a wavelet transformation (Torrence and Compo 1999) because it enables the identification of changes in the periodicity of signals through time (Rigozo et al. 2003), unlike a Fourier transformation that identifies periodic components of a time series regardless of the location or frequency in time (Cazelles et al. 2008). Wavelet analysis is appropriate for use with ecological data because it does not assume stationarity in the

time series, but instead allows one to decompose variations in spectral characteristics that vary through time (Torrence and Compo 1999, Cazelles et al. 2008). The two most common wavelet transformations are the Morlet and the Mexican Hat and the Morlet was chosen because the resolution in the frequency domain is higher. The Mexican Hat transformation can isolate smaller changes in the temporal domain, but we are able to explore variability through time using other techniques (e.g. PCA; Mi et al. 2005.). Morlets are considered complex, resulting in the integration of negative and positive peaks in the data. Complex-valued wavelets are better for representing oscillations because they capture both amplitude and phase regardless of direction. This is important for identifying the presence of inter-decadal climate signals in tree growth time series when the question is whether or not changes are occurring in tree growth coincident with ENSO events.

Wavelet transformations were conducted for both the ENSO index time series and for each regional standardized chronology (Appendix 3.1). Then, a cross-wavelet analysis was performed to measure the correlation of spectra between ENSO and tree growth in each region. I did not perform a wavelet analysis on the PDO index, because the time series is not long enough to capture the longer wavelengths of the different phases.

I tested the results of the cross-wavelet analysis using a chi-squared test with a significance level of $\alpha = 0.10$. One can assume that the wavelet power spectrum has a mean and that deviations from that mean can be tested for significance (Torrence and Compo 1997). Because both the tree-ring and ENSO time series are normally distributed, a chi-squared distribution can be used to test for significance (Torrence and Compo 1997). Significance level is determined by multiplying the mean spectrum by the 95^{th} percentile value of χ^2, requiring 2 degrees of freedom because 2 time series are being tested. Significant portions of the power

spectrum are denoted by black contours, and can be interpreted based on their location in temporal space. Dashed lines represent the cone of influence, which is the portion of the data that cannot be included in interpretation. Errors occur at the beginning and end of the wavelet power spectra because it is assumed in the calculations that the data are cyclic (Torrence and Compo 1998). To correct for these errors the time series is padded with zeroes at the beginning and end to increase the total length, but this decreases the amplitude near the edges of the wavelet transformation. These edge effects influence interpretation of the data and are demarcated within the cone of influence.

All analyses were conducted in the R Statistical Computing Environment (R Core Team 2013), specifically the dplR (Bunn 2008) and biwavelet packages.

4. RESULTS

4.1 ENSO, PDO, and climate

An exploratory analysis of the relationship among ENSO, PDO, and regional climatic variability shows that El Niño event years (warmer sea surface temperatures) are more common than La Niña event years (cooler sea surface temperatures), so the effect of the former is more pronounced. El Niño years bring anomalously lower precipitation to the Pacific Northwest and Northern Rockies and higher precipitation to the Southwest and only occasionally to California (Figure 3.3). The signal is less clear in the Central Rockies and Southern Rockies, but event years still coincide with extremes in precipitation (Figure 3.3). El Niño years correspond with higher temperature anomalies, especially in the Pacific Northwest, Northern Rockies, and Central Rockies (Figure 3.4). In the more southerly regions, the signal is mixed, even in the

Southwest where a clear relationship with precipitation exists. Warmer phases of the PDO bring consistently warmer temperatures during ENSO event years (Figure 3.4). Temperature anomalies are, on average, higher during PDO warm phases (Figure 3.4).

4.2 ENSO, PDO, and tree growth

The PC1 of each regional set of plot-scale chronologies was extracted, and event years were plotted over the time series of PC1 scores (Figure 3.5). Some time series are longer than the climate data series, and thus include more event years than in Figures 3.3 and 3.4. Percent variability explained varies by region: Pacific Northwest (34%), Northern Rockies (56%), Central Rockies (44%), Southern Rockies (47%), California (47%), and Southwest (65%). The clearest associations between low and high growth years with ENSO events are seen in the Southwest, with high growth years occurring during El Niño (more precipitation) and the converse occurring with La Niña (less precipitation). It appears that extreme tree growth does coincide with ENSO events, but it is unclear whether extremes always coincide with El Niño or La Niña years (Figure 3.5).

Correlations for Oct–Mar values of the "Best" Index with watershed-scale tree ring indices are weak (≤ 0.30) for all sites (Figure 3.6), although anything above 0.16 is significant at $\alpha = 0.05$. The strongest correlations are found in the Southwest, eastern Oregon, and California coast. SEA results show that El Niño has a stronger influence on winter precipitation, and La Niña has a stronger influence on growing season precipitation (Table 3.3). Growing season temperatures are mostly affected in regions at northern latitudes. Precipitation was significantly different in extreme growth years for the Pacific Northwest ($p = 0.014$) and the Southwest ($p =$

0.018). Temperature was significantly different in extreme growth years for the Pacific Northwest (p=0.005), Southern Rockies (p=0.062), and Southwest (p=0.062).

The PC1 from each region was compared to warm and cool phases of the PDO (Figure 3.7). The percent variability explained for each region is the same as displayed in Figure 3.5. Dominant variability in tree growth does not strongly coincide with phases of PDO consistently throughout the entire time series. The most recent warm phase of the PDO does appear to drive variability in tree growth in all regions except the Northern Rockies. Lagged responses are evident in the Central and Southern Rockies. The effect is weakest in the Southwest, but the amplitudes of variability are coincident with peaks in the PDO time series.

4.3. Cross-wavelet analysis

All of the cross-wavelet analyses resulted in significant wavelet-coherence, with increased coherence beginning in the late 1960s in all regions (Figure 3.8). When the two time series are coherent, changes in amplitude and phase in both time series are occurring simultaneously or have a lagged effect. The period signifies the duration of changes in power, which is displayed in terms of changes in the temporal domain. Wavelet-coherence increased in frequency and the period decreased (1-7 years) since the mid-late 1970s in all regions except the Southern Rockies. Before 1960, wavelet-coherence occurred at longer periods, ranging from 7 to 10 years. A distinct 14-year period, which varies in time and is centered around 1990, is evident in all regions. The Pacific Northwest exhibits the clearest wavelet-coherence, with fewer similarities in power outside of the significance contours. Cross-wavelet analyses of the Northern and Central Rockies reveal a similar pattern, with coherence in the power spectra in a

20-year period (1880–1900), a 10-year period (1910 – 1920), and small periods around 1940 and 1950. The Southern Rockies have a distinct low frequency response to ENSO during a 20-year period (1880–1900) at the beginning of the time series; however, the low frequency response seen in other regions during the most recent decades is not present in this region.

5. DISCUSSION

Regional variations in inter-decadal precipitation patterns are affected by variability in the strength and timing of ENSO events. Consistent with previous findings, a clear relationship between precipitation and ENSO exists on extreme ends of the dipole (Brown and Comrie 2004, Wise 2012). High and low peaks in precipitation are evident in the Pacific Northwest and Southwest during El Niño and La Niña years, and this relationship stays consistent through the entire period of analysis (Figure 3. 3). The effect of ENSO on precipitation and streamflow in the Pacific Northwest (Mote et al. 2003) and Southwest (D'Arrigo et al. 2005) is well documented, and my results confirm that extreme climate in these regions is driven by ENSO variability. Climate in the Northern Rockies and California is also affected by ENSO variability, but the pattern is less consistent (Figure 3.3). After El Niño events, the Northern Rockies tend to have warm spring and winter periods with anomalously low precipitation (Redmond and Koch 1991, Harshburger et al. 2002, Heyerdahl et al. 2008), a pattern that is corroborated with the dataset analyzed in this study (Figure 3.3). Schonher and Nicholsen (1998) conducted a thorough analysis of ENSO-mediated precipitation in California and concluded that ENSO events modulate precipitation across the state, but that the magnitude of influence varies regionally with the least consistency in northern California (the location of my study sites).

Close proximity to the dipole decreases the effect of ENSO in northern California and in the Central and Southern Rockies (Figure 3.2). The clearest connection between ENSO and regional-scale climate is seen in the most northerly and southerly areas of the western United States.

The relationship between temperature and ENSO is less restricted to the extremes of the dipole and can be seen across all regions. El Niño event years, in particular, bring warmer temperatures throughout my study regions (Figure 3.4). This is a reasonable response to the ENSO atmosphere-ocean teleconnection, because anomalously warm water in the Pacific Ocean drives the phenomenon (Li et al. 2013), and above average air temperatures have been observed during El Niño events (Halpert and Ropelewski 1992). The Southwest displays an opposite effect, where lower temperatures are associated with El Niño events (Figure 3.4). Other studies have reported this pattern, in which higher and lower temperatures in the northern and southern latitudes coincide with El Niño events (Ropelewski and Halpert 1986). An explanation of the temperature difference is the strength and location of the Pacific North American (PNA) teleconnection pattern during an El Niño, which produces a trough over the Gulf of Alaska, a ridge over northern North America and a trough in the Southwest (Leathers et al. 1991). Scientists have argued that ENSO events amplify the PNA, and therefore the opposite effects of the PNA on temperature in western North America are exaggerated during an ENSO event (Renwick and Wallace 1996, Shabbar and Khandekar 1996). Although the temperature relationship is distinctly different in the Southwest, the rest of the study region experiences above-average temperatures during ENSO events.

The complex relationship between PDO and regional climate is not as easily interpreted because the PDO does not occur as events, but instead as warm and cool phases. Warm and cool

phases do not appear to modify the magnitude of precipitation, but La Niña years do occur more frequently during the cool phase of the PDO, which has implications for regional precipitation patterns. Average temperature anomalies are higher during warm phases of the PDO, because conditions are amplified when PDO and ENSO occur in phase (Wise 2010). It is hypothesized that the PDO is forced by ENSO, so parsing out the direct effects of one climatic mode of variability from the other is difficult (Newman et al 2003). However, interpretations of ENSO-related changes in precipitation and temperature need to be contextualized in terms of warm and cool phases of the PDO.

ENSO-related climatic effects are evident in the tree-ring time series analyzed. Results of the climate analysis strongly support that precipitation and temperature are controlled by ENSO at inter-decadal time scales. Douglas-fir is clearly a water-limited species in most of its range (Littell et al., 2008), but this limitation is regulated by the interrelationship between temperature and precipitation (Restaino et al. *in preparation*), so variability or directional trends in either precipitation or temperature have direct consequences for water availability.

In all regions, strong ENSO events are seen in the cross-wavelet results (Figures 3.8), but the inter-relationship between the two time series is most evident in the Pacific Northwest and Southwest. These results are consistent with our climate data analysis—ENSO affects climate most at extreme ends of the dipole—therefore tree growth is most linked to ENSO in these regions. The relationship between tree growth and ENSO has strengthened in recent decades, which is consistent with findings that the severity of ENSO has also changed in this time period (Shongart et al. 2004, Appendix 3.2). Synchrony between ENSO and RWIs is also evident in the Northern Rockies and California, but the relationship is weaker. The correlation analysis did not yield strong results (Appendix 3.1, Figure 3.6), and the strongest relationships were not

consistent with results of the cross-wavelet analysis. This highlights the importance of analyzing these types of data in the frequency domain, in which the relevant metric is amplitude of the indices and not raw data.

ENSO events occur every 3-7 years but the cross-wavelet analysis does not suggest wavelet coherence at this same frequency, suggesting a non-stationarity in the inter-decadal climate-growth response. A significant increase in wavelet coherence is evident in the most recent decades across all regions, which coincides with the transition from cool to warm phase PDO. One explanation is that the shift from one long-lived phase to the next is a time of increased climatic variability, which ultimately influences tree growth. The shift from warm to cool is also seen in the power spectra in the early 1940s in the Pacific Northwest, Northern Rockies, Southern Rockies, and California. Alternatively, the increased coherence could predominately be a result of the warm phase PDO, suggesting that the effects of ENSO events on growth were amplified during the last warm phase PDO. Precipitation extremes on opposite ends of the dipole are exaggerated when PDO and ENSO are in phase (Figure 3.2), so growth is more responsive during these time periods. The power spectra do not show directional changes in the time series, but simply that changes exist. For example, trees in the Southwest respond very favorably to more precipitation (growth increases), and trees in the PNW respond unfavorably to less precipitation (growth decreases), but the change in precipitation is controlled by El Niño events. Results of regional PCA also supports this inference, where variability in growth is not coincident with PDO until the most recent warm phase in all regions except for the Southwest. The increased wavelet coherence in all regions can be explained by different regional responses to El Niño events and potentially the increases in events caused by a warm phase PDO (Figure 3.7). The longest duration El Niño events (1911-1915, 1990-1994, 2002-

2006; Appendix 3.2) are also evident in the power spectra (Figure 3.8), suggesting that when climate is modified by ENSO for longer periods of time, tree growth is more significantly altered. More frequent and longer El Niño events during a warm phase PDO coupled with higher ambient air temperatures (Figure 3.4) modify forest growing environments, resulting in an increased ENSO signal in tree-ring chronologies.

ENSO and PDO, two dominant atmosphere-ocean circulation patterns, modify regional climate and consequently alter the growing environment for coniferous forests. Relationships between tree growth and broad-scale climatic variability are most distinct at the extremes of the ENSO dipole, and when ENSO and PDO are in phase. It is important to decipher the chain of causes linking growth variability to climate teleconnections; it is not ENSO directly that is modifying tree growth, but instead the changes in regional climate that are caused by ENSO. Although the mechanisms causing changes in climate are not operating at the same scale as tree growth, the relationship is manifest via changes in regional climate.

It is unclear how the frequency and intensity of ENSO events will change in a warmer climate (Collins et al. 2010, Vecchi and Wittenberg 2010, Guilyardi et al. 2009). It is hypothesized that ENSO events could intensify, weaken, or not change at all, but ENSO events and associated climatic variability are certain to persist (Vecchi and Wittenberg 2010, Deser et al. 2012). Although future periodicity and strength of ENSO events are unclear, some studies suggest that increased sea-surface temperatures will be most pronounced at the equator, leading to an "El Niño-like" climate change (Collins 2005, Collins et al. 2010). If this occurs, we may expect changes in storm-track activity and high and low pressure system development consistent with El Niño events. ENSO warm phases can therefore be used to illustrate time periods of higher temperatures with varying levels of precipitation that arise from El Niño events. Climate

models project that atmospheric temperatures will continue to increase, but the timing and magnitude of future precipitation are uncertain (IPCC 2013). ENSO event years provide a reference point for understanding how climate responds to anomalous sea surface temperatures, and ultimately how tree growth responds to the different climatic conditions that arise during these years.

6. REFERENCES

Adams, J. B., M. E. Mann, and C. M. Ammann. 2003. Proxy evidence for an El Nino-like response to volcanic forcing. Nature **426**: 274-278.

Bailey, R. G. 2004. Identifying ecoregion boundaries. Environmental Management 34: S14-S26.

Barlow, M., S. Nigam, and E. H. Berbery. 2001. ENSO, Pacific decadal variability, and US summertime precipitation, drought, and stream flow. Journal of Climate **14:** 2105-2128.

Bradshaw, G. A., and B. A. McIntosh. 1994. Detecting climate-induced patterns using wavelet analysis. Environmental Pollution **83**: 135-142.

Brown, D. P., and A. C. Comrie. 2004. A winter precipitation 'dipole' in the western United States associated with mulitdecadal ENSO variability. Geophysical Research Letters **31**: 1-4.

Case, M. J., and D. L. Peterson. 2005. Fine-scale variability in growth-climate relationships of Douglas-fir, North Cascade Range, Washington. Canadian Journal of Forest Research **35**: 2743-2755.

Cayan, D. R., M. D. Dettinger, H. F. Diaz, and N. E. Graham. 1998. Decadal variability of precipitation over western North America. Journal of Climate **11:** 3148–3166.

Cazelles, B., M. Chavez, D. Berteaux, F. Ménard, J. O. Vik, S. Jenouvrier, and N. C. Stenseth. 2008. Wavelet analysis of ecological time series. Oecologia **156**: 287-304.

Chen, P. Y., C. Welsh, and A. Hamann. 2010. Geographic variation in growth response of Douglas-fir to interannual climate variability and projected climate change. Global Change Biology **16**: 3374-3385.

Collins, M. 2005. El Niño-or La Niña-like climate change? Climate Dynamics **24**: 89-104.

Collins, M., S. I. An, W. Cai, A. Ganachaud, E. Guilyardi, F. F. Jin, M. Jochum, M. Lengaigne, S. Power, A. Timmermann, G. Vecchii, and A. Wittenberg. 2010. The impact of global warming on the tropical Pacific Ocean and El Niño. Nature Geoscience **3**: 391-397.

Cook, E.R., and L.A. Kairiukstis (Ed.) 1990. Methods of dendrochronology: Applications in the Environmental Sciences. Kluver Academic Publishers, The Netherlands.

D'Arrigo R., E. Cook, R. Wilson, R. Allan, and M. Mann. 2005. On the variability of ENSO over the past six centuries. Geophysical Research Letters **32**: 1-4.

Davis, R. E. 1976. Predictability of sea surface temperatures and sea level pressure anomalies over the North Pacific Ocean. Journal of Physical Oceanography **6**: 249-266.

Deser, C., A. Phillips, V. Bourdette, and H. Teng. 2012. Uncertainty in climate change projections: the role of internal variability. Climate Dynamics **38:** 527-546.

Dettinger, M. D., D. R. Cayan, H. F. Diaz, D. M. Meko. 1998. North-south precipitation patterns in western North America on interannual-to-decadal timescales. Journal of Climate **11**: 3095-3111.

Diaz, H. F., M. P. Hoerling, and J. K. Eischeid. 2001. ENSO variability, teleconnections and climate change. International Journal of Climatology **21**: 1845-1862.

Fritts, H. C. 1976. Tree rings and climate. Academic Press, New York.

Gedalof, Z. E., D. L. Peterson, and N. J. Mantua. 2005. Atmospheric, climatic, and ecological controls on extreme wildfire years in the northwestern United States. Ecological Applications **15**: 154-174.

Gershunov, A., and T. P. Barnett. 1998. Interdecadal modulation of ENSO teleconnections. Bulletin of American Meterological Society **79**: 2715-2725.

Griesbauer, H. P., and D. S. Green. 2010a. Assessing the climatic sensitivity of Douglas-fir at its northern range margins in British Columbia, Canada. Trees, Structure and Function **24**: 375-389.

Griesbauer, H. P., and D. S. Green. 2010b. Regional and ecological patterns in interior Douglas-fir climate-growth relationships in British Columbia, Canada. Canadian Journal of Forest Research **40**: 308-321.

Guilyardi, E., A. Wittenberg, A. Fedorov, M. Collins, C. Wang, A. Capotondi, G. J. Van Oldenborgh, and T. Stockdale. 2009. Understanding El Niño in ocean-atmosphere general circulation models: progress and challenges. Bulletin of the American Meteorological Society **90**: 325-340.

Halpert, M. S., and C. F. Ropelewski, C. F. 1992. Surface temperature patterns associated with the Southern Oscillation. Journal of Climate **5:** 577-593.

Harshburger, B., H. Ye, and J. Dzialoski. 2002. Observational evidence of the influence of Pacific SSTs on winter precipitation and spring stream discharge in Idaho. Journal of Hydrology **264**: 157–169.

Hessl, A. E., D. McKenzie, and R. Schellhaas. 2004. Drought and Pacific Decadal Oscillation linked to fire occurrence in the inland Pacific Northwest. Ecological Applications **14**: 425-442.

Heyerdahl, E. K., L. B. Brubaker, and J. K. Agee. 2002. Annual and decadal climate forcing of historical fire regimes in the interior Pacific Northwest, USA. The Holocene **12**: 597-604.

Heyerdahl, E. K., P. Morgan, J. P. Riser. 2008. Multi-season climate synchronized historical fires in dry forests (1650-1900), northern Rockies, USA. Ecology **89:** 705-716.

Holmes, R. L. 1999. User's manual for program COFECHA. University of Arizona Press, Tucson, AZ.

IPCC. 2013. Summary for Policymakers. In: Climate Change 2013: The Physical Science Basis. Contribution of Working Group I to the Fifth Assessment Report of the Intergovernmental Panel on Climate Change [Stocker, T.F., D. Qin, G.-K. Plattner, M. Tignor, S.K. Allen, J. Boschung, A. Nauels, Y. Xia, V. Bex and P.M. Midgley (eds.)]. Cambridge University Press, Cambridge, United Kingdom and New York, NY, USA.

Leathers, D. J., B. Yarnal, and M. A. Palecki. 1991. The Pacific/North American teleconnection pattern and United States climate. Part I: Regional temperature and precipitation associations. Journal of Climate **4:** 517-528.

Liang, X., D.P. Lettenmaier, E.F. Wood, and S.J. Burges. 1994. A simple hydrologically based model of land surface water and energy fluxes for general circulation models. Journal of Geophysical Research **99:** 14, 415-424, 428.

Littell, J. S., D. L. Peterson, and M. Tjoelker. 2008. Douglas-fir growth in mountain ecosystems: water limits tree growth from stand to region. Ecological Monographs **78**: 349-368.

Mantua, N. J., and S. R. Hare, Y. Zhang, J. M. Wallace, and R. C. Francis. 1997. A Pacific interdecadal climate oscillation with impacts on salmon production. Bulletin of the

American Meteorological Society **78**: 1069-1079.

Mantua, N. J., and S. R. Hare. 2002. The Pacific decadal oscillation. Journal of Oceanography **58**: 35-44.

McPhaden, M. J., S. E. Zebiak, and M. H. Glantz. 2006. ENSO as an integrating concept in earth science. Science **314:** 1740-1745.

Mi X., H. Ren, Z. Ouyang, W. Wei, and K. Ma. 2005. The use of the Mexican hat and the Morlet wavelets for the detection of ecological patterns. Plant Ecology **179**: 1-19.

Newman, M., G. P. Compo, and M. A. Alexander. 2003. ENSO-forced variability of the Pacific decadal oscillation. Journal of Climate **16:** 3853-3857.

Njissen B.N., D.P. Lettenmaier, X. Liang, S.W. Wetzel, and E.F. Wood. 1997. Streamflow simulation for continental-scale river basins. Water Resources Research **33:** 711-724.

Piechota, T. C., and J. A. Dracup. 1996. Drought and regional hydrologic variation in the United States: associations with the El Niño Southern Oscillation. Water Resources Research **32**: 1359-1373.

Piechota, T. C., J. A. Dracup, and R. G. Fovell. 1997. Western US streamflow and atmospheric circulation patterns during El Niño-Southern Oscillation. Journal of Hydrology **201:** 249-271.

R Core Team. 2013. R: A language and environment for statistical computing. R Foundation for Statistical Computing, Vienna, Austria. ISBN 3-900051-07-0, URL http://www.R-project.org/

Redmond, K. T., and R. W. Koch. 1991. Surface climate and streamflow variability in the western United States and their relationship to large-scale circulation indices. Water Resources Journal **27** :2381–2399.

Renwick, J. A., and J. M. Wallace. 1996. Relationships between North Pacific wintertime blocking, El Niño, and the PNA pattern. Monthly Weather Review **124:** 2071-2076.

Restaino, C. M., D. L. Peterson, and J. Littell. *In preparation.* Higher temperatures decrease tree growth in western US forests.

Rigozo, N. R., L. E. A. Vieira, E. Echer, and D. J. R. Nordemann. 2003. Wavelet analysis of solar-ENSO imprints in tree ring data from southern Brazil in the last century. Climatic Change **60**: 329-340.

Ropelewski, C. F., and M. S. Halpert. 1986. North American precipitation and temperature patterns associated with the El Niño/Southern Oscillation (ENSO). Monthly Weather Review **114:** 2352-2362.

Schneider, N., and B. D. Cornuelle. 2005. The forcing of the Pacific Decadal Oscillation. Journal of Climate **18**: 4355-4373.

Schoengart, J., W. J. Junk, M. T. F. Piedade, J. M. Ayres, A. Hüttermann, M. Worbes. 2004. Teleconnection between tree growth in the Amazonian floodplains and the El Nino–Southern Oscillation effect. Global Change Biology **10**: 683-692.

Schoennagel, T., T. T. Veblen, W. H. Romme, J. S. Sibold, E. R. Cook. 2005. ENSO and PDO variability affect drought-induced fire occurrence in Rocky Mountain subalpine forests. Ecological Applications **15**: 2000-2014.

Schonher, T., and Nicholson, S. E. 1989. The relationship between California rainfall and ENSO events. Journal of Climate **2**: 1258-1269.

Shabbar, A., and M. Khandekar, M. 1996. The impact of el Nino-Southern oscillation on the temperature field over Canada: Research note. Atmosphere-Ocean **34**: 401-416.

Smith, C.A., and P. Sardeshmukh. 2000. The effect of ENSO on the intraseasonal variance of surface temperature in winter. International Journal of Climatology **20:** 1543-1557.

Stahle D. W., R. D. D'Arrigo, P. J. Krusic, M. K. Cleaveland, E. R. Cook, R. J. Allan, J. E. Cole, R. B. Dunbar, M. D. Therrell, D. A. Gay, M. D. Moore, M. A. Stokes, B. T. Burns, J. Villanueva-Diaz, and L. G. Thompson. 1998. Experimental dendroclimatic reconstruction of the Southern Oscillation. Bulletin of the American Meteorological Society **79**: 2137–2152.

St George, S. 2014. An overview of tree-ring width records across the Northern Hemisphere. Quaternary Science Reviews **95**: 132-150.

Stokes, M. A., and T. L. Smiley. 1968. An introduction to tree-ring dating. University of Chicago Press, Chicago, Illinois, USA.

Swetnam, T.W. and J.L. Betancourt. 1990. Fire-Southern Oscillation relations in the southwestern United States. Science **249**: 1017-1020.

Torrence, C., and G. P. Compo. 1998. A practical guide to wavelet analysis. Bulletin of the American Meterological Society **79**: 61-78.

Vinnikov, K. Y., A. Robock, N. A. Speranskaya, C. A. Schlosser. 1996. Scales of temporal and spatial variability of midlatitude soil moisture. Journal of Geophysical Research **101**: 7163-7174.

Watson, E., and B. H. Luckman. 2002. The dendroclimatic signal in Douglas-fir and ponderosa pine tree-ring chronologies from the southern Canadian Cordillera. Canadian Journal of Forest Research **32**: 1858-1874.

Williams, A. P., C. D. Allen, A.K. Macalady, D. Griffin, C. A. Woodhouse, D. M. Meko, T. W. Swetnam, S. A. Rauscher, R. Seager, H. D. Grissino-Mayer, J. S. Dean, E. R. Cook, C. Gangodagamage, M. Cai, and N. G. McDowell. 2013. Temperature as a potent driver of regional forest drought stress and tree mortality. Nature Climate Change **3**: 292-297.

Wise, E. 2010. Spatiotemporal variability of the precipitation dipole transition zone in the western United States. Geophysical Research Letters **37**: 1-5.

Vecchi, G. A., and A. T. Wittenberg. 2010. El Niño and our future climate: where do we stand? Wiley Interdisciplinary Reviews: Climate Change **1**: 260-270.

Zhang, Y., J. M. Wallace, D. S. Battisti. 1997. ENSO-like interdecadal variability: 1900-93. Journal of Climate **10**: 1004-1020.

7. TABLES

Table 3.1. Locations and mean annual climate parameters for all study watersheds. PPT = precipitation; TMAX = maximum temperature, TMIN = minimum temperature.

Region	State	# of trees	Property Name	Latitude	Longitude	Elevation (m)	Annual PPT (mm)	Annual TMAX (C)	Annual TMIN (C)
Pacific Northwest	Washington	76	North Cascades National Park	48.94038	-121.40010	1048.3	1972.02	10.01	1.09
Pacific Northwest	Washington	70	Olympic National Park	47.74623	-123.20605	1031.2	1880.0	10.5	2.3
Pacific Northwest	Washington	72	Olympic National Park	47.82603	-123.99620	530.6	3366.11	13.97	4.85
Pacific Northwest	Washington	67	North Cascades National Park	48.30747	-120.65660	989.0	1057.11	11.53	1.18
Pacific Northwest	Oregon	85	HJ Andrews Experimental Forest	44.23159	-122.13355	1179.48	2354.92	13.69	2.97
Northern Rockies	Montana	81	Glacier National Park	48.58777	-113.88410	1323.0	871.66	10.40	-1.56
Northern Rockies	Montana	68	Glacier National Park	48.49320	-113.35914	1726.7	1013.97	8.66	-1.35
Northern Rockies	Idaho	70	Idaho Panhandle National Forest	48.98723	-116.62731	1177.0	839.49	10.70	0.71
Northern Rockies	Idaho	71	Idaho Panhandle National Forest	48.82964	-116.46036	1257.7	893.43	10.46	1.04
Central Rockies	Idaho	72	Payette National Forest	45.13659	-116.41832	1911.23	1197.58	10.35	-2.21
Central Rockies	Montana	92	Gallatin National Forest	45.87449	-110.89657	1985.79	714.94	10.03	-3.21
Central Rockies	Oregon	31	Umatilla National Forest	44.99897	-118.98660	962.09	430.40	16.60	1.28
Central Rockies	Oregon	74	Wallowa-Whitman National Forest	45.71603	-117.40513	1689.11	1303.74	10.45	0.54
Southern Rockies	Wyoming	83	Bridger-Teton National Forest	43.48059	-110.70658	2299.71	690.78	9.96	-3.28
Southern Rockies	Colorado	89	Gunnison National Forest	38.44524	-106.36330	2987.68	646.73	10.03	-4.58
Southern Rockies	Colorado	59	Roosevelt National Forest	40.42530	-105.32592	2145.03	473.74	14.79	0.89
California	California	72	UC Angelo Reserve	39.72647	-123.63349	526.60	2088.75	19.45	5.61
California	California	57	BLM Headwaters Reserve	40.64037	-124.07719	485.21	1501.19	18.59	7.49
California	California	91	Plumas National Forest	39.94591	-121.09904	1404.67	1168.17	17.60	3.61
California	California	41	Stanislaus National Forest	37.97359	-120.07321	1282.42	1113.76	18.86	5.24
Southwest	Arizona	40	Grand Canyon National Park	36.24806	-112.04188	2525.52	651.18	14.23	-0.23
Southwest	New Mexico	74	Valles Caldera National Preserve	35.98106	-106.59204	2850.17	687.44	11.66	-1.05
Southwest	New Mexico	30	Chama River Wilderness	36.27471	-106.61508	2424.13	518.11	15.22	1.71
Southwest	Utah	43	Henry Mountains	38.06987	-110.79483	2919.51	725.61	10.97	-2.01

Table 3.2. Summary of El Niño and La Niña extreme event years, defined as ± 1.28 °C departure of sea surface temperatures. A summary of 5-month running means is available at http://www.esrl.noaa.gov/psd/people/cathy.smith/best/table.txt.

El Niño	La Niña
1877-1878	1872-1873
1888-1889	1878-1879
1896-1897	1889-1890
1899-1900	1917-1918
1902-1903	1950
1905	1955
1925-1926	1973-1974
1930-1931	1975-1976
1940-1941	1988
1965-1966	2007-2008
1972-1973	
1982-1983	
1987	
1991-1992	
1997-1998	
2002-2003	
2009-2010	

Table 3.3. Results (p-values) from superposed epoch analysis that tested for significance between regional climate variables and El Niño and La Niña event years. El Niño and La Niña years bring significant changes in winter precipitation both in the year of and the year after the event. Growing season temperatures are higher preceding an El Niño year. Year 1 is year of the ENSO event, and Year 2 is the subsequent year. PNW = Pacific Northwest, NR = Northern Rockies, CR = Central Rockies, SR = Southern Rockies, CA = California, SW = Southwest.

EL NIÑO

Region	Year	GS PPT	Winter PPT	GS TMAX
PNW				
	Year 1	0.046	0.005	0.001
	Year 2			
NR				
	Year 1		0.001	0.001
	Year 2			0.038
CR				
	Year 1		0.023	0.001
	Year 2		0.018	
SR				
	Year 1		0.047	
	Year 2			
CA				
	Year 1			0.021
	Year 2	0.1	0.05	
SW				
	Year 1		0.011	
	Year 2			

LA NIÑA

Region	Year	GS PPT	Winter PPT	GS TMAX
PNW				
	Year 1		0.002	0.01
	Year 2	0.009		
NR				
	Year 1	0.065	0.003	0.065
	Year 2	0.01		0.1
CR				
	Year 1			
	Year 2	0.003		
SR				
	Year 1	0.064		
	Year 2		0.002	
CA				
	Year 1	0.001	0.095	
	Year 2	0.019		
SW				
	Year 1	0.064	0.036	
	Year 2		0.036	

PPT = Preciptation; TMAX = Maximum Temperature; GS = Growing Season

8. FIGURES

Figure 3.1. Distribution of study locations in the western United States. Grey depicts the distribution of Douglas-fir, and triangles indicate the location of plots in each location.

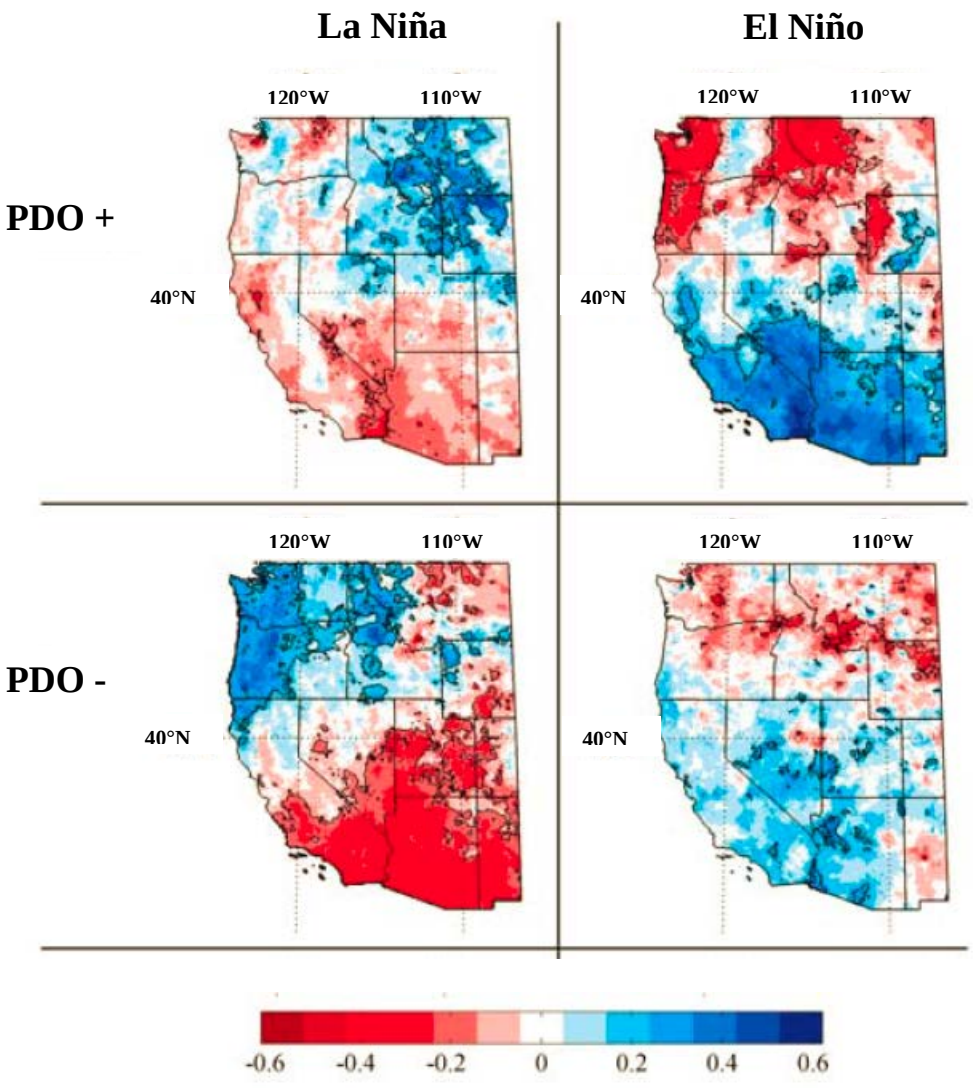

Figure 3.2. Precipitation anomalies depicting the El Niño dipole as illustrated in Wise (2010). Positive and negative values indicate low and high precipitation, respectively. When the El Niño Southern Oscillation and Pacific Decadal Oscillation are in phase the position of the dipole shifts and becomes stronger.

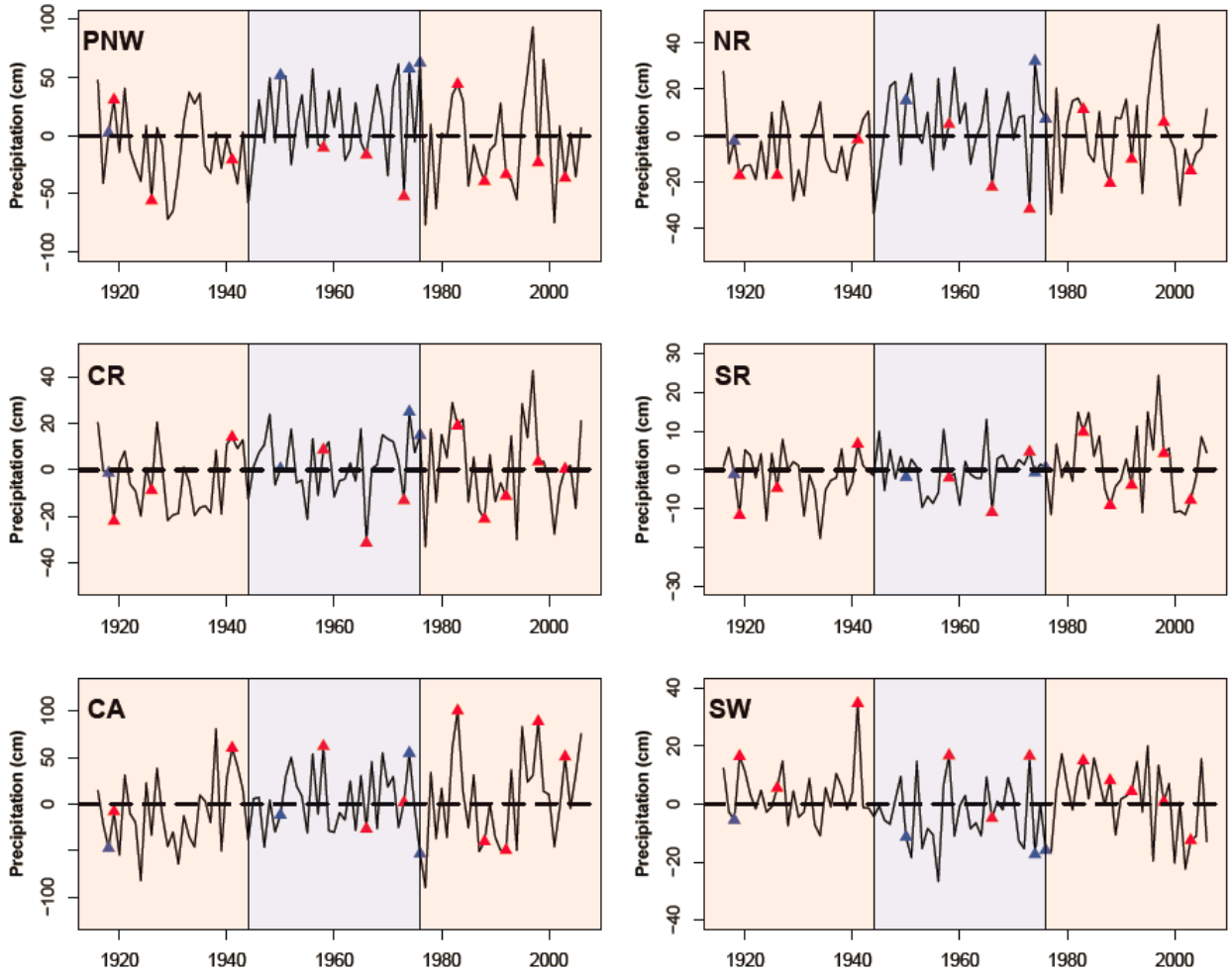

Figure 3.3. El Niño (red triangles) and La Niña (blue triangles) events overlaid on precipitation anomalies. Regions are denoted in the upper left. PNW = Pacific Northwest, NR = Northern Rockies, CR = Central Rockies, SR = Southern Rockies, CA = California, SW = Southwest. Phases of the Pacific Decadal Oscillation are represented in light red (warm) and blue (cool). El Niño event years bring opposite effects with below and above average precipitation in the PNW and SW, respectively. The effect of event years is also seen in CA and NR but is much weaker in the CR and SR, which can be explained by the location of these sites in the transitional zone of the ENSO dipole.

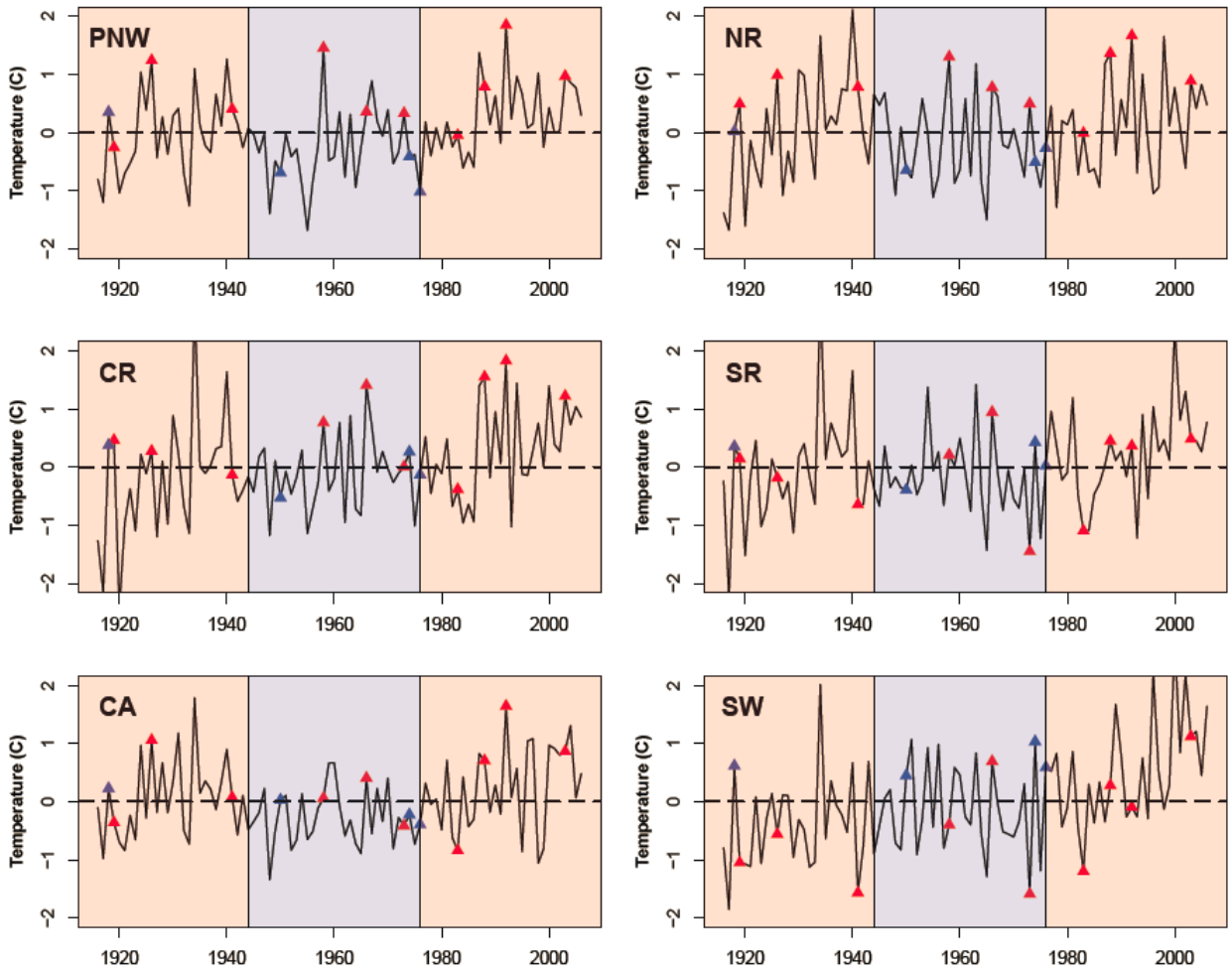

Figure 3.4. El Niño (red triangles) and La Niña (blue triangles) events overlaid on maximum temperature anomalies. Regions are denoted in the upper left. PNW = Pacific Northwest, NR = Northern Rockies, CR = Central Rockies, SR = Southern Rockies, CA = California, SW = Southwest Phases of the Pacific Decadal Oscillation are represented in light red (warm) and blue (cool). In the more northerly latitudes, El Niño years have consistently higher temperatures. The signal is more mixed in centrally located sites. In the SW, El Niño events have historically brought lower temperatures but in the most recent decades warmer temperatures are coinciding with these events. Temperature anomalies are higher during the warm phases of the PDO. Both high and low peaks in temperature do occur during ENSO event years across all regions.

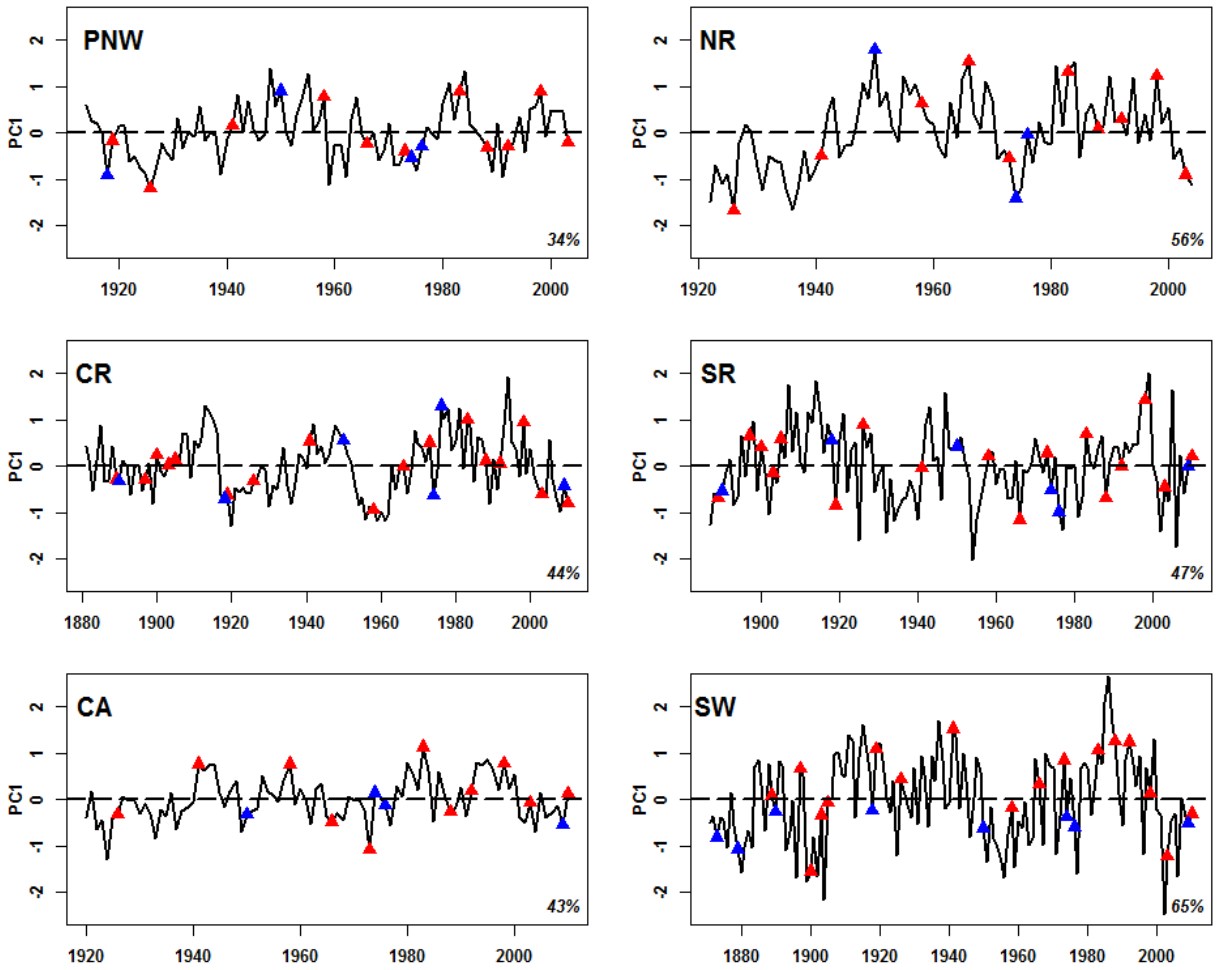

Figure 3.5. El Niño (red) and La Niña (blue) events overlaid on the first principal component of regional tree-ring time series. Percent variability explained by the principal component is indicated on the bottom right. Extremes in growth are not always linked to ENSO events, but some synchrony can be seen in the PNW, SW, NR and CA. The highest variability is observed in the SW and SR, whereas the lowest variability is in CA and the PNW. Length of times series vary based on common time periods of chronologies used in the PCA. PNW = Pacific Northwest, NR = Northern Rockies, CR = Central Rockies, SR = Southern Rockies, CA = California, SW = Southwest.

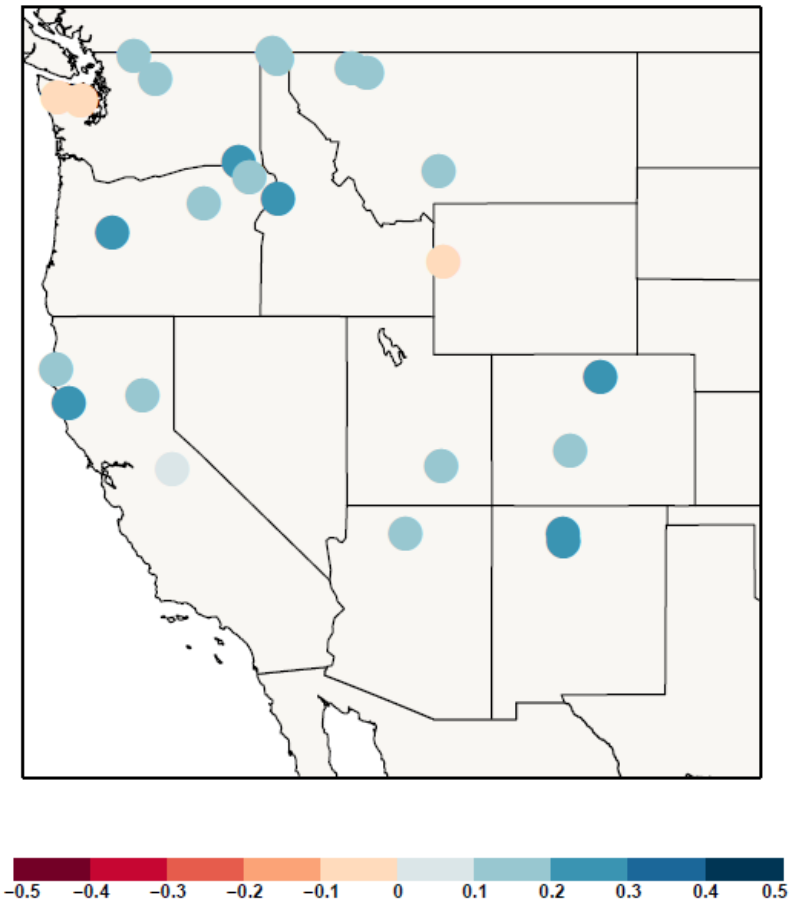

Figure 3.6. Pearson's product-moment correlations between the Oct-Mar "Best" Index and tree-ring indices for all study sites. Correlations are weak (≤ 0.30) for all sites, although values >0.16 or <-0.16 are significant at $\alpha = 0.05$. The strongest correlations are found in the Southwest, eastern Oregon and the California coast. Weak correlations with the ENSO index are consistent with findings in St. George (2014). See Appendix 3.1 for coefficients and significance level.

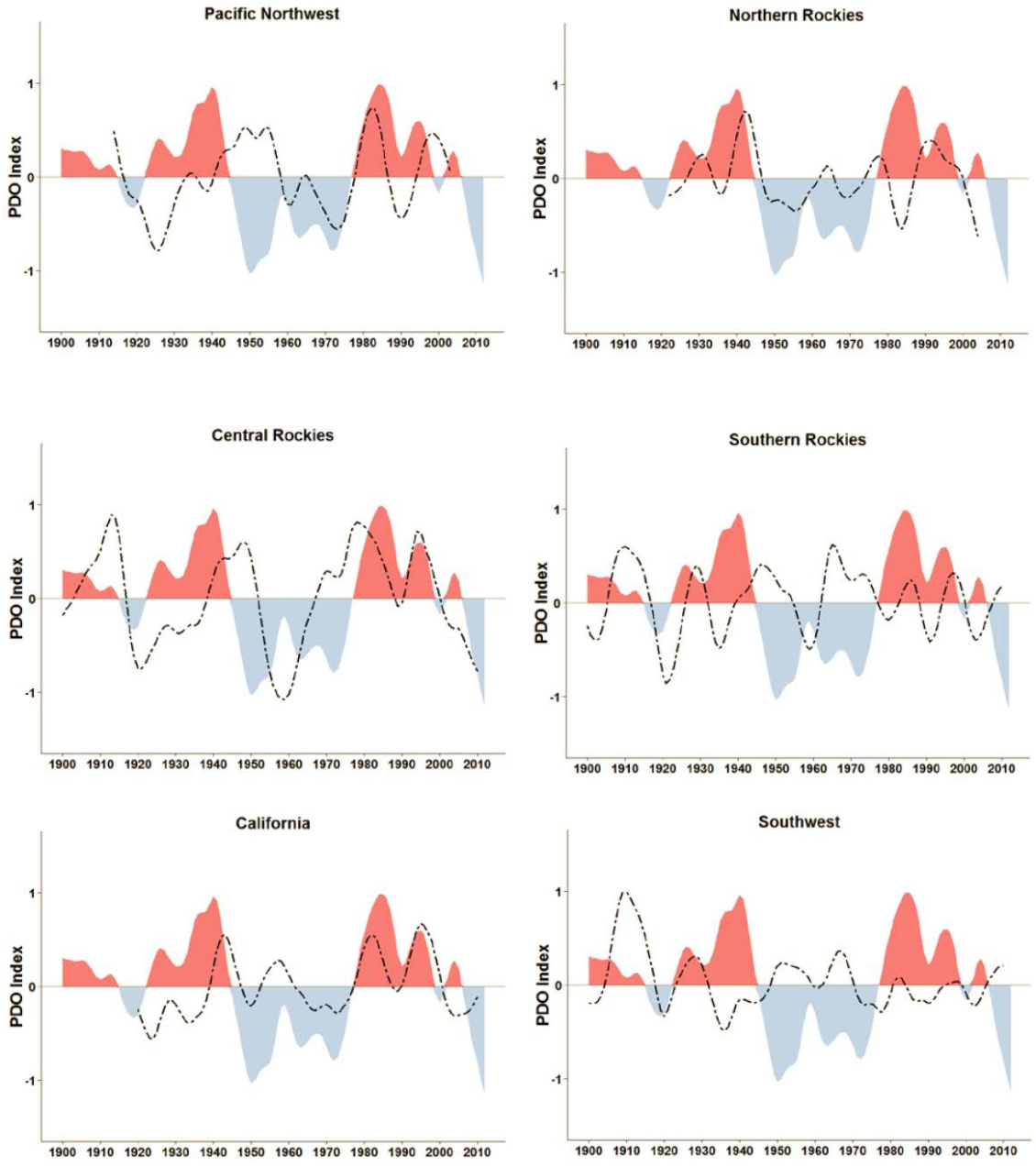

Figure 3.7. First principal component (PC1) of each regional time series overlaid on different phases of the Pacific Decadal Oscillation (PDO). Warm phases are denoted in red and cool phases in blue. All times series are smoothed with a 10-year smoothing spline**.** Regions vary in the growth response to PDO and there is little commonality among regions in the inter-decadal signal. PC1 for each region appears to respond to PDO either positively (Pacific Northwest, Central Rockies, and California) or negatively (Northern Rockies, Southern Rockies, and Southwest).

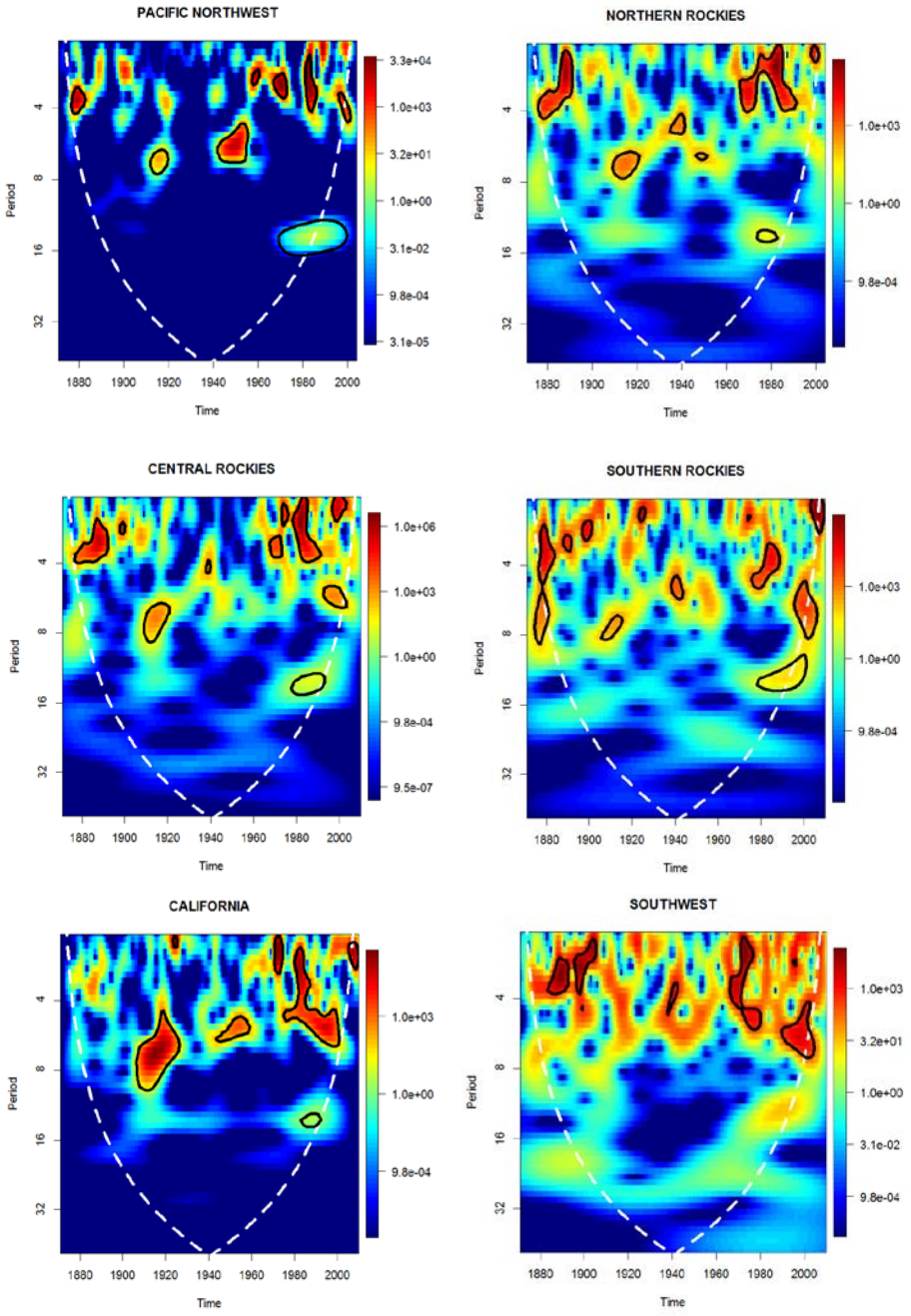

Figure 3.8. Results of cross-wavelet analysis of tree growth and El Niño Southern Oscillation displayed in Plots of the bias-corrected power normalized by the variance for all regions. Wavelet-coherence is evident in all regions, ranging between low frequency and high frequency throughout the time series. Wavelet-coherence has increased in recent decades (coinciding with the latest warm-phase PDO), and is occurring at smaller periods for all regions except the Southern Rockies. Portions of the time series within the cone of influence should not be interpreted, because edge effects result in inaccurate wavelet transformations.

9. APPENDICES

APPENDIX 3.1. Correlations between ring width index and October – March Best Nino Index.

Site	Degrees of freedom	rho	p-value	Lower CI	Upper CI
AZGC	138	0.162	0.055	-0.004	0.320
CAAG	138	0.227	0.007	0.063	0.378
CAHW	138	0.120	0.157	-0.047	0.280
CAPL	138	0.120	0.157	-0.047	0.280
CAST	138	0.057	0.503	-0.110	0.221
COMP	138	0.105	0.217	-0.062	0.266
CORO	138	0.250	0.003	0.087	0.399
IDBL	138	0.236	0.005	0.073	0.387
IDBO	132	0.111	0.201	-0.060	0.275
IDTR	132	0.193	0.026	0.024	0.351
MTGT	138	0.127	0.134	-0.040	0.287
MTLM	132	0.122	0.161	-0.049	0.286
MTTM	132	0.121	0.165	-0.050	0.284
NMCH	138	0.299	0.000	0.140	0.443
NMVC	138	0.217	0.010	0.053	0.369
ORHJ	138	0.203	0.016	0.039	0.357
ORUT	138	0.124	0.145	-0.043	0.284
ORWT	138	0.259	0.002	0.097	0.407
ORWW	138	0.191	0.024	0.026	0.346
UTHM	138	0.159	0.061	-0.007	0.316
WACR	132	0.125	0.151	-0.046	0.288
WADR	132	-0.020	0.815	-0.189	0.150
WAHR	132	-0.013	0.885	-0.182	0.157
WAST	132	0.123	0.155	-0.047	0.287
WYJK	138	-0.006	0.945	-0.172	0.160

APPENDIX 3.2. Time series and morlet transformations of the El Niño Southern Oscillation "Best" Index and regional tree-ring indices.

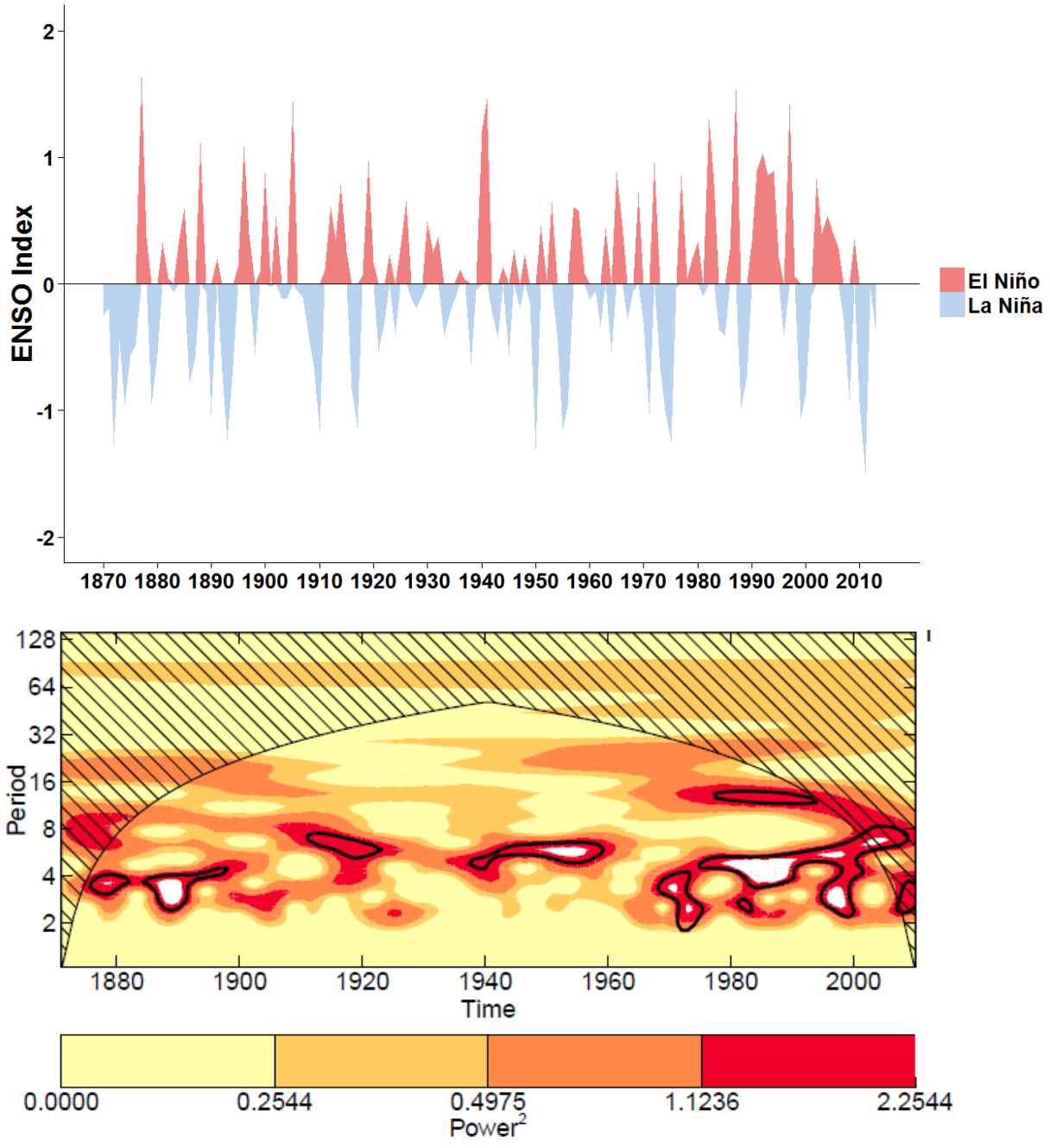

Figure 1. Morlet transformation of El Niño Southern Oscillation Index (ENSO) with contours highlighting significant portions of the power spectra ($\alpha = 0.10$). The area inside the cone of influence should not be interpreted. It is evident that ENSO is on a 4-8 year return interval, and the amplitude and duration of events has increased in recent decades.

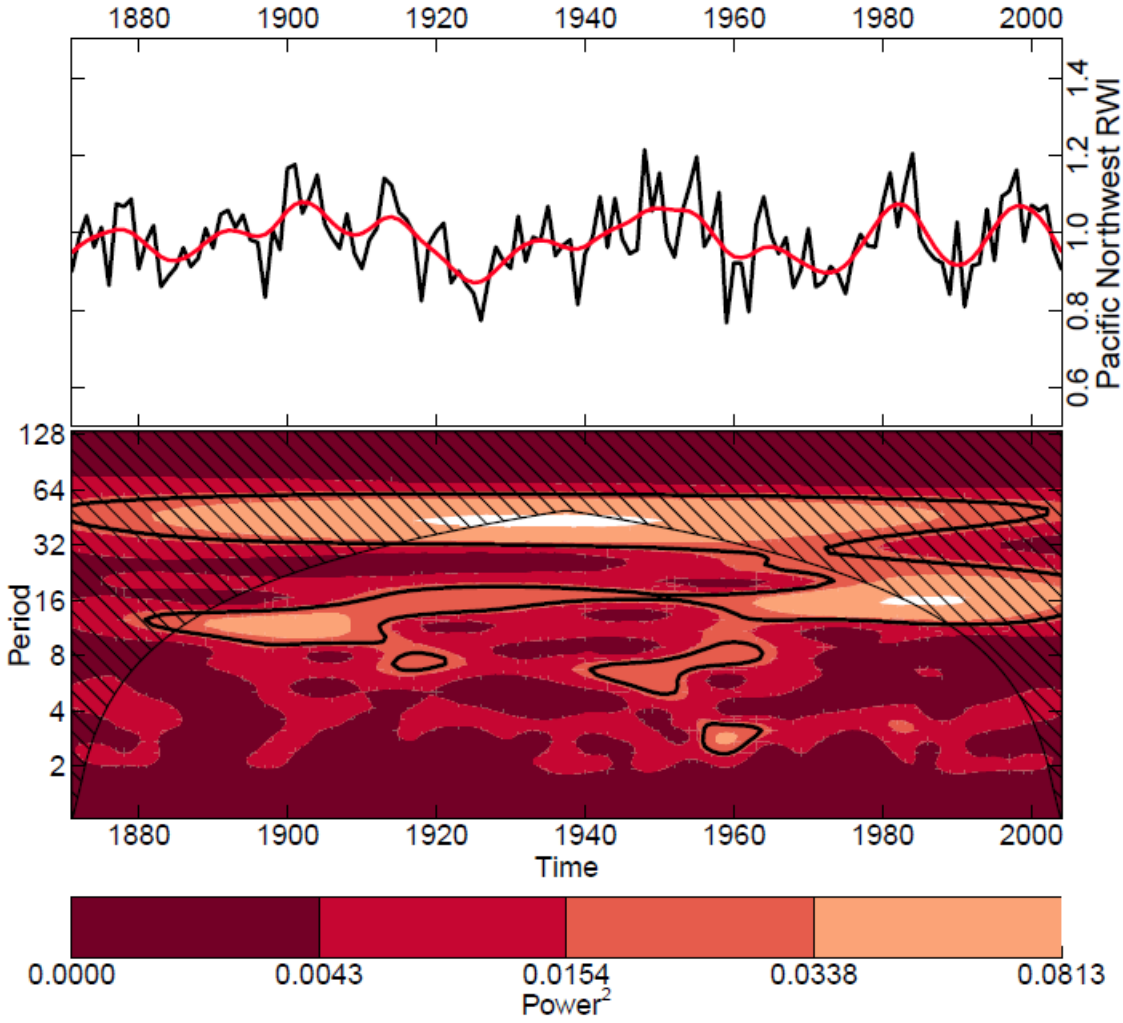

Figure 2. Morlet transformation of Pacific Northwest tree-ring indices with contours highlighting significant portions of the power spectra ($\alpha = 0.10$). The area inside the cone of influence should not be interpreted. Variability in power is evident at the inter-decadal scale but is significant only at the 8–10 year scale from 1900 to 1960, which could be a response to a cool-phase Pacific Decadal Oscillation.

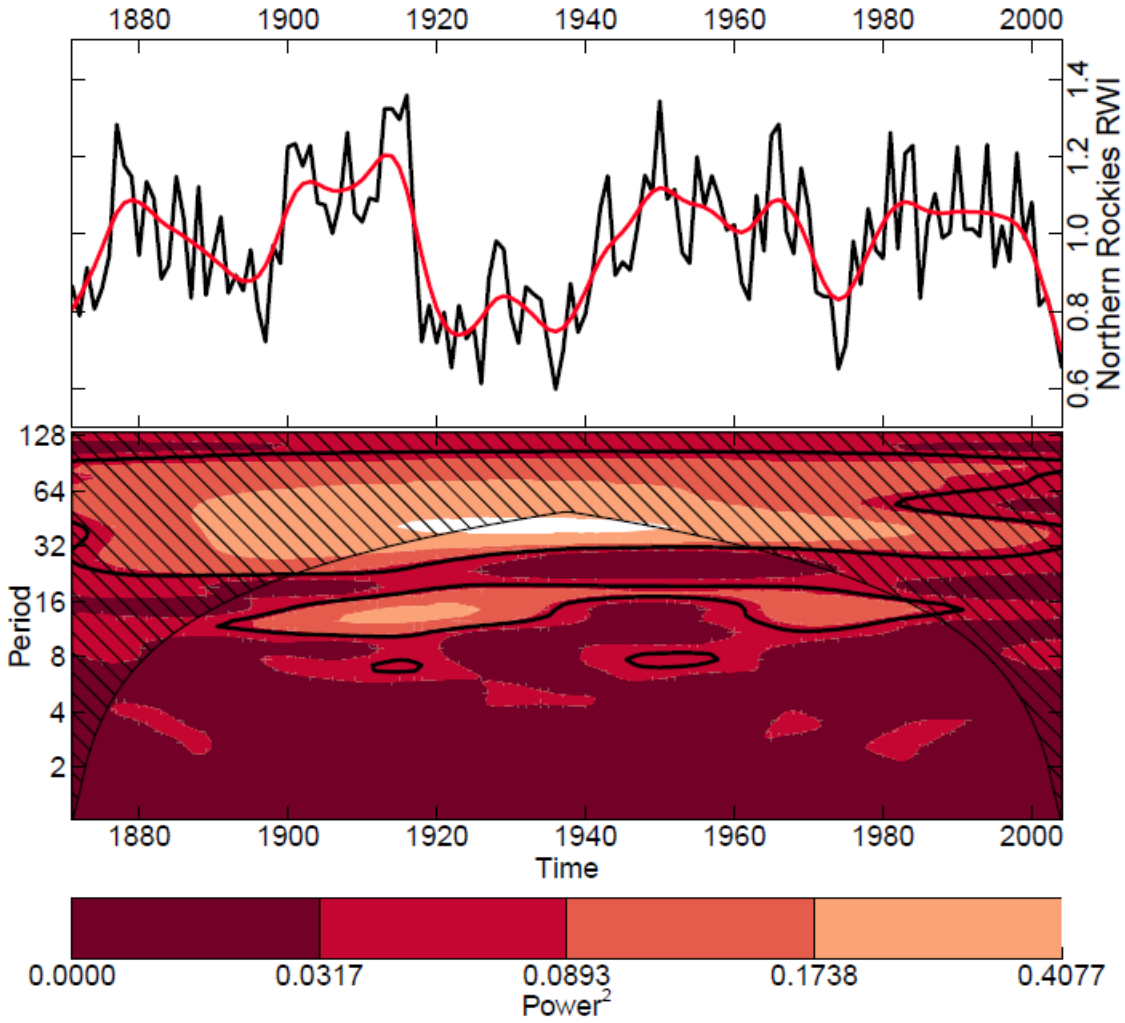

Figure 3. Morlet transformation of Northern Rockies tree-ring indices with contours highlighting significant portions of the power spectra ($\alpha = 0.10$). The area inside the cone of influence should not be interpreted. Less inter-decadal variability is evident in this region.

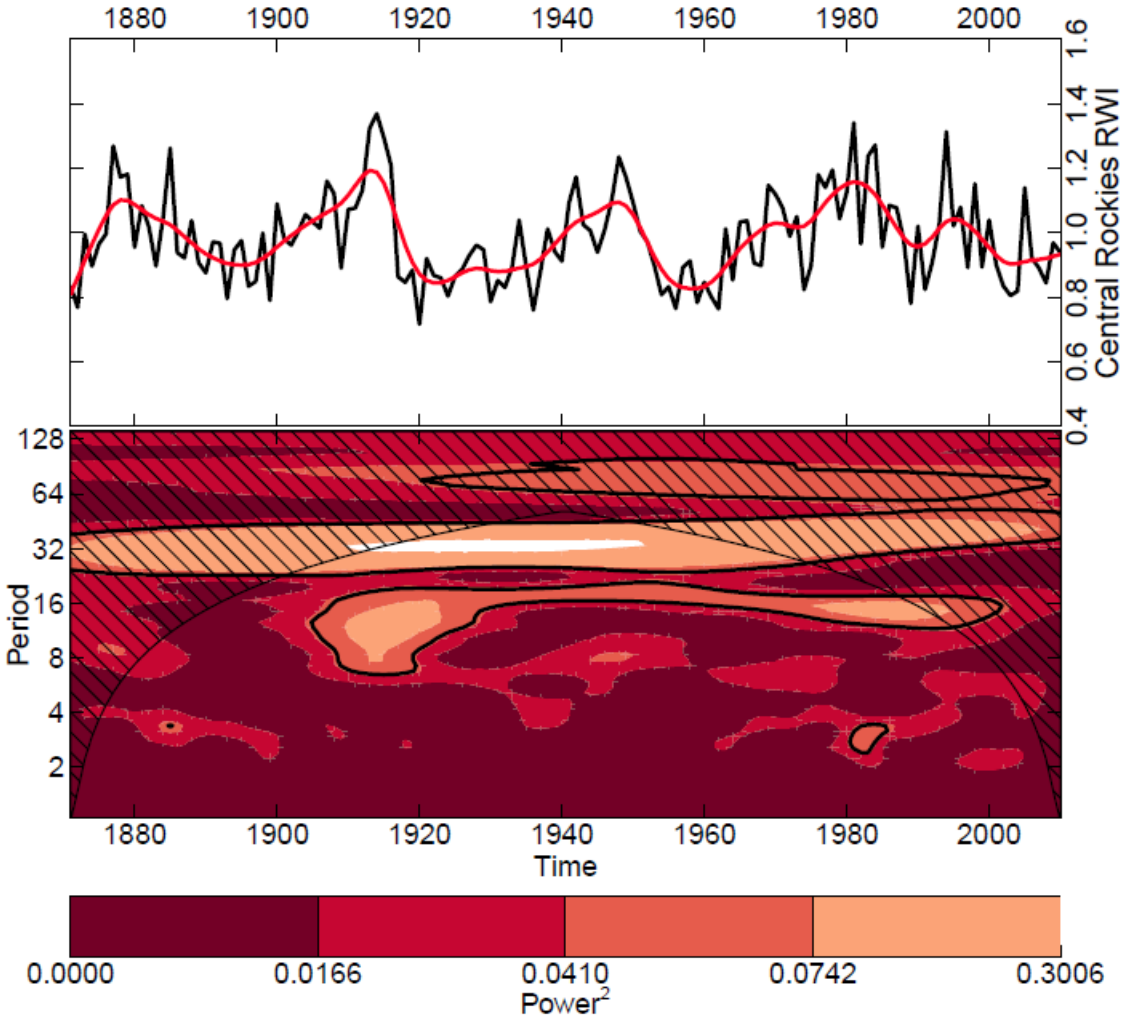

Figure 4. Morlet transformation of Central Rockies tree-ring indices with contours highlighting significant portions of the power spectra ($\alpha = 0.10$). The area inside the cone of influence should not be interpreted. An 8–16 year signal is persistent through the 21st century.

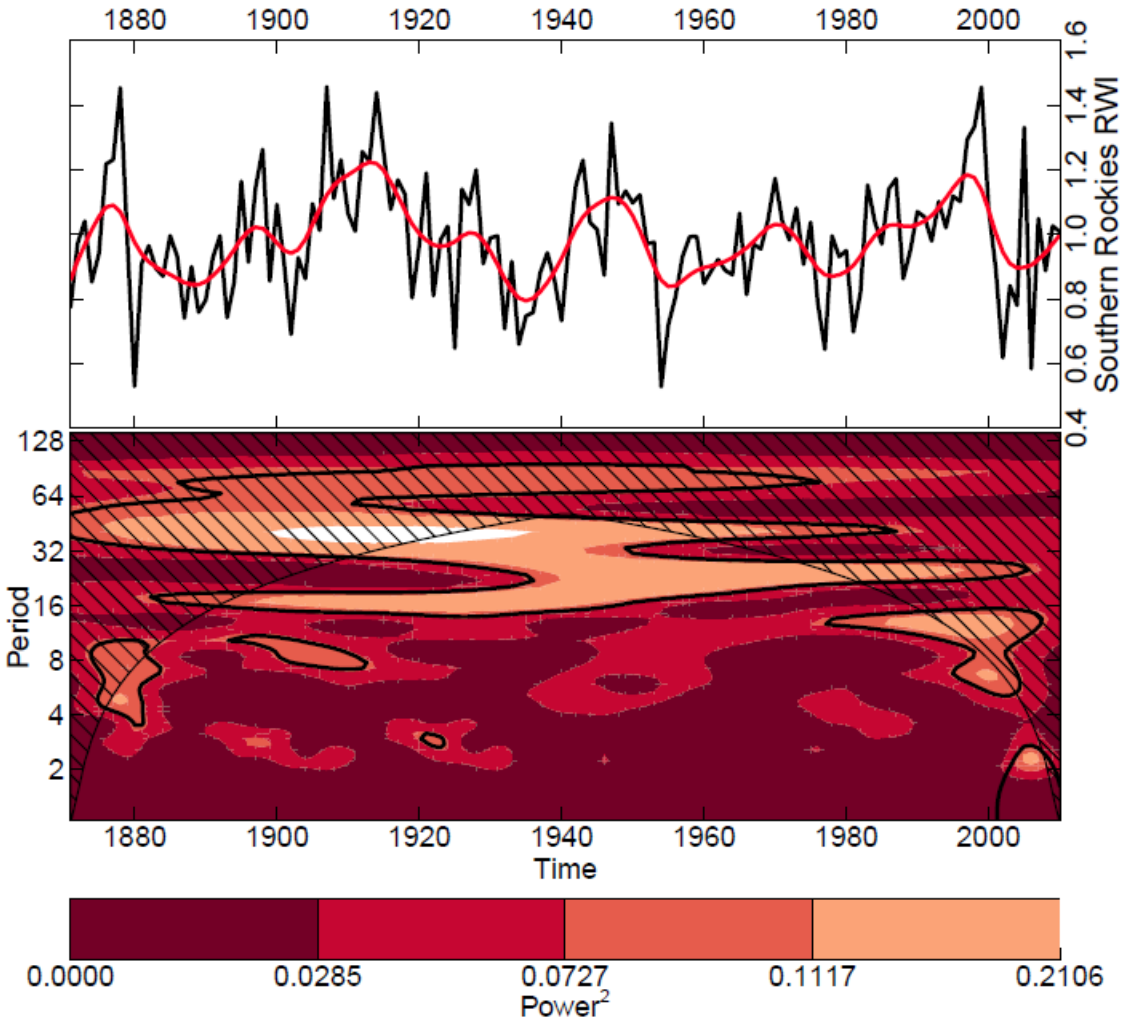

Figure 5. Morlet transformation of Southern Rockies tree-ring indices with contours highlighting significant portions of the power spectra ($\alpha = 0.10$). The area inside the cone of influence should not be interpreted. An 8–16 year signal is persistent through the 21st century.

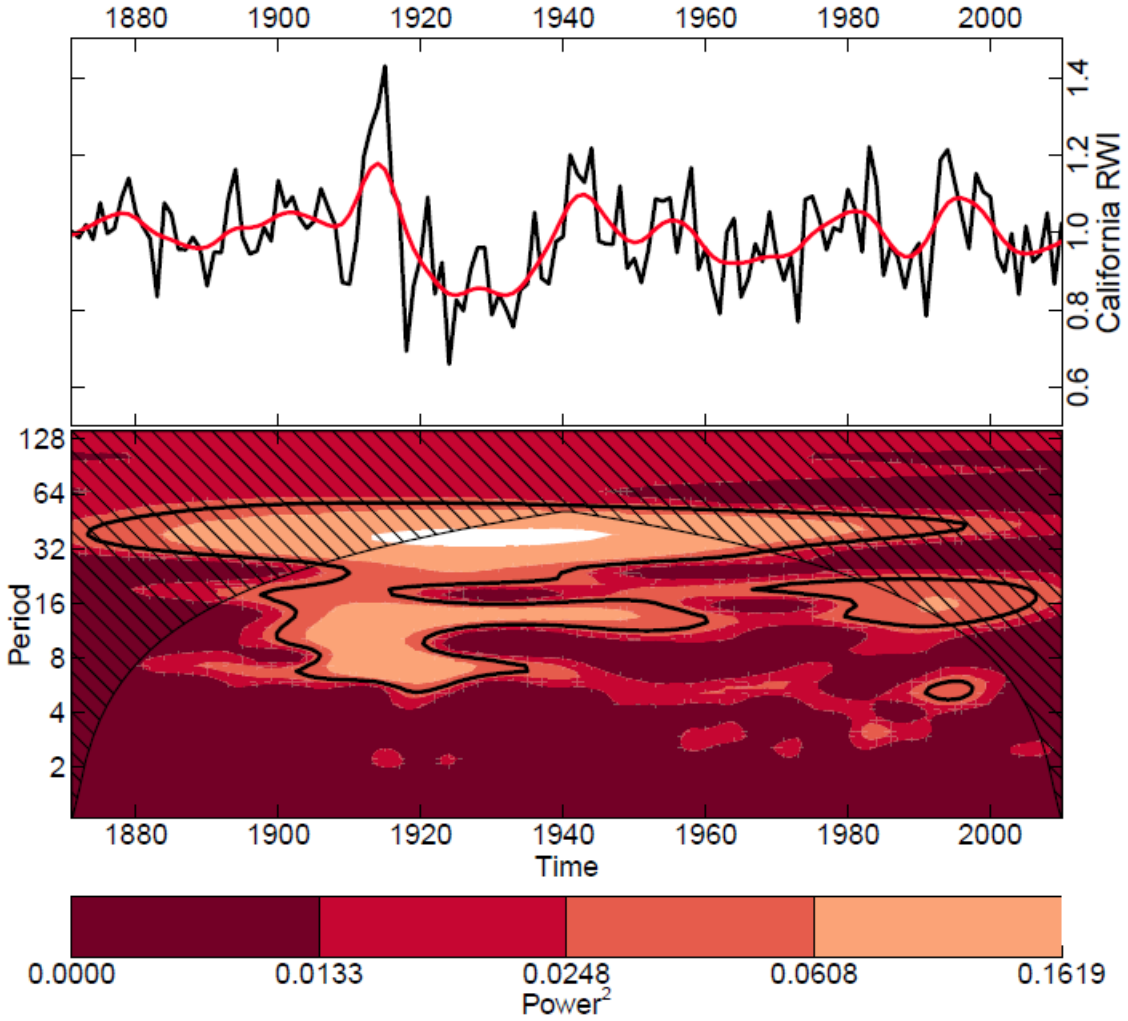

Figure 6. Morlet transformation of California tree-ring indices with contours highlighting significant portions of the power spectra ($\alpha = 0.10$). The area inside the cone of influence should not be interpreted.

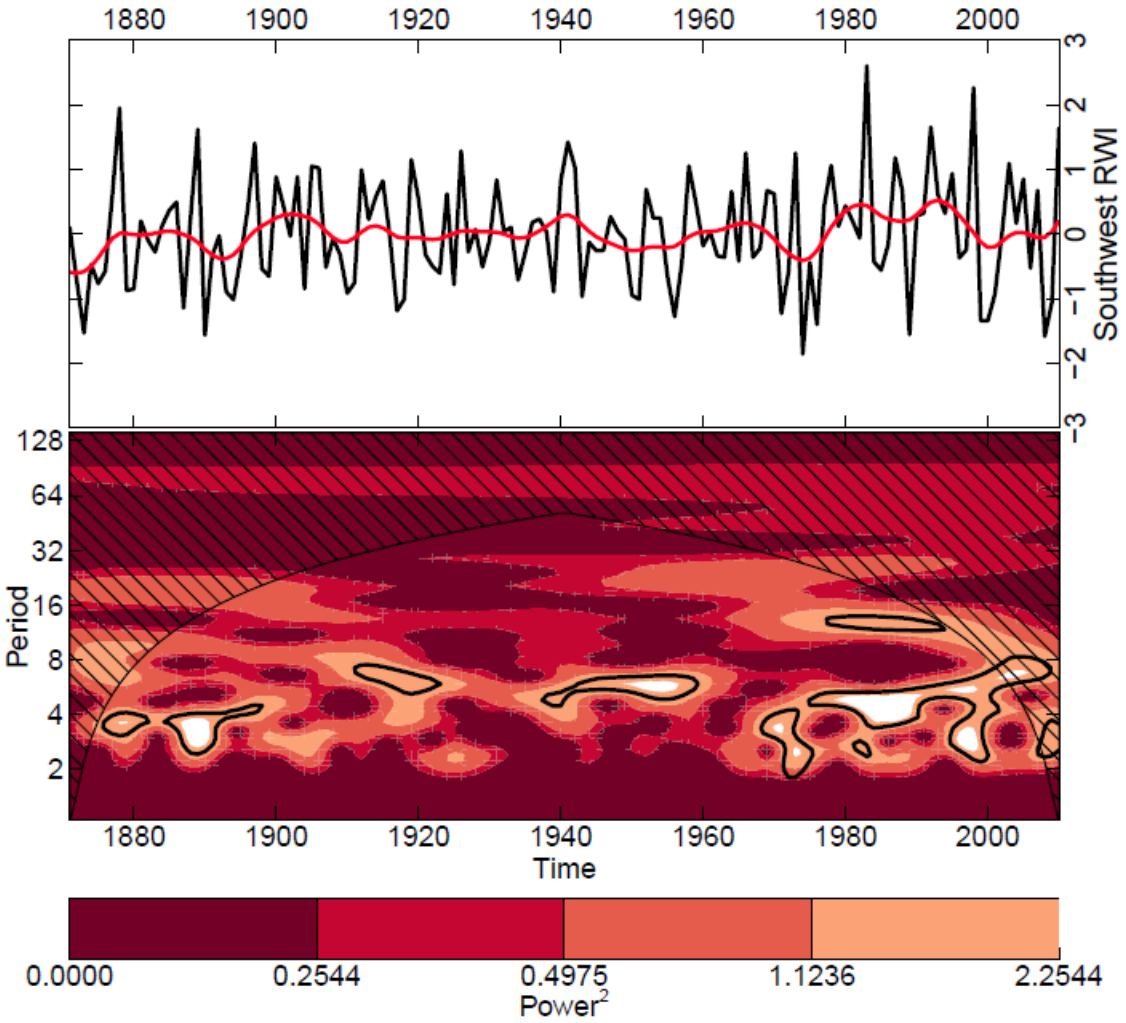

Figure 7. Morlet transformation of Southwest tree-ring indices with contours highlighting significant portions of the power spectra ($\alpha = 0.10$). The area inside the cone of influence should not be interpreted. Variability at inter-decadal scale (4-10 years) is obvious.

Chapter 4

Conclusion

1. OVERVIEW

I used a comprehensive network of Douglas-fir (*Pseudotsuga menziesii*) tree-ring data to quantify relationships between climate and tree growth. A hierarchical, multi-scale sampling approach was used to collect tree cores across the entire range of the species in the United States. Data collection was stratified based on variability in growing environments, climate, and geographic dispersion. This multi-scale sampling approach was built upon and added to work completed by Littell et al. (2008). Other datasets covering a continental scale have been pieced together from the International Tree Ring Database (Chen et al. 2010), and have a shorter common time period and have included only trees from extreme populations. Our dataset covers (1) the entire United States range of the species, (2) climate space of the species, (3) all dominant mountain ranges in the western United States, (4) elevations spanning from sea level to 3300 m, and (5) open to closed canopy forests. We now have the most extensive set of chronologies for one species in the world.

Tree growth data were combined with a novel climate dataset, which includes typical climate variables as well as "plant relevant" variables. Data extracted from the Variable Infiltration Capacity Hydrologic Model (VIC) included precipitation, temperature, potential evapotranspiration, actual evapotranspiration, and vapor pressure deficit. Climatic water deficit was calculated as a function of actual evapotranspiration minus potential evapotranspiration. Few other tree-ring studies have used deficit variables as the main variables in their analyses. The relationship between tree growth and climate was analyzed at four spatial scales (plot,

watershed, region, and continent) and three temporal scales (monthly, interannual, and interdecadal). Chronologies were created at all four scales, and tree growth data were also aggregated via principal components analysis. I used a combination of Pearson's product-moment correlations, ordinary least squares regression, superposed epoch analysis and cross-wavelet analysis to assess the relationship between chronologies and climatic variability. A thorough treatment of relationships at all scales allows for robust inference that considers how mechanisms that alter tree growth vary through space and time.

2. KEY FINDINGS

2.1 Trees respond to climate at multiple scales

Chapter 2 and 3 results demonstrate that variability in continental, regional, and local climate is recorded in annual tree rings, proving that tree growth is responsive to climate at multiple scales. Individual trees respond to the local microclimate, but conditions at this scale are embedded within local and regional interannual climate patterns. At larger scales (regional to continental), interdecadal climatic variability is often forced by major modes of the atmosphere-ocean circulation system (Cayan et al. 1998, Barlow et al. 2001). In some cases, trees can record variations in climate at all aforementioned scales. For example, lower precipitation, higher temperatures, and a longer growing season can decrease soil moisture storage which is a major limiting factor for tree growth. These types of conditions can arise as a function of monthly or even daily variations in weather, but are also characteristic of La Niña or El Niño events, depending on the proximity to the ENSO dipole. ENSO events are recorded by

trees in this study, supporting the conclusion that variation in ring width reflects limitations in growing environments at multiple scales.

2.2 Temperature regulates water availability

Results suggest that integrated climate variables (climatic water deficit and vapor pressure deficit) are more closely linked to growth variability than either precipitation or temperature alone. Correlation statistics are much higher with the integrated variables, and are higher in the Chapter 2 analysis than other studies. Therefore, variables that integrate water and energy reflect how plants "sense" climate and are more useful in parameterizing climate sensitivity in Douglas-fir. All analyses confirm that Douglas-fir is sensitive to water availability and soil moisture, but results suggest that the inter-relationship between temperature and precipitation more accurately predicts growth limitations. Therefore, to fully understand the relationship between tree growth and water one must consider how temperature regulates limitations to growth. Increased ambient air temperature alters vapor pressure deficit which modifies the soil-plant-atmosphere continuum, increasing water potential gradients and atmospheric demands on water stored both in the plant and soil (Breda et al. 2006). Temperature drives evaporative demand, relative humidity and dew point, all of which influence boundary layer and stomatal conductance (Irvine et al. 2001, Warren et al. 2004). The effects of temperature are also indirectly felt via changes in vapor pressure deficit which also regulates stomatal conductance (Oren 1999). Temperature is projected to increase without commensurate increases in precipitation; therefore, we can expect increased temperature and deficits to cause decreased growth.

Water and energy were considered as the two dominant limiting factors in Douglas-fir growth, which leaves several other aspects of the growing environment unmentioned. Light availability is a limiting factor in forests of the Pacific Northwest (Lewis et al., 2000, Franklin et al. 2002), especially old growth forests where dominant canopies filter photosynthetically active radiation. Soil substrate and nutrient availability also limit the establishment and success of mature individuals (Keyes and Grier 1981). In addition, limitations to growth differ with the age and life stage of forest species (Niinemets 2010). This study considers only climate-driven limiting factors to growth on mature, dominant and co-dominant trees.

2.3 All dominant trees respond to climatic variability

Many previous dendrochronological studies have targeted the most exposed trees in order to extract the strongest climate signal (aiding in reconstruction of climate variables), and are not suitable for assessing climate-growth relationships broader populations of trees. Consequently, many climate-growth interaction studies have included data from only these most exposed trees. The dataset analyzed here includes trees growing across a range of elevations and on a variety of topographic positions, proving that a dominant climate response can be observed in entire populations not just those in the extreme ends of a species distribution**.**

3. FUTURE DIRECTIONS

3.1 Assessing variability through time

All of the analyses addressed how climate-growth relationships vary through space, but did not address how they vary through time. I would like to further investigate the stationarity of climate-growth responses using a moving-correlation analysis. An exploratory analysis of this question suggests that indeed correlations have decreased at some sites and increased at others, but the direction of change varies with climate variable. Calculating correlations in moving windows reduces degrees of freedom, so the results would be less robust than those reported here. Further consideration is needed to identify the best method to assess how the response to climate is changing over time.

3.2 Projecting future growth

In my own future work, I will use these data to project future climate-growth relationships in Douglas-fir. Growth projections will be considered in two main contexts: (1) growth models, and (2) changing growing environments. I am collaborating with professors at the University of Arizona Laboratory of Tree-Ring Research to use my Douglas-fir data to parameterize a process-based growth model that will forecast western United States species distributions based on climatic niche. Albright and Peterson (2013) presented a method for forecasting changing growth environments. I will use my growth data with simulated climate projections from VIC to define how the climate niche of Douglas-fir will shift in climate space. Although the species is predominantly water limited, some locales exhibit energy limitations. Forests that are predominantly energy limited may transition to water limited (Littell et al. 2010, Albright and Peterson 2013), and my analysis would test this hypothesis for Douglas-fir across its range.

3.3 Multiple species and competition

The sampling and analytical approach used in this dissertation provide a model for conducting future studies with different dominant forest species in either the western or eastern United States or other continents. While the amount of effort required to assemble this type of dataset is large, the consistency and lack of sampling bias make these data more appropriate for addressing forest vulnerability and stress response. Gathering growth data of this type is crucial for understanding the impacts of climate change on forest ecosystems, and is arguably time-sensitive because older trees are being lost to insects, disease and wildfire. Certain domestic species of interest include ponderosa pine (*Pinus ponderosa*), Engelmann spruce (*Picea engelmannii*), subalpine fir (*Abies lasiocarpa*), and lodgepole pine (*Pinus contorta* var. *latifolia* and *Pinus contorta* var. *murryana*). All of these species have a large geographic extent and encompass a breadth of growing environments. Any future effort would also consider competition, as none of these species grow in pure stands. It is hypothesized that competition mediates the growth response to climate, but it is unclear how and to what degree (Carnwath et al. 2012). Future work would incorporate a multi-species sampling approach to assess how forest communities respond to climatic variability.

4. FINAL THOUGHTS

Work presented in this dissertation represents a new method for considering how forests may respond to future climatic variability. Thorough field sampling across a wide range of growing environments differentiates this work from others that have focused only on extreme environments. I provide a template for how to conduct this type of field research and an

analytical framework for considering processes that occur at multiple scales. This work is all retrospective and does not provide projections of future growth. Instead, I provide scientific information regarding the intricate relationship between tree growth and climate that can be used in future studies that consider growth response to a changing climate.

4. REFERENCES

Albright, W. L., and D. L. Peterson. 2013. Tree growth and climate in the Pacific Northwest, North America: a broad-scale analysis of changing growth environments. Journal of Biogeography **40**: 2119-2133.

Bréda, N., R. Huc, A. Granier, and E. Dreyer. 2006. Temperate forest trees and stands under severe drought: a review of ecophysiological responses, adaptation processes and long-term consequences. Annals of Forest Science **63**: 625-644.

Carnwath, G. C., D. W. Peterson, and C. R. Nelson, C. R. 2012. Effect of crown class and habitat type on climate–growth relationships of ponderosa pine and Douglas-fir. Forest Ecology and Management **285**: 44-52.

Chen, P. Y., C. Welsh, and A. Hamann. 2010. Geographic variation in growth response of Douglas-fir to interannual climate variability and projected climate change. Global Change Biology **16**: 3374-3385.

Lewis, J. D., R. B. McKane, D. T. Tingey, and P. A. Beedlow. 2000. Vertical gradients in photosynthetic light response within an old-growth Douglas-fir and western hemlock canopy. Tree Physiology **20:** 447-456.

Franklin, J. F., T. A. Spies, R. Van Pelt, A. B. Carey, D. A. Thornburgh, D. R. Berg, D. B. Lindenmayer, M. E. Harmon, W. S. Keeton, D. C. Shaw, K. Bible, J. Chen. 2002. Disturbances and structural development of natural forest ecosystems with silvicultural implications, using Douglas-fir forests as an example. Forest Ecology and Management **155:** 399-423.

Irvine, J., B. E. Law, P. M. Anthoni, and F. C. Meinzer. 2002. Water limitations to carbon exchange in old-growth and young ponderosa pine stands. Tree Physiology **22**:189-196.

Keyes, M. R., and C. C. Grier. 1981. Above-and below-ground net production in 40-year-old Douglas-fir stands on low and high productivity sites. Canadian Journal of Forest Research **11:** 599-605.

Littell, J.S., D.L. Peterson, and M. Tjoelker. 2008. Douglas-fir growth in mountain ecosystems: water limits tree growth from stand to region. Ecological Monographs **78**: 349-368.

Littell, J. S., E. E. Oneil, D. McKenzie, J. A. Hicke, J. A. Lutz, R. A. Norheim, and M. M. Elsner. 2010. Forest ecosystems, disturbance, and climatic change in Washington State, USA. Climatic Change **102**: 129-158.

Niinemets, U. 2010. Responses of forest trees to single and multiple environmental stresses from seedlings to mature plants: Past stress history, stress interactions, tolerance and acclimation. Forest Ecology and Management **260**: 1623-1639.

Oren, R., J. S. Sperry, G. G. Katul, D. E. Pataki, B. E. Ewers, N. Phillips, and K. V. R. Schäfer. 1999. Survey and synthesis of intra- and interspecific variation in stomatal sensitivity to vapour pressure deficit. Plant, Cell and Environment **22**: 1515-1526.

Warren, C. R., N. J. Livingston, and D. H. Turpin. 2004. Water stress decreases the transfer conductance of Douglas-fir (*Pseudotsuga menziesii*) seedlings. Tree Physiology **24**: 971-979.